NON-INVASIVE MEASUREMENT OF THE INTERNAL TEMPERATURE OF HEAT-GENERATING BODIES

by

DEAN RAYMOND ANTHONY

THESIS

Submitted in partial fulfillment of the requirements
For the degree of Master of Science in Mechanical Engineering at
The University of Texas at Arlington
December, 2016

Arlington, Texas, USA

Supervising Committee:

Ankur Jain, Supervising Professor
Ratan Kumar
Albert Tong

ACKNOWLEDGEMENTS

Help from everyone in the Microscale Thermophysics Lab, Daipayan Sarkar, Derek Wong, Dr. David Wetz, and Dr. Ankur Jain is gratefully acknowledged.

This material is based upon work supported by the National Science Foundation under NSF CAREER Grant No. CBET-1554183 and NSF Grant No. CBET-1623892. Financial Support from Office of Naval Research through DURIP Award #N00014-14-1-0752 for acquisition of infrared camera is gratefully acknowledged. Heat pipe assistance from Dr. Winston Zhang, Novark Technology Inc. is also gratefully acknowledged.

DEDICATION

This work is dedicated to my wife, Jocelyn Anthony, for all of her understanding and support during this time.

ABSTRACT

Non-Invasive Measurement of the Internal

Temperature of Heat-Generating Bodies

Dean Raymond Anthony, M.S.

The University of Texas at Arlington, 2016

Supervising Professor: Ankur Jain

While the surface temperature of a heat-generating solid body can be measured using a variety of methods, there is a scarcity of techniques that exist for non-invasively measuring the temperature inside the solid body. Internal temperature measurement is very desirable as mere measurement of surface temperature gives no indication of the internal temperature. The highest temperature, usually located at the core of the body, dictates system performance and safety. For example, Li-ion cells provide good energy storage and conversion characteristics, but unfortunately suffer from safety problems related to overheating due to insufficient heat removal during operation. The following thesis presents a technique to non-invasively measure the core temperature of a heat generating solid body for both steady state and transient cases, utilizing the theoretical relationship between the core and surface temperatures of the body. This method is experimentally validated by determining the core temperature of various heat generating

cylindrical bodies - a thermal test cell and a Li-ion cell - using infrared temperature measurement on the surface, and comparing with measurements from embedded thermocouples within each cell. There is excellent agreement throughout the heat generation period between the predicted core temperature and measurements from the embedded thermocouple. These measurements demonstrate an accurate, non-invasive measurement method for real-time, core temperature monitoring. This thesis also investigates thermal performance of a Li-ion cell with a heat pipe inserted into the core. It is shown that active cooling of the protruding tip of the heat pipe results in maximum thermal benefit, which is shown to reduce the core temperature to as low as, or even lower than the surface temperature. This work contributes towards fundamental thermal metrology, and toward effective thermal management techniques for future Li-ion cell manufacturer designs, with possible applications in a wide variety of engineering systems.

LIST OF FIGURES

TABLE OF CONTENTS

CHAPTER 1

INTRODUCTION

Temperature directly affects the safety, performance, and reliability of a number of engineering systems relevant for energy conversion. Many physical processes that happen in such systems are closely connected to the temperature field. Measurement of temperature is a critical step in the monitoring process for engineering systems involving heating and cooling [1]. For example, accurate measurement of temperature for a Li-ion cell is a critical research challenge for ensuring performance, safety and reliability of systems that utilize Li-ion cells for energy conversion and storage [2]. The amount of heat generated in a typical cylindrical 26650 Li-ion cell is not relatively large, but due to poor thermal conductance of the cell, this causes significant temperature rise [3]. Accurate temperature measurement of the cell, particularly the peak temperature that occurs at the core of the cell is critical for effective thermal management and thermal control. Surface temperature measurements alone do not provide enough information about the internal temperature profile. The surface temperature is in most cases not as large as the core, which may be much hotter and in need of immediate cooling. While several experimental methods exist for measurement of the surface temperature of a solid body, there is a deficit of experimental techniques available for non-invasively measuring the internal temperature of a body. Internal measurement of a number of physical quantities such as stress, chemical composition, morphology, crystal structure, etc. made possible using different measurement methods [1], make apparent the lack of a similar method for internal measurement of temperature.

The second chapter presents a contactless, non-intrusive method for the measurement of the core temperature inside a heat-generating solid body. A theoretical heat transfer model is developed to show that the core temperature of a heat-generating, solid cylinder can be measured using appropriate integrals of the measured spatial temperature distribution on the cylinder surface. Surface temperature measurement is carried out using infrared thermography on a thermal test cell capable of internal heat generation. Internal temperature measurement based on this approach is carried out for a thermal test cell in a variety of heat generation and convective conditions. These measurements are validated against a thermocouple embedded in the thermal test cell. The two are found to be in very good agreement.

The third chapter presents a similar technique for non-invasively determining the core temperature of a heat generating body, but with a transient condition. This method uses surface temperature measurement using infrared thermography on a thermal test cell and the core temperature is predicted as a function of time. The technique is validated by the same means as in the previous chapter, via an embedded thermocouple in the thermal test cell. Core temperatures determined through this technique are found to be in close agreement with the actual core temperatures over the entire experimental period in a variety of heating and cooling conditions.

The fourth chapter applies the previously mentioned transient core temperature measurement method to the measurement of the core temperature of a 26650 Li-ion cell during high-rate discharge. The core temperature is determined using the same theoretical model, using measurements of the transient temperature field on the outside surface of the cell. Core temperature is measured for multiple discharge rates and varying rate scenarios. In each case, excellent agreement is found compared to independent measurements of the core temperature

using an embedded thermocouple within the Li-ion cell. These experiments demonstrate an effective, non-invasive method for measuring the core temperature of a Li-ion cell in use, which may be helpful for thermal control, performance optimization, as well as the monitoring of phenomena akin to thermal runaway.

Upon careful analysis of the temperature profile throughout the body of a Li-ion cell, the vast disparity between core and surface temperature stands out as a serious concern. Heat removal from a Li-ion cell is an important technological challenge that directly affects performance, reliability and safety of energy conversion and storage systems [4]. Increased temperatures within a Li-ion cell can result in reduced performance, reduced lifetime due to capacity/power fade, self-discharge, and a host of other failure scenarios [4]. Safety of Li-ion cells at large temperatures is also a prominent concern due to the well-known phenomenon of thermal runaway [4]. The large temperature gradient within Li-ion cells highlights the challenge in cooling the entire cell volume by using only surface-based cooling techniques. The benefit of surface cooling is restricted to only that region close to the surface. However, cooling is most crucially needed at the core of the cell, which is the most difficult to thermally access. Insertion of a heat pipe into a Li-ion cell may be an effective strategy for cooling the cell core. A heat pipe is a passive heat transfer device that provides highly directional heat transfer between two bodies [4].

The fifth chapter provides an experimental investigation into thermal performance enhancement due to heat pipe insertion in a cylindrical 26650 Li-ion cell. Reduction in core temperature of the cell due to the presence of a heat pipe in a variety of operating conditions is examined. Experimental data show that by directing the heat pipe at the core of the cell where temperature is usually the highest and where cooling is most needed, the core temperature can

decrease to a point that is as low as the surface temperature, resulting in excellent cooling and thermal uniformity within the cell. The experimental insight provides a fundamental characterization of thermal performance of heat pipes inserted into Li-ion cells. Based on this work, heat pipe cooling could be evaluated by manufacturers for enhanced safety and performance in future Li-ion cell designs.

References

[1] D. Anthony, D. Sarkar, A. Jain, Contactless, non-intrusive core temperature measurement of a solid body in steady-state, *Int. J. Heat Mass Transfer*, **101**, 2016, pp. 779-778. DOI: 10.1016/j.ijheatmasstransfer.2016.05.073

[2] D. Anthony, D.Sarkar, A. Jain, Non-Invasive, transient measurement of the core temperature of a solid body. *Sci. Rep*., **6** (35886), 2016, pp. 1-10. DOI: 10.1038/srep35886

[3] D. Anthony, D. Wong, D. Wetz, A. Jain, Non-Invasive Measurement of Internal Temperature of a Li-ion Cell During High-Rate Discharge, *Energy*, in review, 2016.

[4] D. Anthony, D. Wong, D. Wetz, A. Jain, Improved Thermal Performance of a Li-ion Cell Through Heat Pipe Insertion, *J. Electrochem. Soc.*, in review, 2016.

CHAPTER 2:

CONTACTLESS, NON-INTRUSIVE CORE TEMPERATURE MEASUREMENT OF A SOLID BODY IN STEADY-STATE

Dean Anthony, Daipayan Sarkar, Ankur Jain*

Mechanical and Aerospace Engineering Department
University of Texas at Arlington, Arlington, TX, USA.

* – Corresponding Author: email: jaina@uta.edu;
500 W First St, Rm 211, Arlington, TX, USA 76019
Ph: +1 (817) 272-9338; Fax: +1 (817) 272 2952

D. Anthony, D. Sarkar, A. Jain, Contactless, non-intrusive core temperature measurement of a solid body in steady-state, *Int. J. Heat Mass Transfer*, **101**, 2016, pp. 779-778.

DOI: 10.1016/j.ijheatmasstransfer.2016.05.073

Abstract

Accurate measurement of temperature is critical for understanding thermal behavior and monitoring safety and performance of engineering systems involving heating and cooling. While a number of methods are available for measurement of temperature on the outside surface of solid bodies, there is a lack of contactless, non-invasive methods for determining temperature inside solid bodies. Development of such methods is likely to impact a wide range of engineering systems. This paper describes and validates a method for measurement of internal temperature of a solid body based on measurement of the temperature distribution on its outside surface. A theoretical model is developed for determining the core temperature of a cylinder based on surface temperature measurement. This method is validated by determining the core temperature of a thermal test cell using infrared temperature measurement on the surface, and comparing with measurements from an embedded thermocouple. The two measurements are found to agree well with each other in a variety of heat generation and cooling conditions. While this validation is presented for a cylindrical body, the method lends itself easily to bodies of other shapes. This work contributes towards fundamental thermal metrology, with possible applications in a wide variety of engineering systems.

Keywords: Temperature Measurement; Internal Temperature; Infrared Thermography; Analytical Thermal Modeling.

1. Introduction

Temperature directly affects the performance, safety and reliability of a variety of engineering systems relevant for energy conversion. Most physical processes that occur in such systems are closely coupled to the temperature field. For example, in a Li-ion cell,

electrochemical reactions during energy storage and conversion determine the temperature field in the cell [1-4], which, in turn, affects the rate of these electrochemical reactions [5]. Measurement of temperature is a critical step for ensuring safety, reliability and high performance of engineering systems involving heating and cooling, as well as for fully understanding coupled, multiphysics phenomena that occur in such systems. In general, temperature is measured based on a linear change in a measurable characteristic as a function of temperature [6-7]. This includes electrical resistance [8], thermal expansion [8], reflectance [9], circuit resonant frequency [10], color [11], surface radiation [12], etc. A variety of temperature measurement methods, varying in their accuracy and complexity have been used to measure transient and steady state temperature either at discrete locations, or over an entire surface.

While a number of methods are available for temperature measurement on the outside surface of a solid, there is a relative lack of methods for non-invasively measuring temperature inside solids. Internal temperature measurement is relatively more challenging, particularly when a remote, contactless method is desired, but is also very important, since the safety and performance of systems depends critically on the internal temperature, which for heat-generating bodies is typically higher than the outside surface temperature. One example to illustrate this is a nuclear fuel rod, which is usually cylindrical in nature and has relatively low thermal conductivity [13]. Heat generation within the fuel rod due to fission reactions results in a temperature field within the rod, with the core of the rod usually being much hotter than the outside [14-15]. While the outside temperature of the fuel rod can be measured using a variety of surface temperature measurement techniques, measuring the temperature in the core of the fuel rod is not straightforward. In this case, a remote, contactless method for internal temperature measurement that does not disrupt the function of the fuel rod is very desirable. Another example

is a Li-ion cell commonly used for electrochemical energy conversion and storage [1,16]. In a Li-ion cell, electrochemical reactions and electrical impedance results in significant heat generation and temperature rise throughout the cell volume [2,17]. Due to the poor radial thermal conductivity of the Li-ion cell [18], a significant temperature gradient within the cell is known to exist [17,19-20]. Performance optimization and safety of the cell requires information about the peak temperature of the cell, which occurs in the core of the cell, and is difficult to measure [17] as the cell is hermetically sealed, and drilling a hole through the cell to insert a temperature sensor will short circuit and disrupt the electrochemical function of the cell. On the other hand, use of the surface temperature of the cell instead of core temperature is not appropriate, and may lead to severe under-design of the thermal management of the cell. These examples illustrate the need for and importance of contactless, non-intrusive measurement of the internal temperature of engineering systems. Such a measurement method will clearly be of universal appeal.

Internal measurement of a variety of physical quantities other than temperature such as stress, chemical composition, morphology, crystal structure, etc. is possible using various measurement methods [21-24]. For example, internal morphology and chemical composition can be measured using x-ray CT scans [24] that make use of the absorptivity of electromagnetic radiation by different materials. A variety of contactless, non-intrusive methods based on synchrotron x-ray, neutron scattering and ultrasonic waves also exist for internal stress measurement [25]. In comparison, however, there is a distinct lack of contactless, non-intrusive methods for measurement of temperature inside solid bodies. Most present methods provide information about either the surface temperature or the volumetrically averaged temperature, neither of which may be representative of the internal temperature of the solid. Only very limited work exists on measuring internal temperature of solids [26-29]. For example, the temperature

dependence of speed of ultrasonic waves through a solid has been utilized to measure the average temperature along a path through the solid by measuring the time of flight of an ultrasonic wave along that path [28-29]. Measurements along multiple paths through the body have been used in conjunction with information about the nature of the temperature field, obtained from solving governing energy conservation equations, to reconstruct the temperature field [29]. Ultrasonic-based temperature measurement methods, however, do not work well for materials with high rates of ultrasonic attenuation, and may be cumbersome to implement. Internal temperature of a Li-ion cell has been measured through impedance spectroscopy, based on a relationship between the cell temperature and certain electrochemical parameters of the cell [30-32]. However, these methods are very specific to the electrochemical characteristics of this system and do not apply to a general heat-generating body.

This paper presents a contactless, non-intrusive method for measurement of the core temperature in a heat-generating solid body. A theoretical heat transfer model for a heat-generating cylinder is developed to show that the core temperature of the cylinder can be measured using appropriate integrals of the measured spatial temperature distribution on the cylinder surface. Internal temperature measurement based on this approach is carried out for a thermal test cell in a variety of heat generation and convective conditions. These measurements are validated against a thermocouple embedded in the thermal test cell. The two are found to be in very good agreement. While this internal temperature measurement method is demonstrated here for a cylinder, a similar approach could be used for solids of other shapes. The next section presents theoretical models for non-intrusive determination of the core temperature based on surface temperature measurements. This is followed by a section describing the experimental test

setup and methods. Results are presented and discussed next, followed by conclusions and future directions for this work.

2. Mathematical Modeling

Consider a heat generating cylinder for which measurement of internal temperature at r=0 is of interest, and for which temperature distribution on the outside surface is measured. This section presents the derivation of the temperature distribution within the cylinder, from where it is shown that the core temperature of the cylinder can be determined using the surface temperature distribution. Thermal conduction in the cylinder is assumed to be orthotropic, as is the case in several systems of engineering interest [18]. An infinite cylinder is considered in section 2.1, and extension to a cylinder of finite length is discussed in section 2.2.

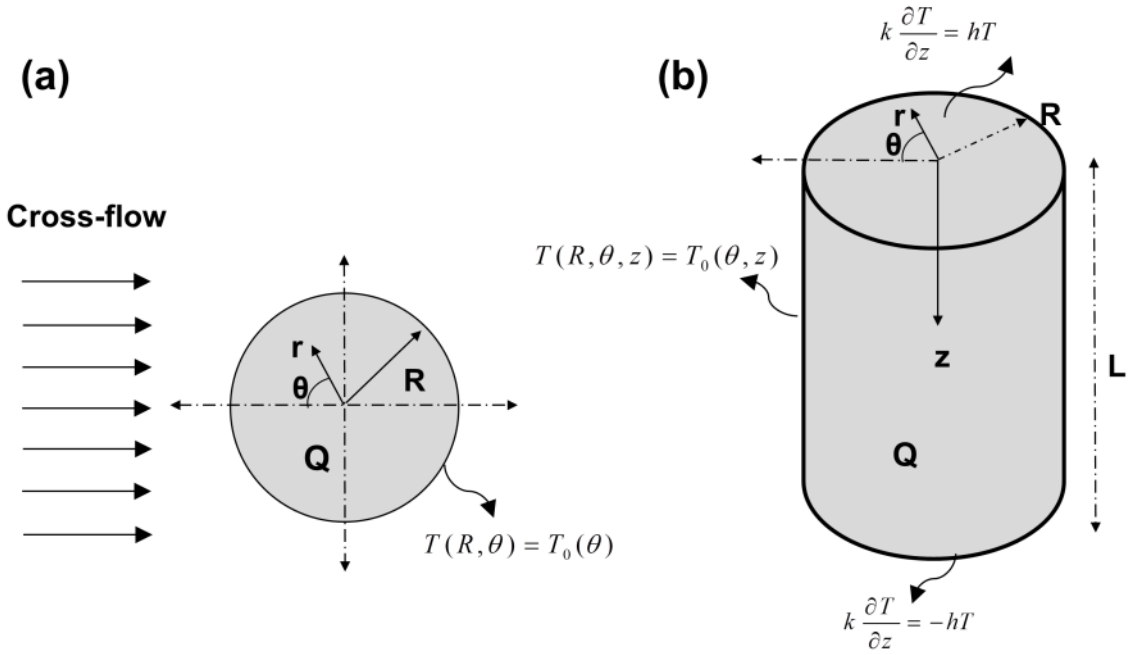

1. Figure 1: Schematic of the geometry of (a) infinite, and (b) finite cylinders analyzed in theoretical models for determining core temperature from outside temperature distribution measurements.

2.1. Infinite Cylinder

Figure 1(a) shows a schematic of the general heat transfer problem analyzed in this section. Consider an infinitely long cylinder of radius R, with volumetric internal heat generation at a rate of Q. The radial and circumferential thermal conductivities are k_r and k_θ respectively. Assume that the temperature distribution along the outer surface at $r=R$ is measured to be a function of θ, given by $T_0(\theta)$. In steady state, the energy conservation equation that governs the temperature field in the cylinder is given by

$$\left(\frac{\partial^2 T}{\partial r^2}+\frac{1}{r}\frac{\partial T}{\partial r}\right)+\frac{k_\theta}{k_r}\left(\frac{1}{r^2}\frac{\partial^2 T}{\partial \theta^2}\right)+\frac{Q}{k_r}=0 \qquad (1)$$

Where $T(r,\theta)$ is the temperature rise above ambient. The temperature distribution within the cylinder is subject to the following boundary conditions:

$$\left.\frac{\partial T}{\partial r}\right|_{r=0}=0 \qquad (2)$$

$$T(R,\theta)=T_0(\theta) \qquad (3)$$

$$T(r,\theta)=T(r,\theta+2\pi) \qquad (4)$$

$$\left.\frac{\partial T}{\partial \theta}\right|_{\theta}=\left.\frac{\partial T}{\partial \theta}\right|_{\theta+2\pi} \qquad (5)$$

Equation (2) represents the requirement for the temperature field to be finite at r=0. Equation (3) accounts for the measured temperature distribution T_0 on the outside surface of the cylinder. Note that if the extent of convective cooling varies significantly around the cylinder, as it does for forced convective cooling, T_0 will be a function of θ. Equations (4) and (5) represent periodicity in temperature and heat flux in the circumferential direction.

In order to determine the core temperature T_{core} at r=0 in terms of the measured temperature distribution $T_0(\theta)$, a solution for the general temperature field $T(r,\theta)$ must be derived. To do so, the temperature field is first transformed as follows,

$$T(r,\theta) = w(r,\theta) + \frac{Q\left(R^2 - r^2\right)}{4k_r} \tag{6}$$

This results into a homogeneous governing equation for $w(r,\theta)$ as follows:

$$k_r\left(\frac{\partial^2 w}{\partial r^2} + \frac{1}{r}\frac{\partial w}{\partial r}\right) + \frac{k_\theta}{k_r}\left(\frac{1}{r^2}\frac{\partial^2 w}{\partial \theta^2}\right) = 0 \tag{7}$$

Subject to

$$\left.\frac{\partial w}{\partial r}\right|_{r=0} = 0 \tag{8}$$

$$w(R,\theta) = T_0(\theta) \tag{9}$$

$$w(r,\theta) = w(r,\theta + 2\pi) \tag{10}$$

$$\left.\frac{\partial w}{\partial \theta}\right|_{\theta} = \left.\frac{\partial w}{\partial \theta}\right|_{\theta+2\pi} \tag{11}$$

A solution for $w(r,\theta)$ can be expressed as follows

$$w(r,\theta) = C_0 + \sum_{m=1}^{\infty} C_m \cos(m\theta)\left(\frac{r}{R}\right)^{m\sqrt{k_\theta/k_r}} \tag{12}$$

This form for $w(r,\theta)$ satisfies the governing equation (7) and all boundary conditions except the one at $r=R$ expressed in equation (9). The coefficients C_0 and C_m in this solution must be chosen in order to ensure that equation (9) is also satisfied.

Note that the core temperature T_{core} is obtained by substituting $r=0$ in equations (6) and (12), resulting in

$$T_{core} = T(r=0,\theta) = C_0 + \frac{QR^2}{4k_r} \tag{13}$$

This shows that the core temperature can be determined only in terms of the first coefficient C_0, and that no further coefficients are needed. To determine C_0, equation (12) is inserted in equation (9) to get

$$C_0 + \sum_{m=0}^{\infty} C_m \cos(m\theta) = T_0(\theta) \tag{14}$$

Finally, integrating Eq. (14) with respect to θ between 0 and 2π eliminates all coefficients except C_0, resulting in

$$C_0 = \frac{1}{2\pi}\int_0^{2\pi} T_0(\theta)\, d\theta \tag{15}$$

From equations (13) and (15), the core temperature may be expressed in terms of the measured outside surface temperature $T_0(\theta)$ as follows

$$T_{core} = \frac{1}{2\pi}\int_0^{2\pi} T_0(\theta)\, d\theta + \frac{QR^2}{4k_r} \tag{16}$$

Equation (16) shows the core temperature of the cylinder can be obtained from the circumferential integral of the measured outside temperature. Note that this measurement approach requires information about the volumetric heat generation rate, which may be known a priori based on the physical mechanism responsible for heat generation, as well as the radial thermal conductivity k_r, which may be known based on the material of the cylinder. The circumferential thermal conductivity k_θ is not needed for measurement of T_{core} even if thermal conduction in the cylinder may be orthotropic.

2.2. Finite Cylinder

This section extends the model presented in section 2.1 to a finite cylinder of length L, and shows how the core temperature $T_{core}(z)$ may be determined from measurement of the outside surface temperature, $T_0(\theta,z)$. Note the z variation in both T_{core} and T_0 due to the finite length of the cylinder. The geometry considered in this section is shown schematically in Figure 1(b). It is assumed that the two axial ends of the cylinder are convectively cooled with a heat transfer coefficient h. Under these assumptions, the steady state governing equation for the temperature field $T(r,\theta,z)$ is given by

$$\left(\frac{\partial^2 T}{\partial r^2}+\frac{1}{r}\frac{\partial T}{\partial r}\right)+\frac{k_\theta}{k_r}\left(\frac{1}{r^2}\frac{\partial^2 T}{\partial \theta^2}\right)+\frac{k_z}{k_r}\frac{\partial^2 T}{\partial z^2}+\frac{Q}{k_r}=0 \qquad (17)$$

Similar to the infinite cylinder case, the temperature field satisfies boundary conditions given by equations (2), (4) and (5). In addition, the following boundary conditions also apply:

$$T(R,\theta,z)=T_0(\theta,z) \qquad (18)$$

$$k\frac{dT}{dz}=hT \qquad \text{at z=0} \qquad (19)$$

$$k\frac{dT}{dz}=-hT \qquad \text{at z=L} \qquad (20)$$

A general solution for this partial differential equation is given by [33]

$$T(r,\theta,z)=\frac{QL^2}{2k_z}\left[\frac{z}{L}\left(1-\frac{z}{L}\right)+\frac{1}{Bi}\right]+\sum_{m=0}^{\infty}\sum_{n=1}^{\infty}C_{m,n}\ I_{m\sqrt{\frac{k_\theta}{k_r}}}\left(\eta_n\sqrt{\frac{k_z}{k_r}}\,r\right)\cos(m\theta)\left[\frac{h}{\eta_n k_z}\sin(\eta_n z)+\cos(\eta_n z)\right] \qquad (21)$$

Where I is the modified Bessel function of the first kind, and $Bi=\frac{h\cdot L}{k_z}$. The eigenvalues η_n are determined from roots of the equation

$$\tan(\eta_n L)=\frac{2(\eta_n\cdot L)Bi}{(\eta_n\cdot L)^2-Bi^2} \qquad (22)$$

From equation (21), the core temperature $T_{core}(z)$ is given by

$$T_{core}(z) = T(r=0,\theta,z) = \frac{QL^2}{2k_z}\left[\frac{z}{L}\left(1-\frac{z}{L}\right)+\frac{1}{Bi}\right]+\sum_{n=1}^{\infty} C_{0,n}\left[\frac{h}{\eta_n k_z}\sin(\eta_n z)+\cos(\eta_n z)\right] \tag{23}$$

Note that setting r=0 in equation (21) eliminates all terms with coefficients $C_{m,n}$, where m>0, in the expression for $T_{core}(z)$. Thus, measurement of $T_{core}(z)$ requires only $C_{0,n}$ coefficients. To determine these coefficients, equation (21) is inserted in equation (18), followed by multiplication with $\left[\frac{h}{\eta_j k_z}\sin(\eta_j z)+\cos(\eta_j z)\right]$, and integration in z and θ. Using the principle of orthogonality for the eigenvalues in the z and θ directions, this results in

$$C_{0,j} = \frac{-\frac{QL^2}{2k_z}F_j + \frac{1}{2\pi}\int_0^{2\pi}\int_0^{L} T_0(\theta,z)\left(\frac{h}{\eta_j k_z}\sin(\eta_j z)+\cos(\eta_j z)\right)dz\,d\theta}{N_j \cdot I_0\left(\eta_j\sqrt{\frac{k_z}{k_r}}R\right)} \tag{24}$$

Where F_j is given by

$$F_j = \int_0^{L}\left(\frac{z}{L}\cdot\left(1-\frac{z}{L}\right)+\frac{1}{Bi}\right)\cdot\left(\frac{h}{\eta_j k_z}\sin(\eta_j z)+\cos(\eta_j z)\right)dz \tag{25}$$

And the norm N_j is given by [34]

$$N_j = \left(\frac{h^2}{(\eta_j k_z)^2}+1\right)\frac{L}{2}+\frac{h}{k_z\eta_j^{\,2}} \tag{26}$$

Equations (23)-(26) provide an analytical expression for the core temperature $T_{core}(z)$ in terms of appropriate circumferential and axial integrals of the measured outside temperature distribution $T_0(\theta,z)$.

Note that, in comparison to the infinite cylinder case, the axial thermal conductivity k_z is required for determining $T_{core}(z)$, since thermal conduction in the axial direction occurs in the finite cylinder.

The theoretical derivations in sections 2.1 and 2.2 provide a contactless, non-intrusive method for measuring the core temperature at r=0 for infinite and finite cylinders respectively.

The theoretical treatment shows that these temperatures can be obtained using appropriate integrals of the measured temperature distribution on the outside surface of the cylinder. While this discussion is specific to a cylinder, this approach could also be used for a body of any shape, provided one is able to solve the thermal conduction problem within the body, similar to the approach presented here for a cylinder. The solution of the thermal conduction problem for a body of a given shape provides the relationship between the core and outside temperatures, similar to equations (16) and (23).

The next section discusses experiments carried out to validate this core temperature measurement approach using a thermal test cell.

3. Experiments

Experiments are carried out to validate the method described in section 2 to measure the core temperature of a cylinder using outside surface temperature measurements. This section describes components of the experimental setup, as well as the experimental procedure for validation.

3.1. Thermal Test Cell

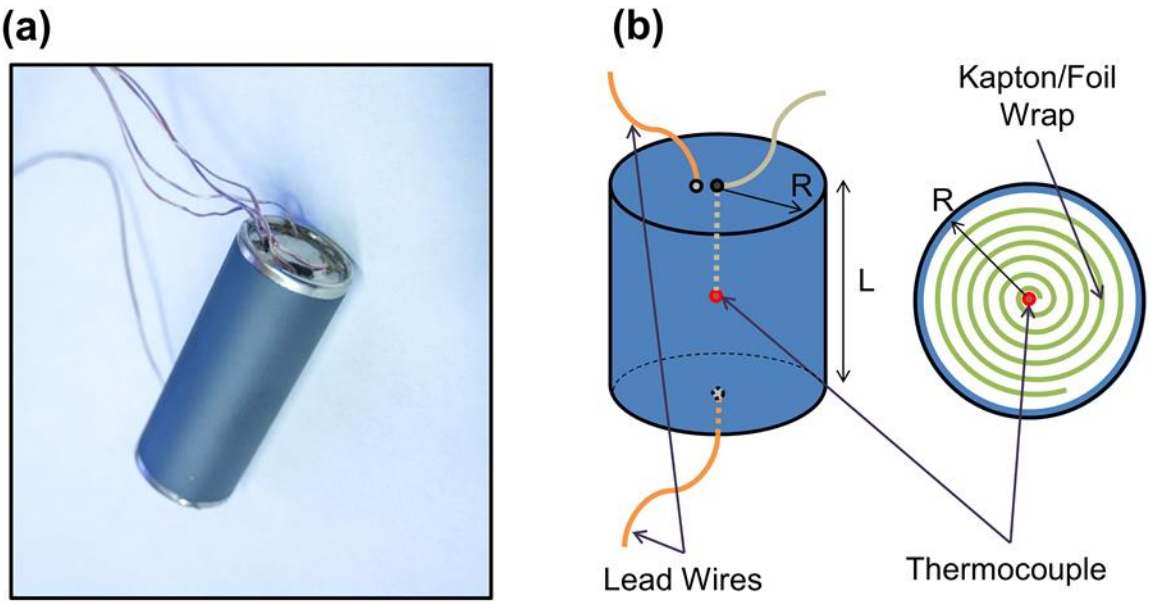

2. Figure 2: (a) Picture and (b) Schematic of the thermal test cell for remote, non-invasive core temperature measurement in steady state.

A cylindrical thermal test cell capable of volumetric heat generation through Joule heating is designed and fabricated for these experiments. A picture and a schematic diagram of the thermal test cell are shown in Figures 2(a) and 2(b) respectively. Thin metal foil of thickness 0.025 mm is first insulated by adhering Kapton tape on its surface. The foil-Kapton sandwich is rolled around a thin rod to form a cylinder of height 65 mm and radius 13 mm. A T-type thermocouple is placed at the inner core during this rolling process. Thin metal wires are soldered to the two ends of the metal foil to provide electrical access to the metal foil. The roll is then lowered inside a hollow Aluminum casing. Electrical current through the metal foil inside the roll provides volumetric heating throughout the test cell. The lead wires are routed out of the casing along with the thermocouple wire. Remaining volume inside the casing is filled with uncured poly-dimethylsiloxane, a commonly used electrically insulating soft polymer, followed by curing at room temperature. A dessicator is used to remove most air bubbles from the mixture of PDMS and curing agent prior to pouring. The long cure time ensures removal of any

remaining air bubbles. PDMS filling is carried out in two steps in order to expel all air inside the test cell. Once filled with PDMS and cured, the test cell is sealed with an epoxy. Lead wires coming out of the test cell provide the capability of passing a heating current through the metal foil, as well as measuring the temperature of the thermocouple embedded in the core of the cell. The thermocouple measurements facilitate validation of core temperature measurement method described in section 2. Note the black color of the outer surface of the test cell in Figure 2(a) due to application of a graphite film to facilitate infrared (IR) temperature measurement.

3.2. Measurement of Radial Thermal Conductivity of Thermal Test Cell

As shown in equation (16), the radial thermal conductivity k_r is needed for determining the core temperature of the thermal test cell. Experiments are carried out to measure k_r, based on the temperature response due to adiabatic heating of the test cell at the outer radial surface [18]. This method has been described in detail in a recent paper [18]. A T-type thermocouple is first attached to the outer surface of the cell at mid-height (r=R,z=H/2). A thermal epoxy is used for improving thermal contact between the cylinder surface and the thermocouple bead. A flexible Kapton heater is then wrapped around the test cell to provide radial heatingThe entire test cell is then insulated using fiberglass insulation tape, and placed in a vacuum ambient (-75 kPa (gage)) to minimize unaccounted heat loss from the test cell. The cell is suspended on thin paper arms to minimize thermal conduction loss through surface area contact. It has been shown [18] that in this case, the temperature distribution at the outer surface is given by

$$\theta(R,t) = \frac{2Q''}{\rho C_p R}t + \frac{Q''R}{4k_r} - \frac{2Q''R}{k_r}\sum_{n=1}^{\infty}\frac{1}{(\lambda_n R)^2}\exp\left(-\frac{k_r\lambda_n^{\,2}}{\rho C_p}t\right) \tag{27}$$

Where Q'' is the applied heat flux, and eigenvalues λ_n are obtained from roots of the equation $J'_0(\lambda_n R)=0$. J_0 denotes Bessel function of the first kind of order 0. As a result, the radial thermal conductivity k_r may be determined by comparing the intercept of temperature measured by the thermocouple as a function of time, with the second term in equation (27). For this experiment, electric current is provided by a Keithley 2612A power supply, potential difference is measured by a Keithley 2100 digital multimeter, and thermocouple measurements are carried out through NI-9213 thermocouple module and LabView data acquisition software. Note that this experiment is separate from the main, core temperature measurement experiment, and is carried out only for radial thermal conductivity measurement.

3.3. Experimental Setup for Temperature Measurement

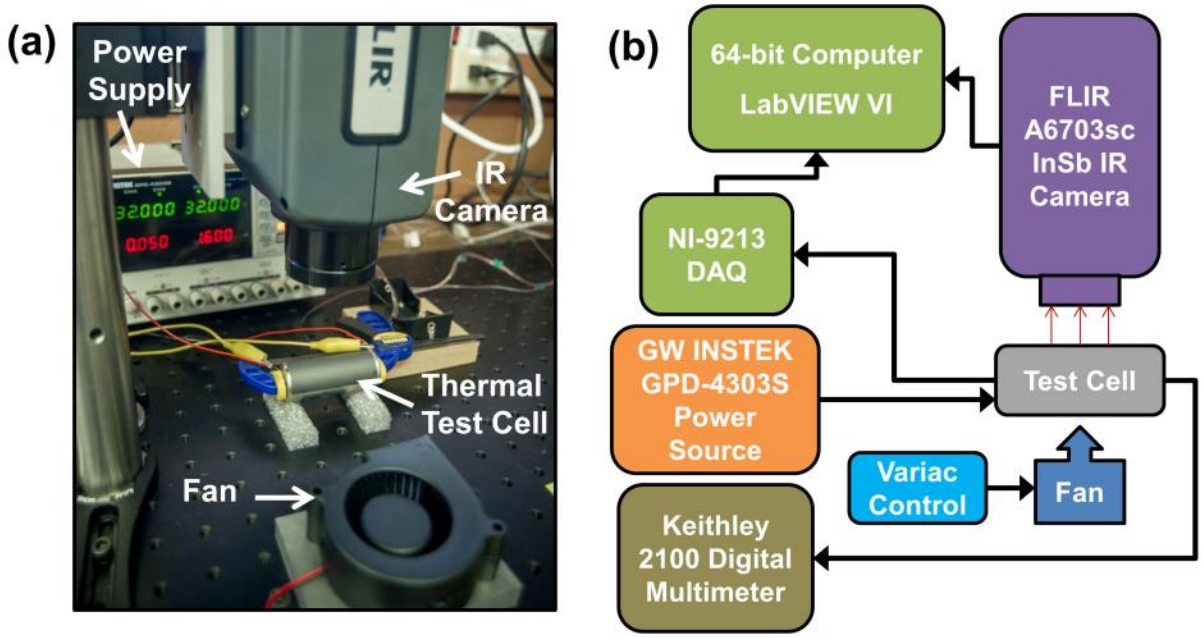

3. Figure 3: (a) Picture and (b) Schematic of the experimental test set up for remote, non-invasive core temperature measurement in steady state.

Figure 3(a) shows a picture of the experimental setup for core temperature measurement. Figure 3(b) shows a block diagram representing the data acquisition process and various

instruments used in the experiment. A FLIR A6703sc InSb infrared camera is mounted above an optical breadboard. The thermal test cell is placed directly under the camera, and is mounted on two thin, foam risers to minimize thermal conduction from the cell to the breadboard. In order to improve the accuracy of infrared temperature measurement, the outer surface of the thermal test cell is coated with a thin graphite film using a DGF-123 graphite aerosol spray. The resistive metal foil in the thermal test cell is connected to a GW INSTEK GPD-4303S power supply for supplying the heating current. Two additional probe wires monitor the potential difference across the test cell using a Keithley 2100 digital multimeter in order to monitor the heat generation rate. A small computer fan, Fugetek HT-07530D12, is placed approximately 10 cm away from the test cell at the same height as the cell axis, so that air from the fan directly impinges upon the outer surface of the test cell. The fan speed can be controlled using a power controller. A vane anemometer is used to measure the air speed. Data acquisition from the IR camera is carried out through an ethernet cord using ResearchIR software. LabView software is used for data acquisition from the thermocouple through a NI-9213 thermocouple module.

3.4. IR Camera Calibration

Accuracy of infrared-based temperature measurement depends critically on the quality of calibration carried out. In these experiments, the infrared camera is calibrated on an Instec HCS662V thermal stage, which can be set to any desired temperature between -190 °C and 600 °C. In this case, the temperature range of interest is room temperature to 80 °C. The thermal stage is placed on the optical breadboard, directly under the infrared camera, as shown in the inset of Figure 4. Since infrared temperature measurement requires a highly emissive surface, two regions of the metal surface of Instec stage are covered with materials of high emissivity – a black tape and graphite film. The Instec stage is set to a number of temperatures between room

temperature and 80 °C. At each set point, the stage temperature is allowed to reach steady state, and measured through the infrared camera. These measurements are carried without and with specifying emissivity and distance between sample and camera to investigate the effect of these calibration parameters on temperature measurement accuracy.

3.5. Experiments

Once the experiment is set up as described in section 3.3, temperature measurements are carried out on the thermal test cell in a number of conditions. For each case, a heating current is passed for Joule heating. Infrared surface temperature data are taken until the temperature distribution reaches steady state, which is also confirmed through measurement of the core temperature from the embedded thermocouple. The resistance of the test cell is measured in advance using a small test current that minimizes self-heating, and it is confirmed that the resistance does not increase appreciably due to temperature rise during the experiments.

For accurate extraction of surface temperature measurement, a region of interest is built into the measured temperature field from the infrared camera, and temperature across the outer surface at mid-height is extracted. In order to verify that the curved nature of the cylinder surface does not affect temperature measurement accuracy, experiments are carried out to measure temperature around the cylinder in isothermal conditions. A uniform temperature is measured around the cylinder, indicating that cylinder curvature does not affect IR measurement accuracy. Due to the curved surface of the cylinder, the x coordinate across the cylinder's projected view as seen by the infrared camera is converted to the circumferential angle θ. . The axial dependence of temperature is also measured and examined to determine whether there is significant axial thermal conduction, which indicates whether the infinite or finite cylinder model is appropriate

for data analysis.

Three sets of experiments are carried out. First, the steady-state surface temperature distribution on the test cell is measured at a number of heating powers while the cell is cooled in natural convection conditions. Subsequently, these experiments are repeated in the presence of forced convection cooling from the fan operating at a speed of around 3.0 m/s. Finally, a set of experiments is carried out at constant heating power, but with different fan speeds. In these experiments, the heating powers based on Joule heating in the metal foil are chosen in order to match the heating powers expected in Li-ion cells operating at high discharge rates [17]. In each experiment involving air flow from the fan, the flow field is allowed to stabilize for around ten minutes before the heating current is switched on. Sufficient cooling down time is provided between successive experiments to ensure that the cell reaches room temperature before the next experiment. In each experiment, the core temperature of the cell is determined using the theoretical model presented in section 2.1 and the experimentally measured surface temperature distribution. These core temperature measurements are compared against measurements from the embedded thermocouple to validate the measurement method.

4. Results and Discussion

4.1. Calibration of the IR Camera

An HCS622V Instec thermal stage is used for IR camera calibration. Temperature of the stage is measured by the IR camera at a number of set temperatures. Figure 4 summarizes results from this experiment by plotting the measured temperature as a function of set temperature. The ideal 45° line is shown, along which the measurement agrees exactly with the set temperature.

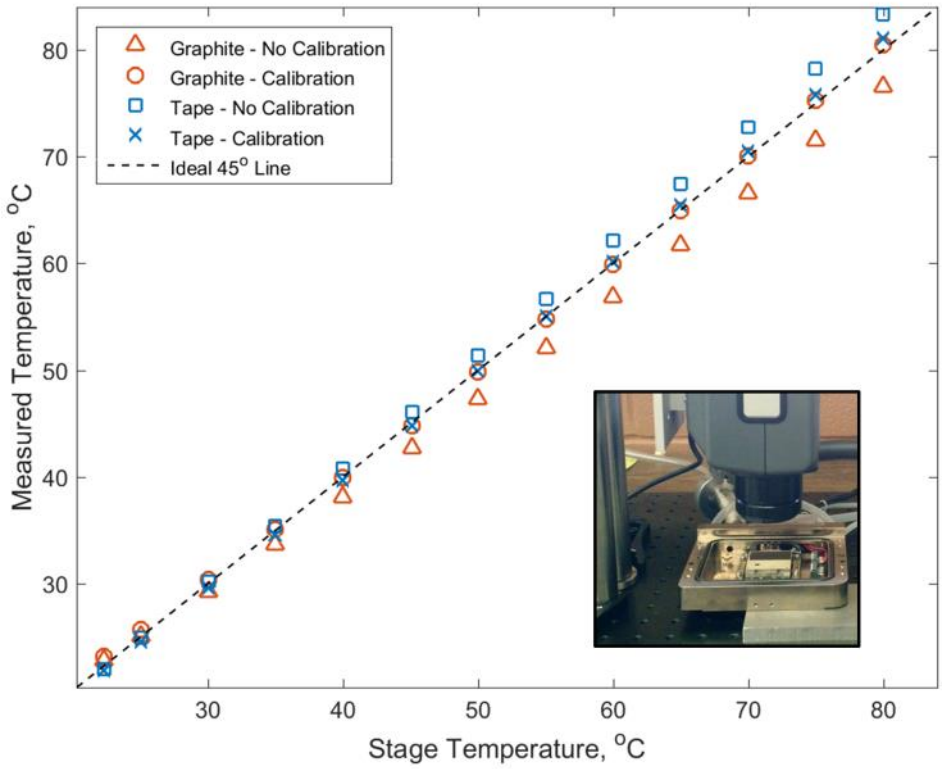

4. Figure 4: Plot of temperature measured by IR camera as a function of set stage temperature for four different surface and calibration conditions. Inset shows a picture of experimental setup.

Four calibration conditions are investigated. The stage temperature is measured with a black tape affixed on the stage, or with a thin film of graphite applied uniformly with a spray in order to improve surface emissivity. In each case, measurements are taken without and with specifying emissivity of the tape or spray, as well as the distance between the sample and camera. Figure 4 shows that there is some deviation between set and measured temperatures when emissivity and distance are not specified, for both black tape and graphite film. When these parameters are specified, the IR camera is able to measure surface temperature very accurately, as seen in Figure 4 where data for these cases are very close to the ideal 45° line. The peak deviation between the stage temperature and IR-based temperature using graphite film is 0.92 °C. While both black tape and graphite film work equally well, only graphite film is used in subsequent experiments, since it is less invasive in terms of affecting the surface properties of the sample, such as

roughness, topography and insulation. It is also found that measurement accuracy is a weak function of specified distance between camera and sample, whereas when surface emissivity is not specified, the IR camera uses a default value, resulting in significant measurement error.

4.2. Measurement of Thermal Conductivity of the Test Cell

Supplementary Figure 1 plots the temperature rise measured by a thermocouple affixed on the outer surface of the thermal test cell during radial thermal conductivity measurements described in section 3.2. Experimental data agree well with the theoretical model, and the measured temperature profile increasing linearly with time after the initial transient period as expected. The intercept of this line is used to determine the radial thermal conductivity of the test cell, resulting in a value of k_r=0.25 W/m-K, which is close to the radial thermal conductivity of a 26650 Li-ion cell [18]. This value lies between the thermal conductivities of constituent materials, with PDMS and Kapton tape having very low, and the metal foil having very high thermal conductivity. Since the overall thermal conductivity of the test cell is based on a series combination of thermal resistances of constituent materials, the measured value of thermal conductivity of the test cell is along expected lines.

4.3. Temperature Measurement in Natural Convection Conditions

Once the IR camera is calibrated, and radial thermal conductivity of the thermal test cell is measured, experiments are carried out to non-invasively determine the core temperature of the thermal test cell through measurements of the outside temperature distribution using the IR camera. These experiments are carried out at different heat generation rates within the test cell, controlled by the amount of electric current passing through, and at different convective cooling conditions, controlled by the speed of the cooling fan which impinges air cross-flow on the

cylinder. In each experiment, the core temperature determined from the theoretical model for an infinite cylinder in section 2 is compared with measurement from the thermocouple embedded in the core of the cell. Data presented later confirm that this is an appropriate model to use.

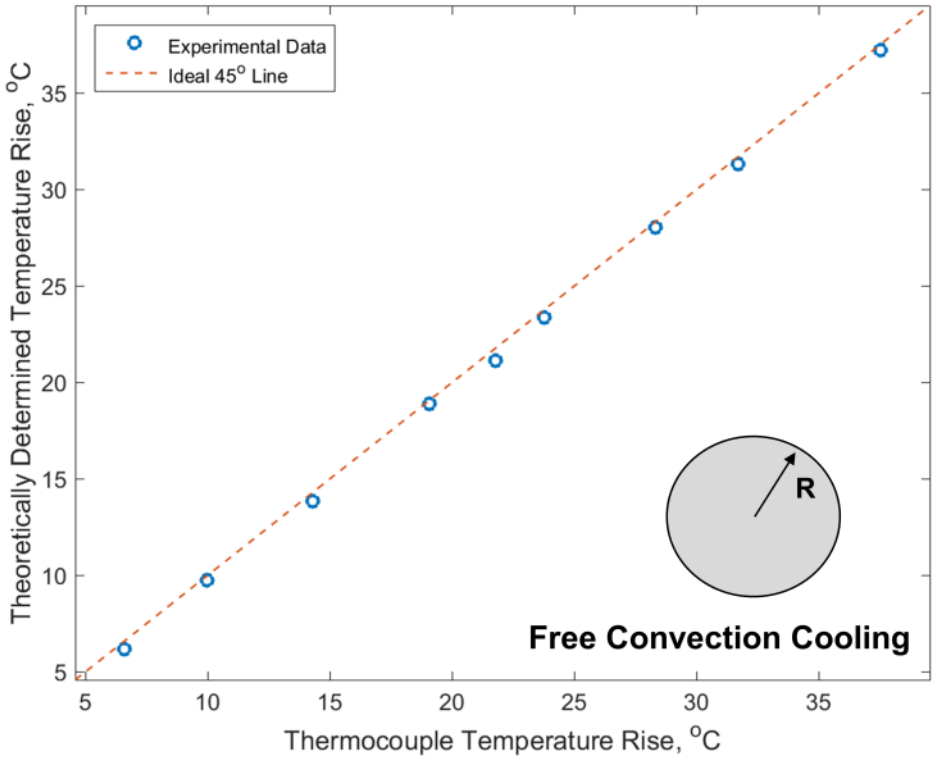

5. Figure 5: Comparison of core temperature determined from infinite cylinder theoretical model and core temperature measured using thermocouple embedded in thermal test cell. Data are taken for a number of heating powers, ranging from 0.31 W to 2.2 W, with free convection cooling conditions. Broken line shows the ideal 45° line.

In the first set of experiments, the cooling fan is not on, so that there is no cross flow, and the test cell cools down through free convection. Figure 5 plots the experimentally measured core temperature, determined using the infinite cylinder model in section 2.2, against the thermocouple temperature measurement for a number of heating powers. The ideal 45° line, along which the two are equal, is also shown. Figure 5 shows that in each case, the core temperature determined from the theoretical model using measurement of the outside temperature distribution is in close agreement with thermocouple measurements. The maximum

error in these measurements is 0.63 °C, which is well within the measurement errors associated with the IR camera and T-type thermocouple. These data demonstrate the capability of the theoretical model to determine the core temperature in a contactless, non-invasive fashion.

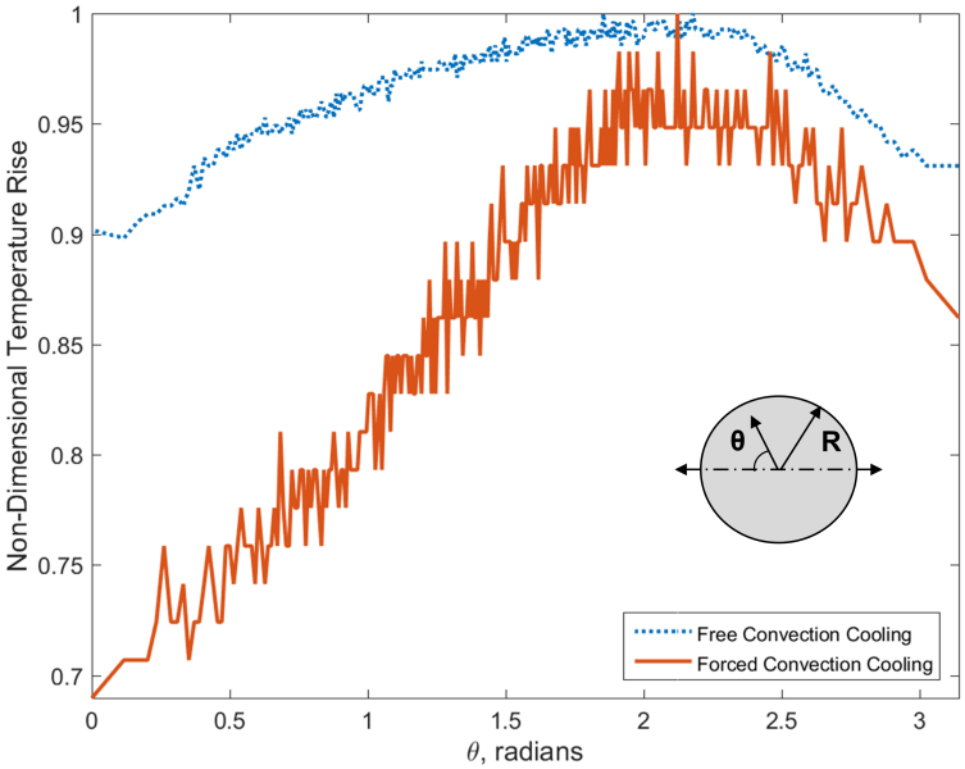

6. Figure 6: Circumferential variation in measured temperature on the outside of the cell in free and forced convection conditions. Data are non-dimensionalized based on peak temperature for each condition.

The circumferential distribution of measured temperature on the outside surface of the test cell for 2.2W heating power is shown in Figure 6, which also plots this distribution for a case of forced convective cooling at the same power. Note that for better visualization, data in this plot are non-dimensionalized based on peak temperature measurement for each cooling condition. It is seen that there is some circumferential variation in the outside temperature measurement for the first set of experiments, but the variation is much greater in the forced convective case. This is along expected lines, as the imposition of a crossflow produces circumferential variation in local convective heat transfer [35], resulting in a circumferentially

varying temperature distribution in the cylinder [33]. In addition, there is greater measurement noise in the forced convection case due to imposition of crossflow over the test cell.

4.4. Temperature Measurement in Forced Convection Conditions

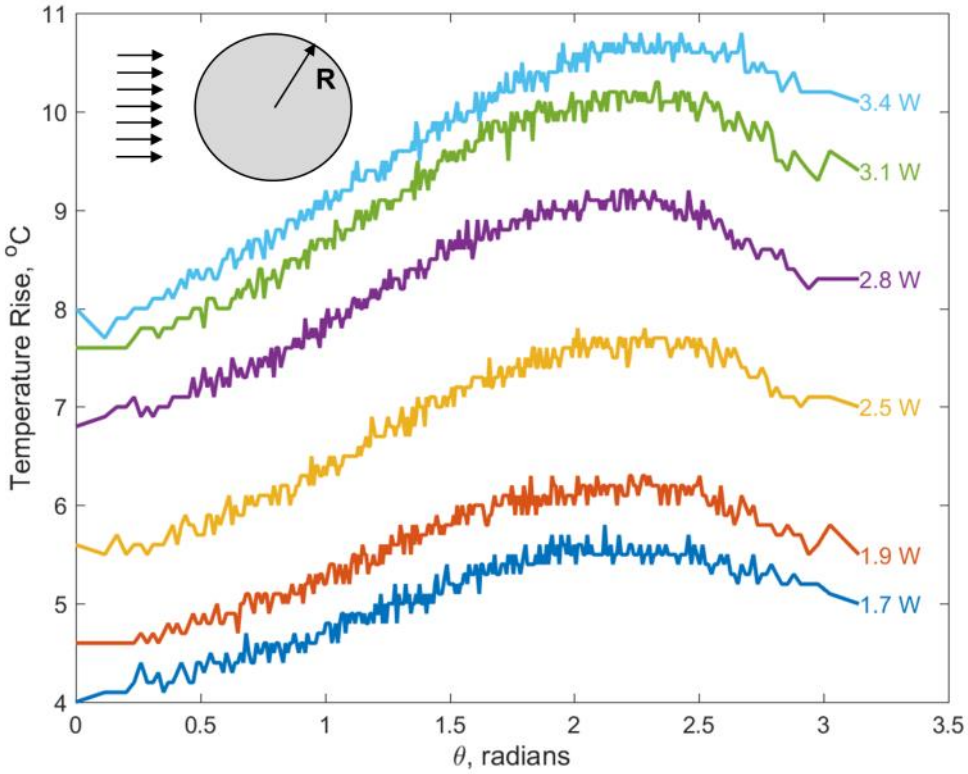

7. Figure 7: Circumferential variation in measured temperature on the outer surface of the cell in forced convection conditions for a number of heating powers.

Experiments described in Section 4.3 are repeated in the presence of cross-flow of air from a fan located around 10 cm from the test cell. Figure 7 plots the circumferential variation in the measured outside temperature for a number of heating powers at fixed fan speed. Temperature curves shift upwards with increasing power, as expected, while the nature of the circumferential variation remains the same. In each case, the measured temperature distribution is integrated to determine the core temperature, as shown in section 2.1. Figure 8 plots these core temperatures against measurements from the embedded thermocouple for each heating power. Figure 8 shows very good agreement between measurements based on the theoretical model and

thermocouple measurements, with a peak deviation of 0.89 °C, well within instrument measurement errors.

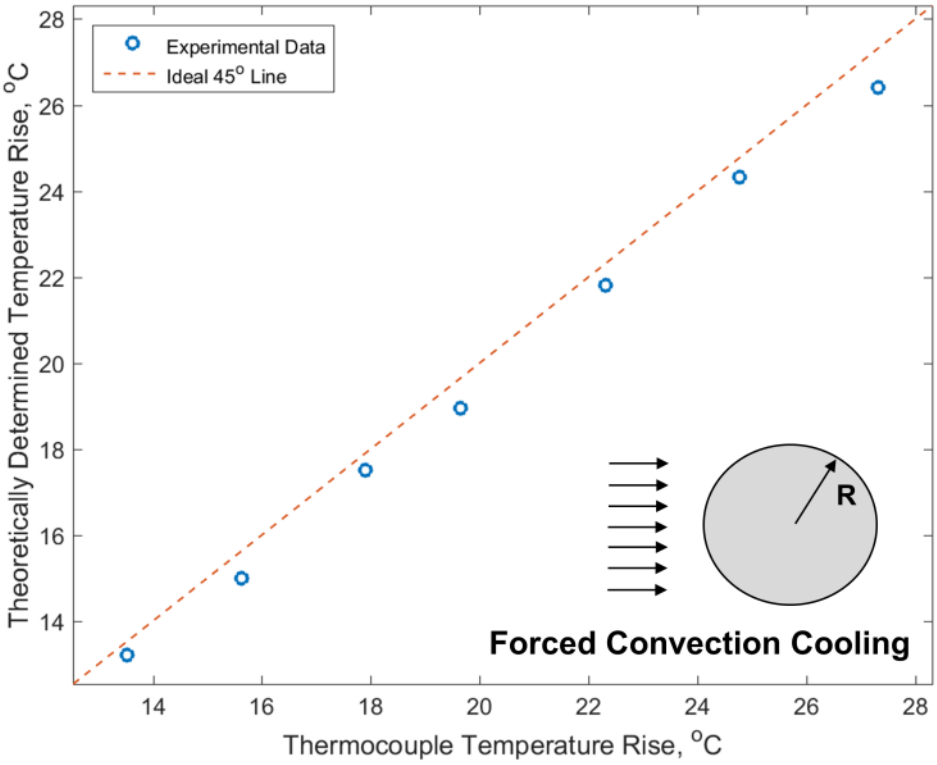

8. Figure 8: Comparison of core temperature determined from infinite cylinder theoretical model and core temperature measured using thermocouple embedded in thermal test cell. Data are taken for a number of heating powers, ranging from 1.68 W to 3.43 W, with forced convection cooling conditions. Broken line shows the ideal 45° line.

Figure 9 plots the measured core temperature rise as a function of heating power, for both free convection and forced convection cooling conditions described above. In both cases, experimental data lie close to linear fits shown in Figure 9 with R^2 values of 0.9943 and 0.9970 respectively, which is expected since temperature rise is a linear function of heating power in the experimental conditions encountered here. The slope of experimental data is lower for the forced convection case, which is also expected, since the presence of cross flow reduces overall thermal resistance, leading to lower temperature rise for a specific power, and lower slope for the relationship between the two.

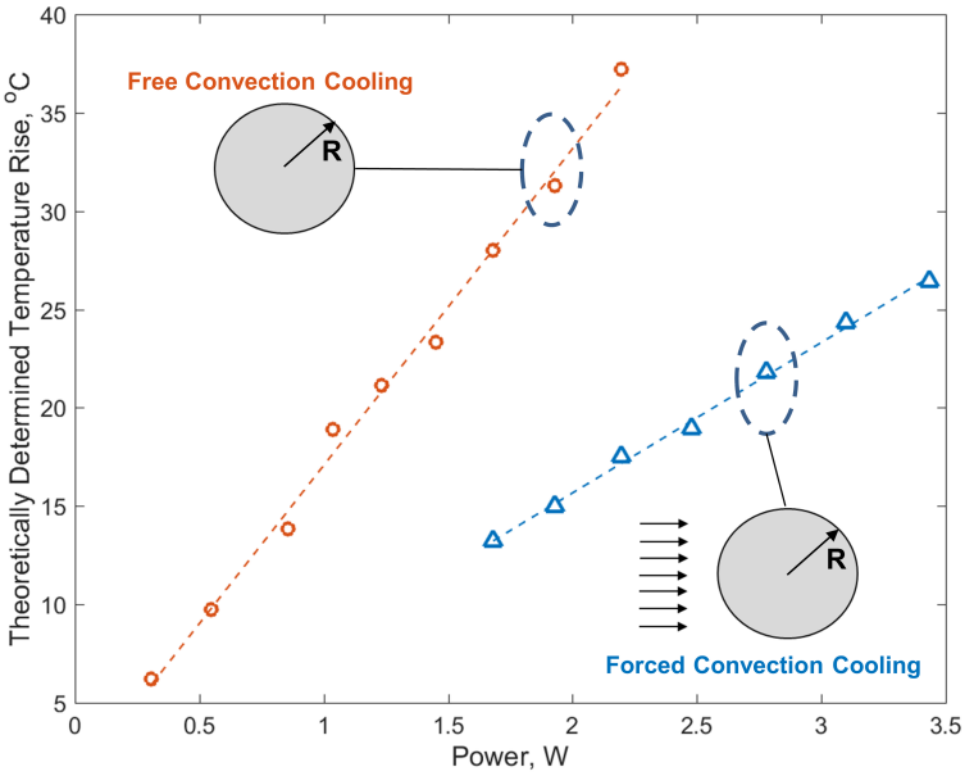

9. Figure 9: Plot of measured core temperature as a function of heating power for both free and forced convection cooling conditions. A linear fit is also shown for each data set.

Finally, a set of experiments are carried at fixed power of 2.2 W, but with a number of air flow speeds. The circumferential variation of temperature rise around the outer surface of the cylinder is presented in Figure 10, which shows, as expected, that the temperature rise reduces as fan speed increases. The nature of the circumferential variation, however, remains the same in each case. Figure 11 summarizes the core temperature determined through the theoretical model against thermocouple measurements. Similar to previous data, there is very good agreement between the two, with a maximum error of 0.77 °C, showing the capability of the theoretical model to determine the core temperature of the test cell in a non-invasive fashion by utilizing the temperature distribution measured on the outside of the cell.

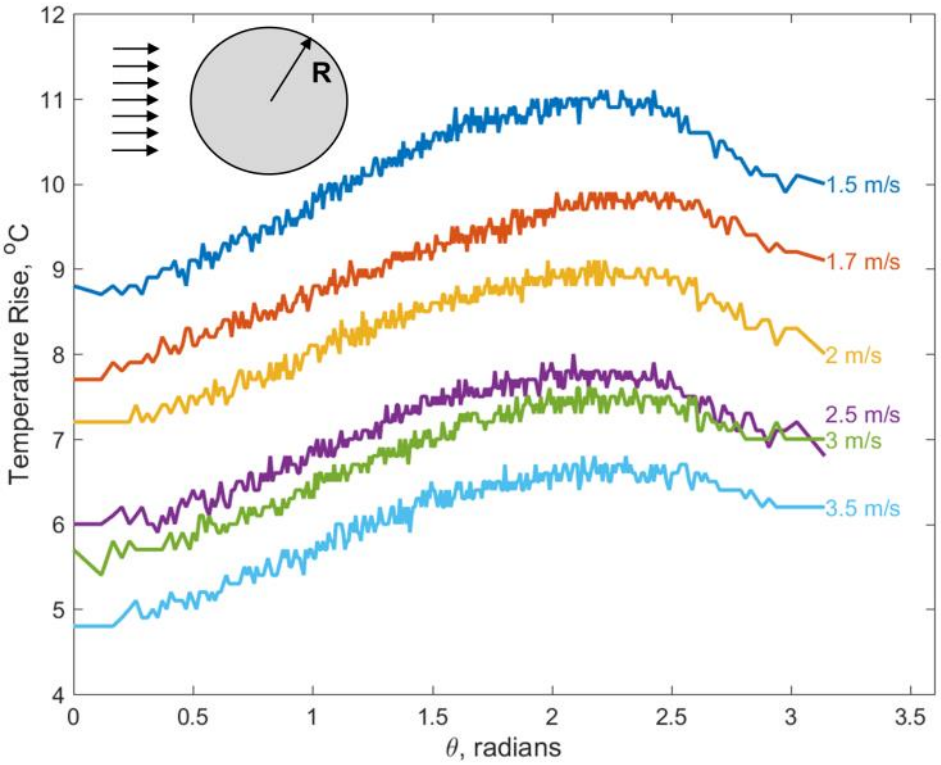

10. Figure 10: Circumferential variation in temperature in forced convection cooling condition for a number of air flow speeds.

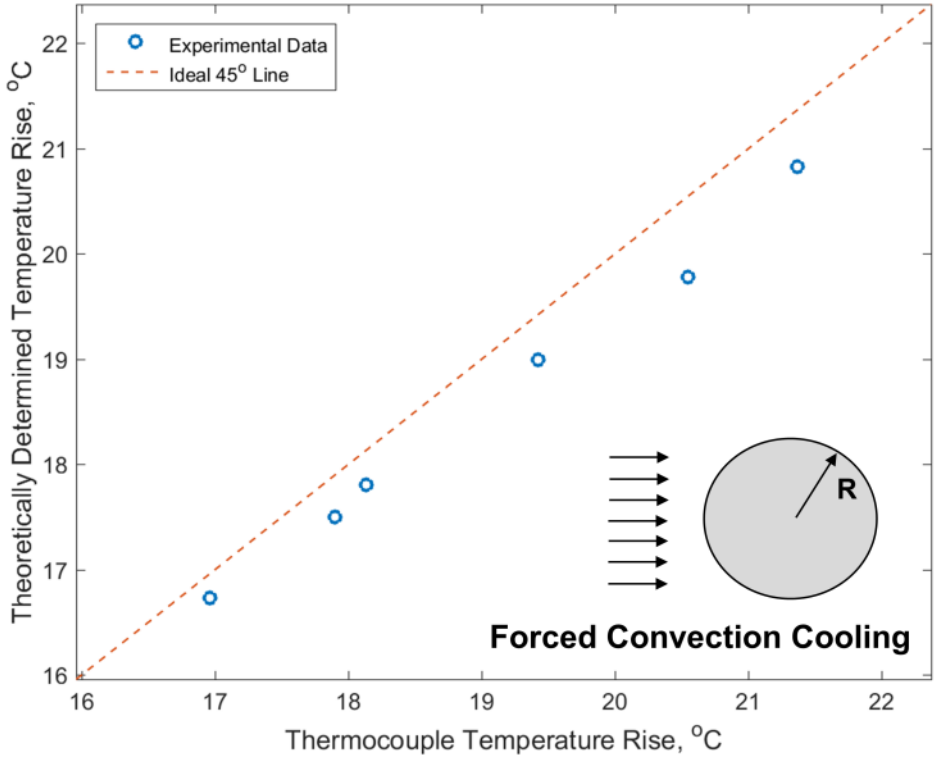

11. Figure 11: Comparison of core temperature determined from theoretical model with thermocouple measurements of forced convection cooling at a number of air flow speeds ranging from 1.5 to 3.5 m/s.

4.5. Comparison of Finite and Infinite Cylinder Models

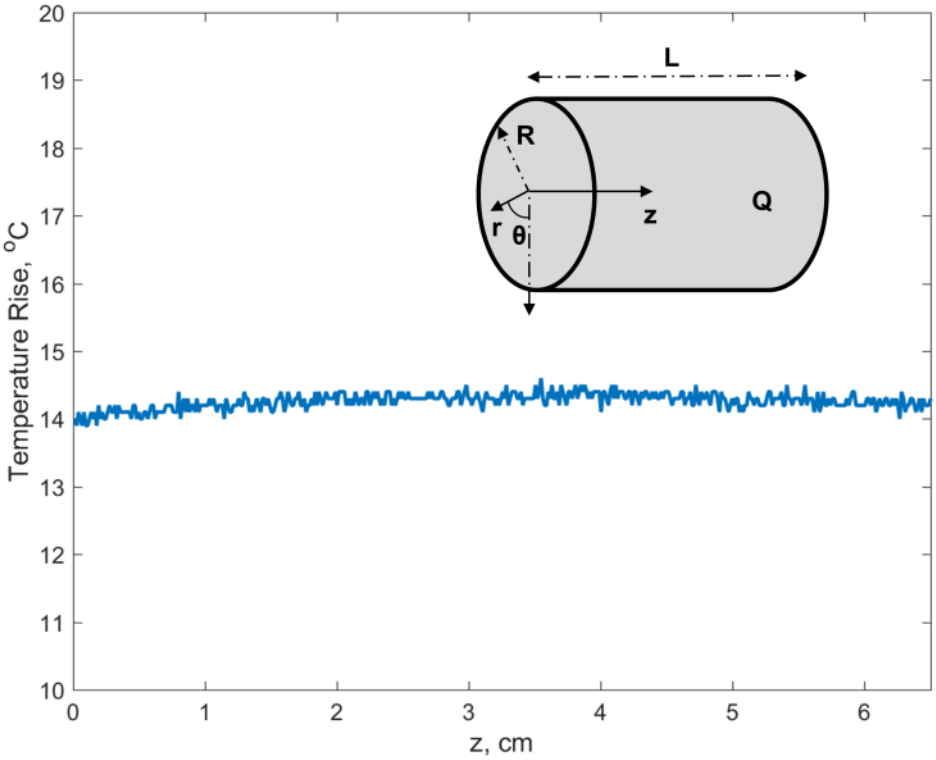

12. Figure 12: Measured outside surface temperature as a function of z for free convection cooling conditions at 1.04 W power.

Experimental data analysis discussed so far uses the infinite cylinder model, which is applicable when there are negligible temperature gradients in the axial direction. Figure 12 plots the measured outside temperature as a function of *z* along the outside surface of the cell with 1.04 W heat generation and free convective cooling. This figure shows negligible axial variation in the outer temperature, which justifies the use of the infinite cylinder model for analyzing experimental data. In order to further examine the regime in which the finite cylinder model may be used, data analysis is carried out using the finite cylinder model on experimental data of the entire outer surface temperature measurement. Figure 13 plots the predicted core temperature from the finite cylinder model for a number of values of the convective heat transfer coefficients on the ends of the cylinder. Figure 13 shows that as the convective heat transfer coefficient

becomes smaller and smaller, the core temperature prediction from the finite cylinder model approaches the thermocouple-measured core temperature, as well as the infinite cylinder model prediction. This is along expected lines, since the two ends of the test cell are insulated during experiments, and hence a small value of the convective heat transfer coefficient is expected. Further, theoretically, a small convective heat transfer at the ends, together with uniform heat generation suppresses axial thermal conduction, and makes thermal conduction in the cylinder almost exclusively radial in nature, thereby obviating the need for using the finite cylinder model.

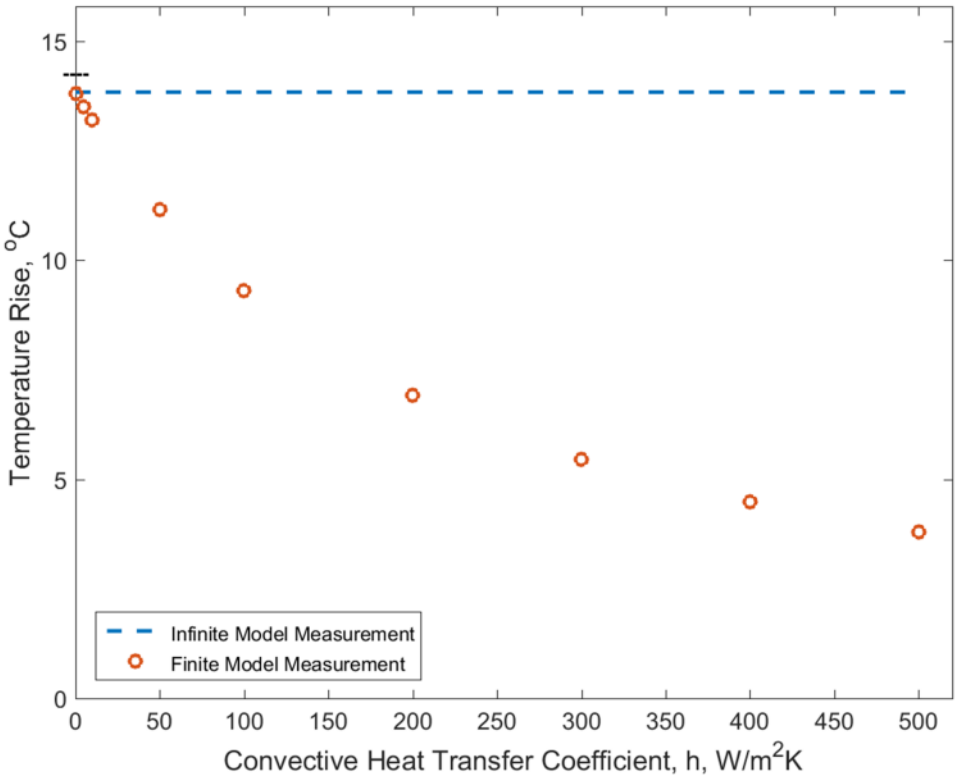

13. Figure 13: Comparison of core temperature predicted by the finite cylinder model for different values of the convective heat transfer coefficient with infinite cylinder model for 1.04 W heat generation and free convective cooling case. Corresponding thermocouple measurement of the core temperature is indicated on the y-axis.

In making the choice for whether the infinite or finite cylinder model is to be used for data analysis, it is recommended to examine the axial variation in the measured temperature

distribution on the outside surface. If the variation is negligible, as is the case in these measurements, the infinite cylinder model would be sufficient.

4.6. Uncertainty Analysis

This sub-section analyzes experimental uncertainty in the two key measurements reported here – measurement of the core temperature through the embedded thermocouple, and through the measurement method discussed here. Uncertainty in the thermocouple measurement is 1 °C, based on manufacturer specifications. Uncertainty in the surface temperature based measurement method arises from three key parameters as shown in equation (16) – uncertainty in heat generation measurement, in thermal conductivity measurement, and in infrared-based outside temperature measurement. Since heat generation is determined using electrical measurements, the uncertainty is expected to be very low due to the high measurement accuracy of Keithley 2612A and Keithley 2100 instruments. As discussed in a recent paper [18], uncertainty in thermal conductivity measurement is estimated to be ±5%. Finally, uncertainty in infrared-based outside temperature measurement is expected to be 0.92 °C, based on infrared calibration described in section 4.1 and Figure 4. As a result, based on error propagation in equation (16), the overall uncertainty in the core temperature measurement from the method described in this paper is estimated to be ±10%, arising mostly due to uncertainty in thermal conductivity measurement and infrared-based temperature measurements. The agreement between the method described in this paper, and embedded thermocouple measurement is within the experimental measurement uncertainty.

5. Conclusions

Non-invasive measurement of temperature inside solid bodies is of significant importance for a wide variety of engineering applications where the body temperature governs performance and reliability. The theoretical model and experimental data presented in the paper establish a novel technique for measuring the inside core temperature of a solid body in steady state using measurements of the outside temperature distribution on the outside of the body. While the results discussed here apply to steady state, an extension to core temperature measurement in transient conditions may be an important future work. The method discussed here can be easily extended to solids of other shapes as long as the thermal conduction problem within the solid could be solved to derive a relationship between the core and outside temperatures, similar to the theoretical treatment described in this paper. These results validate a novel metrology method for temperature measurement inside solid bodies, which may contribute towards thermal design and optimization of a wide variety of engineering systems.

6. Supplementary Material

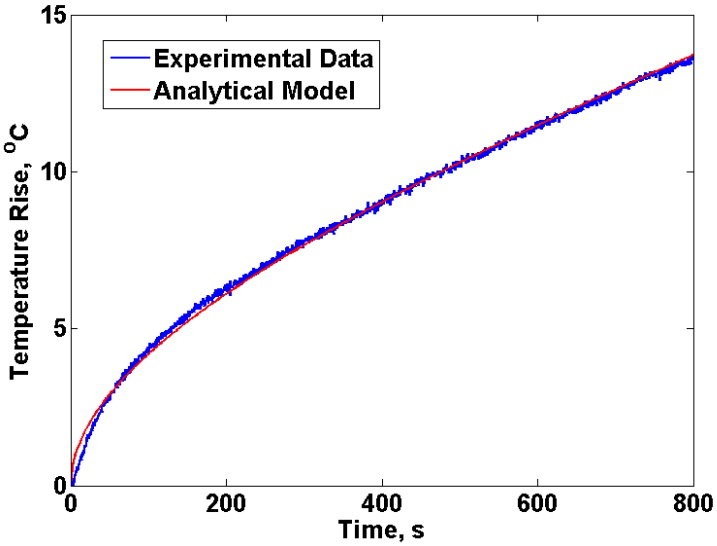

14 - **Figure S1: Comparison of experimentally measured temperature rise with analytical model (equation (27)) for measurement of radial thermal conductivity of the thermal test cell through radial, adiabatic heating.**

Acknowledgments

This material is based upon work supported by the National Science Foundation under NSF CAREER Grant No. CBET-1554183. Financial support from Office of Naval Research through DURIP Award # N00014-14-1-0752 for acquisition of infrared camera is also gratefully acknowledged.

References

[1] J. Goodenough, K.-S. Park, The Li-ion rechargeable battery: a perspective, *J. Am. Chem. Soc.*, **135**, 2013, pp. 1167–1176.

[2] B. Scrosati, J. Garche, Lithium batteries: Status, prospects and future, *J. Power Sources*, **9**, 2010, pp. 2419-2430.

[3] K. Shah, S.J. Drake, D.A. Wetz, J. K. Ostanek, S.P. Miller, J.M. Heinzel, A. Jain, Modeling of steady-state convective cooling of cylindrical Li-ion cells, *J. Power Sources*, **258**, 2014, pp. 374-381.

[4] K. Shah, S.J. Drake, D.A. Wetz, J.K. Ostanek, S.P. Miller, J.M. Heinzel, A. Jain, An experimentally validated transient thermal model for cylindrical Li-ion cells, *J. Power Sources*, **271**, 2014, pp. 262-268.

[5] D. Lisbona, T. Snee, A review of hazards associated with primary Lithium and Lithium-ion batteries, *Process Safety & Env. Protection*, **89**, 2011, pp. 434-442.

[6] L. Michalski, K. Eckersdorf, J. Kucharski, J. McGhee, Temperature Measurement, 2nd Edition, *Wiley*, 2001, ISBN: 978-0-471-86779-1.

[7] D.T. McGee, Principles and Methods of Temperature Measurement, *John Wiley & Sons*, 1988, ISBN: 0-471-62767-4.

[8] P.R.N. Childs., J.R. Greenwood, C.A. Long, Review of temperature measurement, *Rev. Scientific Instruments*, **71** (8), 2000, pp. 2959-2978.

[9] P.E. Raad, P.L. Komarov, M.A. Bettiati, Thermoreflectance temperature measurements for optically emitting devices, *Microelectronics J.*, **45**, 2014, pp. 515-520.

[10] J.J.L. Franco, E. Boemo, E. Castillo, L. Parrilla, Ring oscillators as thermal sensors in FPGAs: Experiments in low voltage, In: Proc. VI Southern Programmable Logic Conf., 2010, pp. 133-137.

[11] T.E. Cooper, R.J. Field, J.F. Meyer, Liquid crystal thermography and its application to study of convective heat transfer, *ASME J. Heat Transfer*, **97**(3), 1975, pp. 442-450.

[12] D.P. DeWiit, G.D. Nutter, Theory and Practice of Radiation Thermometry, 1st Edition, *John Wiley & Sons*, 1988, ISBN: 0-471-61018-6.

[13] Thermophysical Properties of Materials For Nuclear Engineering: A Tutorial and Collection of Data, International Atomic Energy Agency (IAEA), 2008. Available at http://www-pub.iaea.org/MTCD/publications/PDF/IAEA-THPH_web.pdf, accessed Feb 26, 2016.

[14] H. Yapici, O. Ipek, V. Ozceyhan, Temperature distribution in nuclear fuel rod and variation of the neutronic performance parameters in (D-T) driven hybrid reactor system, *Annals of Nuclear Energy*, **28**, 2001, pp. 1825-1850.

[15] C.R. Regis, R.M. Cotta, J. Su, Improved lumped analysis of transient heat conduction in a nuclear fuel rod, *Int. Comm. Heat Mass Transfer*, **27**(3), 2000, pp. 357-366.

[16] D. Linden, T.B. Reddy, 'Handbook of Batteries,' 3rd Ed., McGraw-Hill, New York, 2002.

[17] S.J. Drake, M. Martin, D.A. Wetz, J.K. Ostanek, S.P. Miller, J.M. Heinzel, A. Jain, Heat generation rate measurement in a Li-ion cell at large C-rates through temperature and heat flux measurements, *J. Power Sources*, **285**, 2015, pp. 266-273. [18] S.J. Drake, D.A. Wetz, J.K. Ostanek, S.P. Miller, J.M. Heinzel, A. Jain, Measurement of anisotropic thermophysical properties of cylindrical Li-ion cells, *J. Power Sources*, **252**, 2014, pp. 298-304.

[19] V. Vishwakarma, C. Waghela, Z. Wei, R. Prasher, S.C. Nagpure, J. Li, F. Liu, C. Daniel, A. Jain, Heat transfer enhancement in a Lithium-ion cell through improved material-level thermal transport, *J. Power Sources*, **300**, 2015, pp. 123-131.

[20] C. Forgez, D.V. Do, G. Friedrich, M. Morcotte, C. Delacourt, Thermal modeling of a cylindrical $LiFePO_4$/graphite lithium-ion battery, *J. Power Sources*, **195**, 2010, pp. 2961-2968.

[21] A. Abdul-Aziz, D.J. Roth, R. Cotton, G.F. Studor, E. Christiansen, P.C. Young, Material Characterization and Geometric Segmentation of a Composite Structure Using Microfocus X-Ray Computed Tomography Image-Based Finite Element Modeling, *Journal of Materials Evaluation*, **71**(2), 2013, pp. 167-175.

[22] S. R. Stock, X-Ray Computed Tomography, Characterization of Materials, *John Wiley & Sons, Inc.*, 2012, pp. 1–18. DOI: 10.1002/0471266965.com131

[23] R. Zoughi, Microwave non-destructive testing and evaluation, 1st Edition, *Kluwer Academic Publishers*, 2000, ISBN: 978-90-481-4015-2.

[24] T. Kundu, Ultrasonic nondestructive evaluation: engineering and biological material characterization, *CRC Press*, 2004. ISBN: 13-978-0-203-50196-2.

[25] P.J. Withers, H.K.D.H. Bhadeshia, Residual stress. Part 1 – Measurement techniques, *Materials Sci. & Technol.*, **17**(4), pp. 355-365.

[26] M. Takahashi, I. Ihara., Ultrasonic determination of temperature distribution in thick plates during single sided heating, *Mod. Phys. Lett. B* **22** (11), 2008, 971.

[27] I. Ihara, T. Tomomatsu, In-situ measurement of internal temperature distribution of sintered materials using ultrasonic technique, *Materials Science and Engineering*, **18**, 2011.

[28] H.N.G. Wadley, S.J. Norton, F. Mauer, B. Droney, Ultrasonic measurement of internal temperature distribution, *Phil. Trans. R. Soc. Lond. A*, **320**, 1986, pp. 341-361.

[29] S.J. Norton, L.R. Testardi, H.N.G. Wadley, Reconstructing internal temperature distributions from ultrasonic time-of-flight tomography and dimensional resonance measurements, *Ultrasonics Symposium*, 1983, pp. 850–855.

[30] R.R. Richardson, P.T. Ireland, D.A. Howey, Battery internal temperature estimation by combined impedance and surface temperature measurement, *Journal Power Sources*, **265**, 2014, pp. 254-261.

[31] J.B. Robinson, J.A. Darr, D.S. Eastwood, G. Hinds, P.D. Lee, P.R. Shearing, O.O. Taiwo, D.J.L. Brett, Non-uniform temperature distribution in Li-ion batteries during discharge - A combined thermal imaging, X-ray micro-tomography and electrochemical impedance approach, *Journal of Power Sources*, **252**, 2014, pp. 51-57.

[32] R. Srinivasan, B.G. Carkhuff, M.H. Butler, A.C. Baisden, Instantaneous measurement of the internal temperature in lithium-ion rechargeable cells, *Electrochimica Acta*, **56**, 2011, pp. 6198-6204.

[33] D. Sarkar, K. Shah, A. Haji-Sheikh, A. Jain, Analytical modeling of temperature distribution in an anisotropic cylinder with circumferentially-varying convective heat transfer, *Int. J. Heat and Mass Transfer*, **79**, 2014, pp. 1027-1033.

[34] M.N. Özişik, Heat conduction, 2nd Edition, *John Wiley & Sons, Inc.*, 1980, ISBN: 0-471-05481-X.

[35] W.M. Kays, M.E. Crawford Convective Heat and Mass Transfer, McGraw-Hill, New York, 1993.

CHAPTER 3:

NON-INVASIVE, TRANSIENT DETERMINATION OF THE CORE TEMPERATURE OF A HEAT-GENERATING SOLID BODY

Dean Anthony, Daipayan Sarkar, Ankur Jain*

Mechanical and Aerospace Engineering Department
University of Texas at Arlington, Arlington, TX, USA.

* – Corresponding Author: email: jaina@uta.edu;
500 W First St, Rm 211, Arlington, TX, USA 76019
Ph: +1 (817) 272-9338; Fax: +1 (817) 272 2952

D. Anthony, D.Sarkar, A. Jain, Non-Invasive, transient measurement of the core temperature of a solid body. *Sci. Rep.*, **6** (35886), 2016, pp. 1-10. DOI: 10.1038/srep35886

Abstract

While temperature on the surface of a heat-generating solid body can be easily measured using a variety of methods, very few techniques exist for non-invasively measuring the temperature inside the solid body as a function of time. Measurement of internal temperature is very desirable since mere measurement of surface temperature gives no indication of temperature inside the body, and system performance and safety is governed primarily by the highest temperature, encountered usually at the core of the body. This paper presents a technique to non-invasively determine the internal temperature based on the theoretical relationship between the core temperature and surface temperature distribution on the outside of a heat-generating solid body as functions of time. Experiments using infrared thermography of the outside surface of a thermal test cell in a variety of heating and cooling conditions demonstrate good agreement of the predicted core temperature as a function of time with actual core temperature measurement using an embedded thermocouple. This paper demonstrates a capability to thermally probe inside solid bodies in a non-invasive fashion. This directly benefits the accurate performance prediction and control of a variety of engineering systems where the time-varying core temperature plays a key role.

1. Introduction

While several experimental methods exist for measurement of temperature on the surface of a solid body [1-7], there is a lack of experimental techniques available for non-invasive measurement of temperature inside the body. Development of a technique with similar capability for non-invasive internal temperature measurement will have a dramatic impact on performance, safety and reliability of engineering systems, each of which are directly affected by temperature.

Performance optimization of such systems, including Li-ion cells, is often carried out using surface temperature measurement, which may result in significant error, since surface temperature measurement gives very little indication of the core temperature, which may be much higher for heat-generating bodies.

While the core temperature may in principle be measured by inserting or embedding a temperature sensor inside the solid body [8-10], and optimizing the location of the sensor and accompanying wires [11], this approach is often too intrusive and impractical. As an example, the temperature at the core of a Li-ion cell is of much interest for performance optimization and safety [9], however, due to the presence of electrochemical materials inside the hermetically sealed cell, insertion of a temperature sensor is simply not possible on a large scale. The use of the measured surface temperature for performance optimization and design of safety features is inappropriate, since the greater temperature at the core will govern the design of thermal management to ensure safety. For example, a thermal management system for heat removal based on surface temperature measurement alone is likely to fail due to much higher temperature inside the cell. Further, the advent of a safety problem such as thermal runaway can be accurately predicted by measuring the core temperature, and not the surface temperature [12].

Further, it is also desirable that such a technique should be a direct thermal technique that does not depend on the conversion of temperature rise to another measurable physical parameter. For example, ultrasonic methods that utilize the temperature dependence of ultrasonic wave propagation in solids have been used in the past for estimating temperature profile within a solid body [13,14]. However, these methods only work on dielectric bodies, and further, may not be rapid enough to provide transient temperature distribution.

A method for determining the steady-state core temperature of a solid body was recently developed [15] based on measurement of the surface temperature distribution of the solid body in steady state. However, this technique was applicable only for determining the steady-state core temperature for a uniform heat generation, whereas the transient variation of the core temperature is often much more critical for several reasons. In many cases, the reliability and lifetime of an engineering system is governed by performance during transient operation, and not by steady state performance. Several engineering processes are inherently transient and do not reach a steady-state, thereby limiting the efficacy of a steady-state core temperature measurement method. For example, a process for aggressively discharging a 26650 Li-ion cell may complete within 6-15 minutes [9], whereas the thermal time constant for the cell is much longer [16]. In such a case, the capability of determining the transient core temperature in a non-intrusive fashion will help make real-time decisions to improve performance, safety and reliability. Finally, evolution of temperature of the body in time affects other physical parameters and processes, such as stresses, fatigue, etc. [17]. For these reasons, it is very desirable to develop a method to determine the core temperature of a heat-generating solid body as a function of time in a contactless, non-intrusive fashion.

This paper addresses this critical research need by developing a technique for non-intrusively determining the transient temperature inside a solid, heat-generating body. This method utilizes information from the outside surface temperature distribution measured as a function of time. Based on an adaptation of the general solution for thermal conduction in such a case, it is shown that there exists a relationship between the core temperature and outside surface temperature distribution as functions of time, which could be used to determine the core temperature without the need for physically accessing the core by using appropriate space and

time integrals of the transient temperature distribution on the surface of the body. Surface temperature measurement is carried out using infrared thermography on a thermal test cell capable of internal heat generation, and the core temperature is predicted as a function of time using these data. A thermocouple embedded at the core of this cell provides the actual core temperature measurement, which is used to validate the technique. Core temperature determined through this technique is found to be in close agreement with the actual temperature over the entire experimental period in a variety of heating and cooling conditions.

2. Results and Discussion

2.1. Theoretical Expression for Transient Core Temperature as a Function of Surface Temperature Distribution

Consider a heat-generating infinite cylinder of radius R with constant volumetric heat generation Q within the cylinder, shown schematically in Supplementary Figure S1. Assume the radial thermal conductivity and heat capacity of the cylinder to be k_r and C_p respectively. The surface temperature distribution around the periphery of the cylinder, $T_0(\theta,t)$ is assumed to be known through a measurement. This is a direct thermal conduction problem, variants of which have been solved in the past [18]. For example, a solution for conduction in a heat-generating, isotropic cylinder with a circumferentially uniform temperature imposed on the outer surface has been presented using the method of Green's functions [18]. In this work, a solution is derived to account for circumferential variation in the outside temperature, as well as thermal conductivity anisotropy within the cylinder, both of which are relevant to realistic engineering systems. The detailed derivation in Supplementary Information shows that the temperature at the core of the cylinder, $r=0$, is given as a function of time by

$$T_{core}(t) = T_{1,core}(t) + T_{2,core}(t) = \left[\frac{QR^2}{4k_r} + \sum_{n=1}^{\infty} A_n \exp\left(-\alpha_r \lambda_{0n}^2 \cdot t\right) \right] + \sum_{n=1}^{\infty} B_{0n}(t) \quad (1)$$

In equation (1),

$$A_n = \frac{-\frac{Q}{4k_r} \int_0^R \left(R^2 - r^2\right) \cdot r J_0(\lambda_{0n} r) dr}{N_{r,n}} \quad (2)$$

And,

$$B_{0n}(t) = \frac{\alpha_r \lambda_{0n} R J_1(\lambda_{0n} R)}{N_{r,n}} \int_0^t w_{0I}(\tau) \exp\left[-\alpha_r \lambda_{0n}{}^2 (t-\tau)\right] d\tau \quad (3)$$

Further, in equations (2)-(3), J_m refers to the Bessel function of the first kind and order *m*, and $\alpha_r = \frac{k}{\rho \cdot C_p}$ is the radial thermal diffusivity. Eigenvalues λ_{0n} are obtained from the roots of J_0, and the radial norm $N_{r,n}$ is given by

$$N_{r,n} = \frac{R^2 J_1(\lambda_{0n} R)^2}{2} \quad (4)$$

In equation (3), $w_{0I}(\tau)$ is the circumferentially averaged value of the measured surface temperature $T_0(\theta,t)$, given by

$$w_{0I}(\tau) = \frac{1}{2\pi} \int_0^{2\pi} T_0(\theta, \tau) d\theta \quad (5)$$

In case the heat generation rate within the cell changes with time, given by $Q(t)$, the relationship between the core temperature and surface temperature distribution is given by

$$T_{core}(t) = T_{1,core}(t) + T_{2,core}(t) = L^{-1}\left[\frac{\alpha_r \overline{Q}}{sk_r}\left(1 - \frac{1}{I_0\left(\sqrt{\frac{s}{\alpha_r}}R\right)}\right)\right] + \sum_{n=1}^{\infty} B_{0n}(t) \quad (6)$$

Where L^{-1} refers to the inverse Laplace transform, $\overline{Q}$ is the Laplace transform of $Q(t)$, and I_0 refers to modified Bessel function of the first kind and of order zero. Detailed derivation of equations (1)-(6) is discussed in Supplementary Information.

The solution derived here is along similar lines as one presented by Özişik [18], except that the present solution additionally accounts for circumferential variation of the outside temperature, as well as anisotropy in thermal conductivity within the cylinder. Both of these realistic effects are important to model, since from convective heat transfer theory, temperature on the cylinder surface is known to vary circumferentially, as also evidenced by experimental data described later. Further, in the case of Li-ion batteries, a strong thermal conduction anisotropy is known to exist [19].

While Özişik's solution used the Green's function approach, this paper uses Fourier series expansion and Laplace transforms for time-varying heat generation in order to be consistent with the constant heat generation case. Since heat generation rate for a Li-ion cell is usually available at discrete time steps through experimental measurements [20] or numerical simulation of electrochemistry [21], both of these approaches may need numerical integration – for evaluation of time-domain integral of $Q(t)$ in Green's function approach, and for evaluation of inverse Laplace transforms in the Laplace transform approach.

Supplementary Figure S2 compares the transient core temperature based on this theoretical model with finite-element simulations of the transient temperature field. Refineement in mesh and timestep discretization is carried out in the finite-element simulations until no further change in the solution occurs upon further refinement. The simulation uses approximately 528K elements and 100 timesteps through the entire duration. Two cases are considered with constant and time-varying outside surface temperature. In each case, there is excellent agreement between the theoretical model and finite-element simulation results, with a peak difference between the two of 0.47 °C and 0.70 °C respectively.

Equations (1)-(6) show that the core temperature at any time can be determined through an integral involving the circumferentially-integrated surface temperature distribution at all times prior to the time of interest. This relationship is the basis for a technique for determining the core temperature of a cylinder without invasively inserting a sensor within, but instead by measuring the temperature distribution on its outer surface as a function of time, which could be done using a variety of methods such as infrared thermography. Equations (1)-(6) show that in a thermally anisotropic cylinder, while the general temperature field in the cylinder is a function of the circumferential thermal conductivity $k_{\theta,}$ determining the core temperature requires information only about the radial thermal conductivity k_r and heat capacity C_p, and not k_θ.

2.2. Temperature Measurement Results

Experiments are carried out to non-invasively determine the transient evolution of core temperature of a cylindrical thermal test cell using infrared measurements of the surface temperature distribution based on the model presented in the previous sub-section. The thermal test cell comprises a tightly wound roll of resistive metal foil assembled inside a casing with a

thermocouple embedded at the core of the roll. Electric current passing through the metal foil is used to generate heat at a desired rate throughout the cell volume through Joule heating. Measurements from the embedded thermocouple provide the actual core temperature, which can be used to validate the technique to determine the core temperature using the surface temperature measurement and equations (1)-(6). A number of heat generation rates and external cooling conditions are investigated. Radial thermal conductivity k_r is obtained from a past measurement [15] on the same thermal test cell using an adiabatic heating method where the thermal response of the cell to external heating is used to determine its thermal properties [19], whereas heat capacity C_p is determined from the mass-weighted average of heat capacities of individual material components of the thermal test cell. Figures 1(a) and 1(b) show a picture and schematic of the experimental setup. Figures 2(a) and 2(b) show a picture and a schematic of the thermal

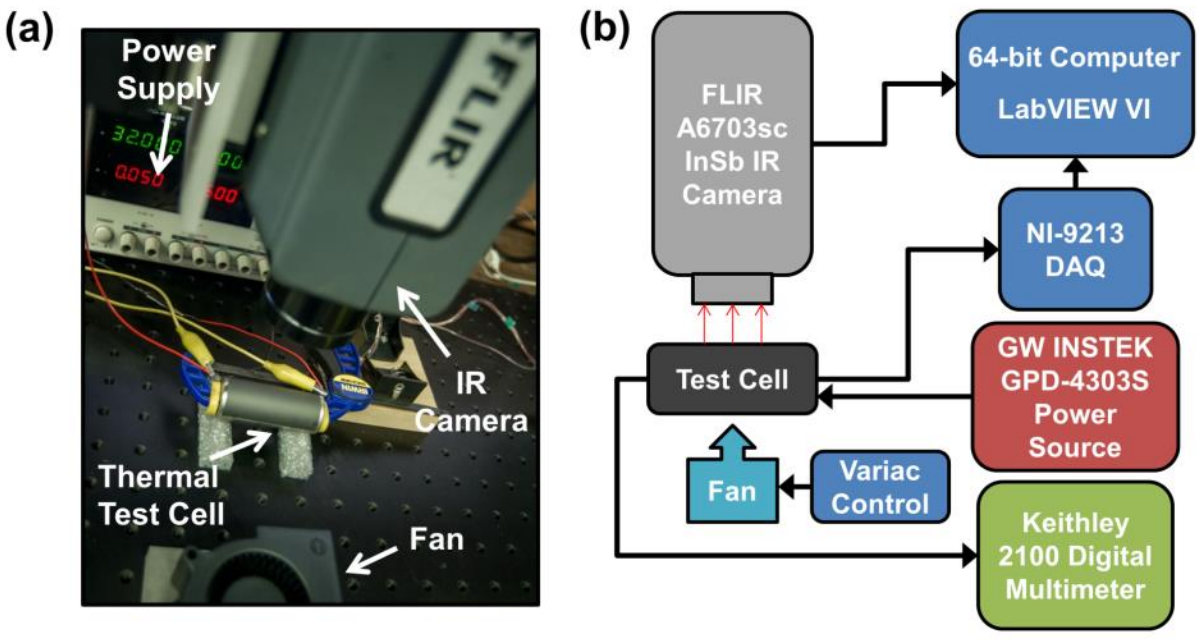

15. Figure 1: (a) Picture of the experimental setup for non-invasive transient core temperature measurement, (b) Schematic of the experimental setup and measurement method.

test cell, showing the volumetric heat generation in the metal foil, as well as the location of the embedded thermocouple.

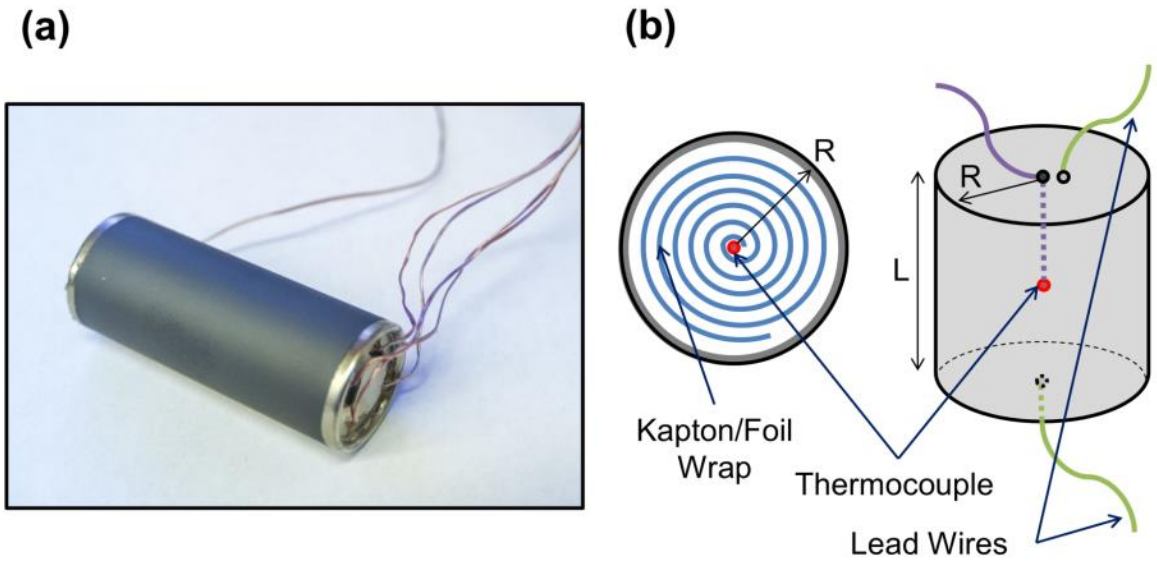

16. Figure 2: Schematic of the thermal test cell (13mm radius and 65mm height) with internal volumetric heat generation and embedded core thermocouple.

Supplementary Figure S3 plots the surface temperature distribution as a function of θ measured by the infrared camera at a number of times following the start of heating for 0.86 W power within the test cell in free convection cooling conditions. The temperature distribution evolves with time, although the nature of θ-dependence remains nearly invariant. There is sharp increase in temperature initially, whereas the rate of change in temperature reduces, as expected, as the test cell approaches thermal steady state.

Figure 3 plots the calculated core temperature for transient experiments at a number of heating powers in free convection cooling conditions. In brief, the surface temperature measurements $T_0(\theta,\tau)$ shown in Supplementary Figure S3 are integrated at each time τ to determine $w_{0I}(\tau)$ according to equation (5). Coefficients $B_{0n}(t)$ are then determined using equation (3), where the coefficient at any given time requires information about w_{0I} at that time and at all prior times. Finally, the core temperature is determined as a function of time using equation (1). For comparison, the core temperature measured by the embedded thermocouple in the test cell

for each power is also plotted in Figure 3. There is excellent agreement over the entire experiment duration between the core temperature predicted by the technique and actual core temperature measurement from the embedded thermocouple. This agreement holds for multiple heating powers. The residual, defined as the difference between measured and analytical temperature rise during an experiment is 0.76 °C at most, which is well within the experimental measurement uncertainty discussed later. In general, the mean of these residuals over the experimental period increases as power increases, but even for measurements at the highest power of 2.2W when the temperature rise is around 37 °C, the mean and standard deviation of the residuals is only 0.30 and 0.21 °C respectively. Supplementary Figure S4 plots the maximum residual between measured and analytical temperature rise as a function of the heating power. In each case, the maximum residual is lower than the experimental uncertainty.

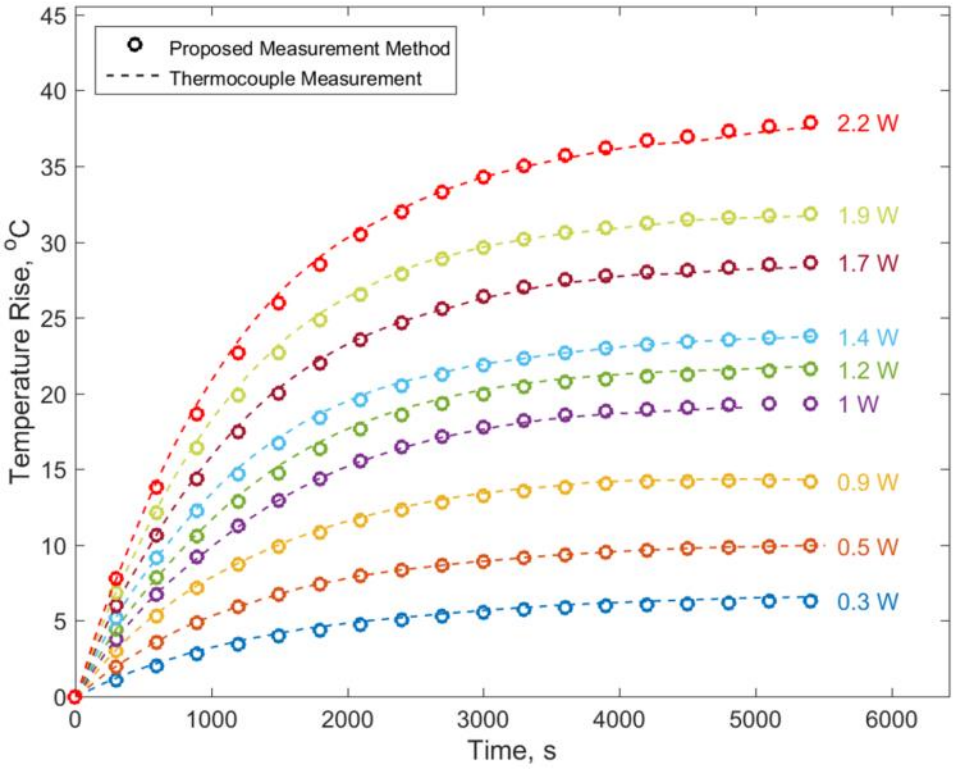

17. Figure 3: Predicted core temperature as a function of time for a number of heating powers in free convection cooling conditions. Actual temperature measured by embedded thermocouple is also shown as broken lines for each power.

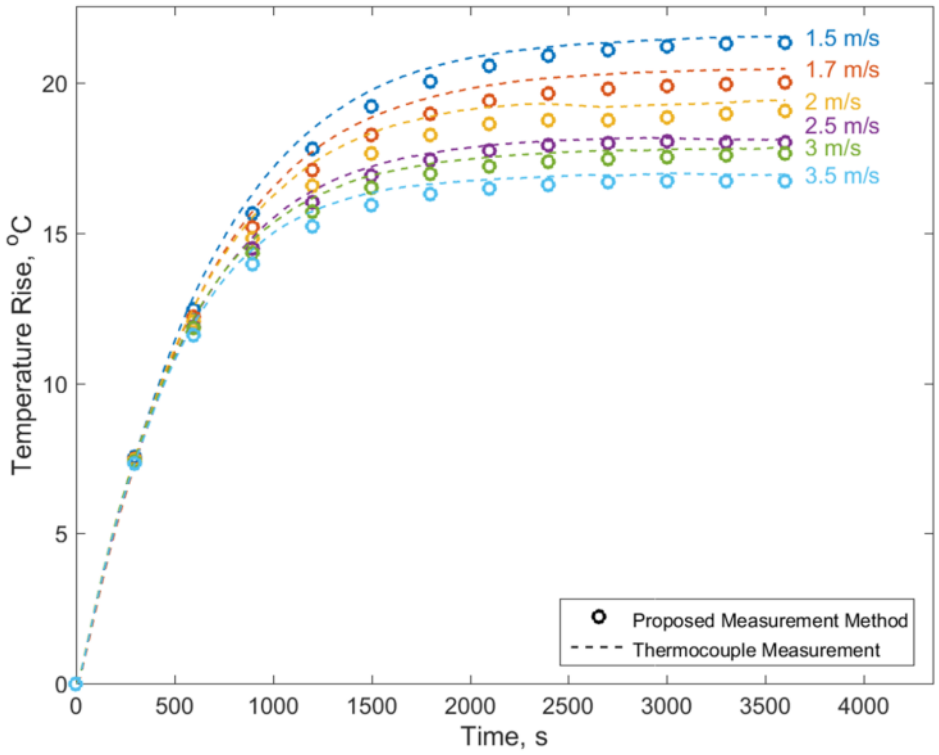

18. Figure 4: Comparison of measured core temperature as a function of time with measurement from core-embedded thermocouple for 2.2 W heating power with different air speeds from a cooling fan.

To further investigate the performance of this, measurements are repeated in the presence of forced convection cooling due to air flow from a fan. Figure 4 plots the core temperature determined as a function of time for a heating power of 2.2 W and at different air speeds. As expected, the temperature reduces as air speed increases. At each air speed, there is excellent agreement between the technique discussed in this paper, and thermocouple measurements of the core temperature. The peak residual between the two over the entire experimental duration is 0.75 °C. The residuals are higher at larger times, but even in the worst case, much below the resolution of the measurement technique. The highest mean and standard deviation of these residuals is 0.46 and 0.23 °C when the temperature rise itself is around 18 °C. These numbers are similar to statistics for the previous Figure.

Time-varying heat generation is often encountered in energy conversion systems. To evaluate the accuracy of this technique in such conditions, a set of experiments are carried out with a time-varying heat generation rate in the thermal test cell. *Q(t)* profiles representative of high-rate cyclic discharge of a Li-ion cell [9] are used. In this case, heat is generated at a large rate during the discharge process, whereas the heat generation rate is much lower or zero during the charge and rest periods between successive discharges. In these experiments, Joule heating in the test cell is switched on and off at 15 minute intervals for three cycles. Experiments are carried out at different powers and in different cooling conditions. Experimental measurements of the surface temperature distribution are analyzed using the theoretical model to determine the core temperature as a function of time. The inverse Laplace transformation in equation (6) is carried out using de Hoog's quotient difference method [22] as implemented by Hollenbeck [23].

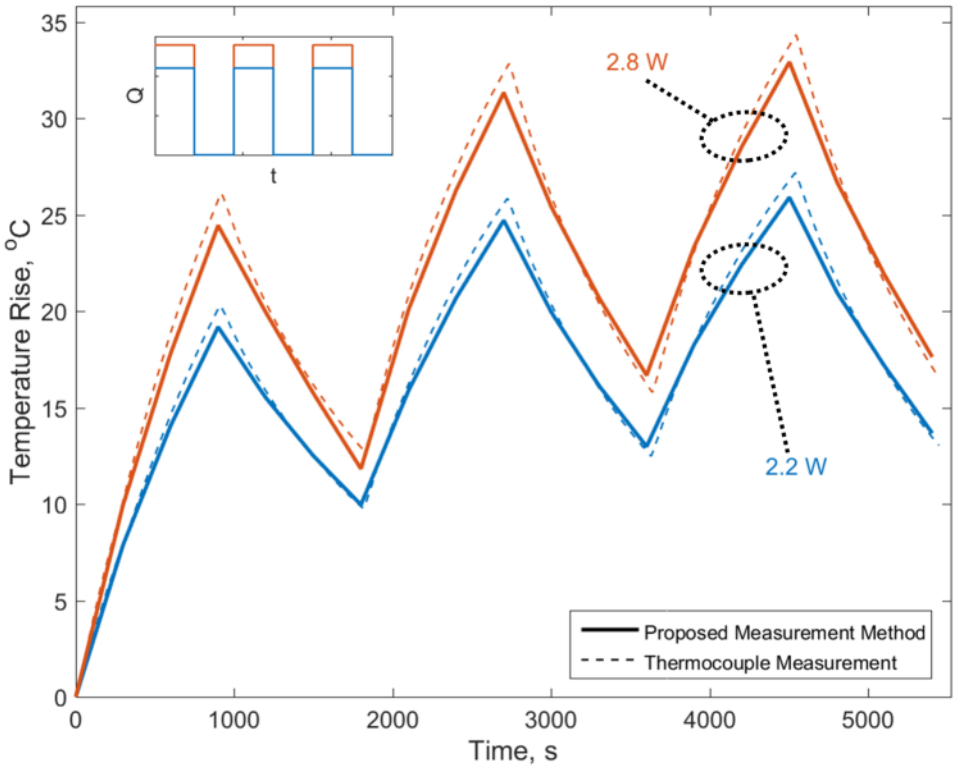

19. Figure 5: Comparison of measured core temperature as a function of time with measurement from core-embedded thermocouple for three cycles of ON-OFF heating with two different heating powers in identical cooling conditions.

Figure 5 plots the core temperature as a function of time predicted by this technique for two different heating powers with free convection cooling. The actual core temperature measurement from the embedded thermocouple is also plotted for both cases. Figure 5 shows that the core temperature is predicted accurately during both parts of the cycles, and over multiple cycles. The peak temperature reached in each cycle is under-predicted only by a few percent.

Figure 6 compares the core temperature with embedded thermocouple data for two cases where the heating power is held constant at 2.78 W, with two different cooling conditions – free convection in the absence of air flow, and forced convection with a 2.5 m/s air flow. As expected, the core temperature reduces when air flow is introduced, and in each case, the core temperature determined from this technique is in good agreement with thermocouple data.

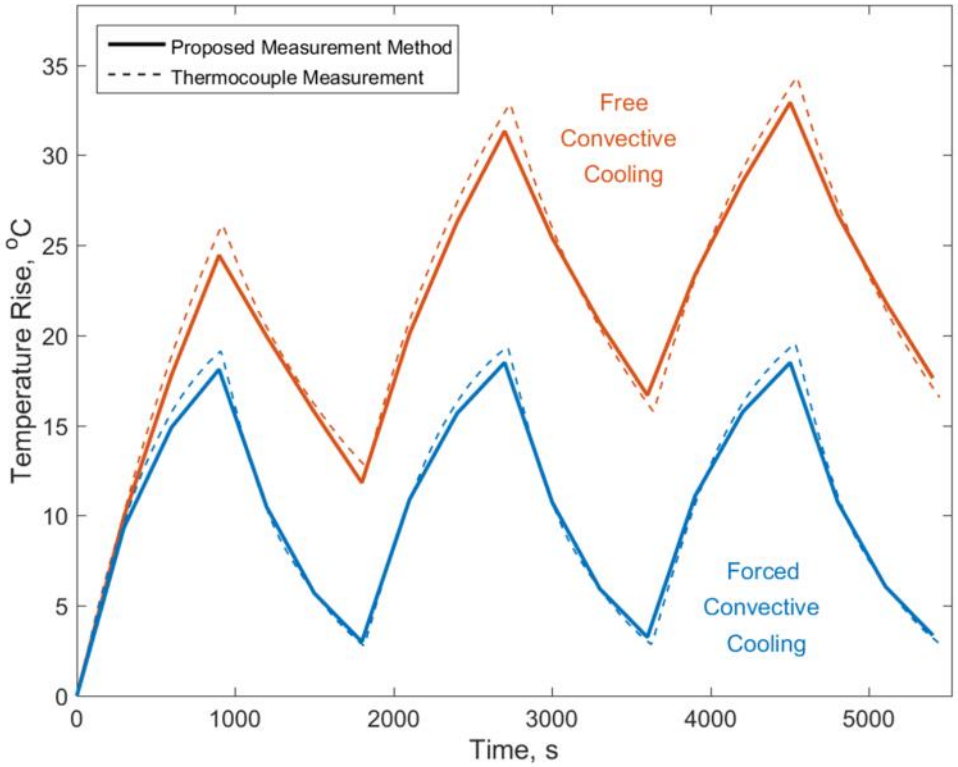

20. Figure 6: Comparison of measured core temperature as a function of time with measurement from core-embedded thermocouple for three cycles of ON-OFF heating with 2.78 W heating power in natural convection and forced convection cooling conditions.

The experiments carried out here, as summarized in Figures 3-6 demonstrate the capability of this technique to accurately determine the core temperature of the cell in a wide variety of experimental conditions including heating powers, cooling conditions and time-varying heating. In each case, the core temperature is determined as a function of time with very good accuracy in a non-intrusive fashion using only surface temperature data. While this paper discusses this technique in the context of a cylindrical body, the technique can be extended easily to bodies of other shapes, as long as an analytical derivation similar to the derivation shown in Supplementary Information can be carried out to determine a relationship between the core temperature and surface temperature of the body.

2.3. Convergence of the Theoretical Model

Supplementary Figure S5 plots the transient core temperature calculation from equation (1) for different numbers of eigenvalues for the $B_{0n}(t)$ term for 0.86 W heating case with free convection cooling. Measurement from the embedded thermocouple is also plotted for comparison. This plot shows that at least 400 eigenvalues are needed for good agreement between the model and thermocouple data. Several other analytical thermal models developed in the past for other applications have required far fewer numbers of eigenvalues [24-25]. However, the large number encountered here is not unexpected. In a limiting case where a constant outside surface temperature T_{out} is imposed on the outer surface of the cylinder with no internal heat generation, it can be shown using equation (1) that the core temperature at large times is given by

$$T_{core}(t \to \infty) = T_{out} \cdot \sum_{n=1}^{\infty} \frac{2}{(\lambda_{n0} R) \cdot J_1(\lambda_{n0} R)} \tag{7}$$

The infinite series in equation (7) can be shown to converge to a value of 1, as expected, but, as shown in Supplementary Figure S6, this convergence is very slow, requiring at least 400 eigenvalues for reaching within 4% of the infinite series sum. This, along with the fact that the outside surface temperature itself changes with time in actual experiments explains the reason for requiring a large number of eigenvalues for accurately computing the model.

2.4. Calibration and Validation of Infrared-Based Surface Temperature Measurements

The accuracy of the technique to determine the core temperature depends critically on the accuracy of surface temperature measurement, carried out in this case with an infrared camera. Experiments are carried out to establish the accuracy of the infrared temperature measurements. In these experiments, the infrared camera is used to measure the temperature of a thermal stage as a function of time. The temperature of the graphite-coated stage is well known through a thermocouple embedded in the stage. Supplementary Figure S7 plots the temperature of the Instec stage during a ramp up from room temperature to 60 °C at a rate of 5 °C/min. The plot compares measurement from the infrared camera with the actual stage temperature measured by the embedded thermocouple. These data clearly show that the infrared camera, when calibrated for the graphite surface is able to accurately measure the surface temperature as a function of time. The peak deviation between the two measurements is 0.31 °C, which is well within the measurement uncertainty of the infrared camera and the embedded thermocouple. Since the rate of temperature change in core temperature experiments is lower than the ramp rate chosen for these validation experiments, these data establish the accuracy of infrared based transient surface temperature measurement.

2.5. Sensitivity and Uncertainty Analysis

An uncertainty analysis is carried out to determine the overall uncertainty in determining the core temperature, as well as to identify key sources of uncertainty. Experimental uncertainty in the core temperature arises primarily from uncertainties in measurement of heat generation Q, radial thermal conductivity k_r, and surface temperature T_0. Uncertainty in heat generation rate is expected to be very small since it is measured electrically using precise measurement instruments. Based on error propagation analysis [26] in experimental measurement of thermal conductivity k_r carried out in the recent past [15,19], the uncertainty in thermal conductivity measurement has been estimated to be ±5% [19]. This represents the expected uncertainty in the thermal conductivity measurement due to propagation of errors involved in measurement of quantities needed for determining thermal conductivity. The uncertainty in infrared-based surface temperature measurement is obtained from the calibration curve (Supplementary Figure S7) to be 0.31 °C. An error propagation analysis [24] of equation (1) shows that the overall uncertainty in core temperature measurement is expected to be around ±10%.

Radial thermal conductivity k_r and heat capacity C_p of the cylinder influence the predicted core temperature as a function of time for the infinite cylinder. Note that the circumferential thermal conductivity k_θ is not required. The sensitivity of measurement results to these thermal properties is examined in Figures 7(a) and 7(b), that plot the predicted core temperature as a function of time for different values of k_r and C_p respectively for a specific case of 0.86 W heating in natural convection conditions. The core temperature measured by the thermocouple is also plotted for reference. Figure 7(a) shows that the core temperature is somewhat sensitive to the value of k_r, indicating that it is important to accurately know beforehand the radial thermal conductivity of the cylinder. For measurements discussed in this

paper, k_r is measured using a recently developed anisotropic thermal conductivity measurement method [19], and the deviation of core temperature measurements from thermocouple data is within the uncertainty associated with k_r measurement and other sources of uncertainty. Figure 7(b) presents a similar plot for the variation of core temperature for different values of C_p, indicating that unlike k_r, the results are not very sensitive to the value of heat capacity.

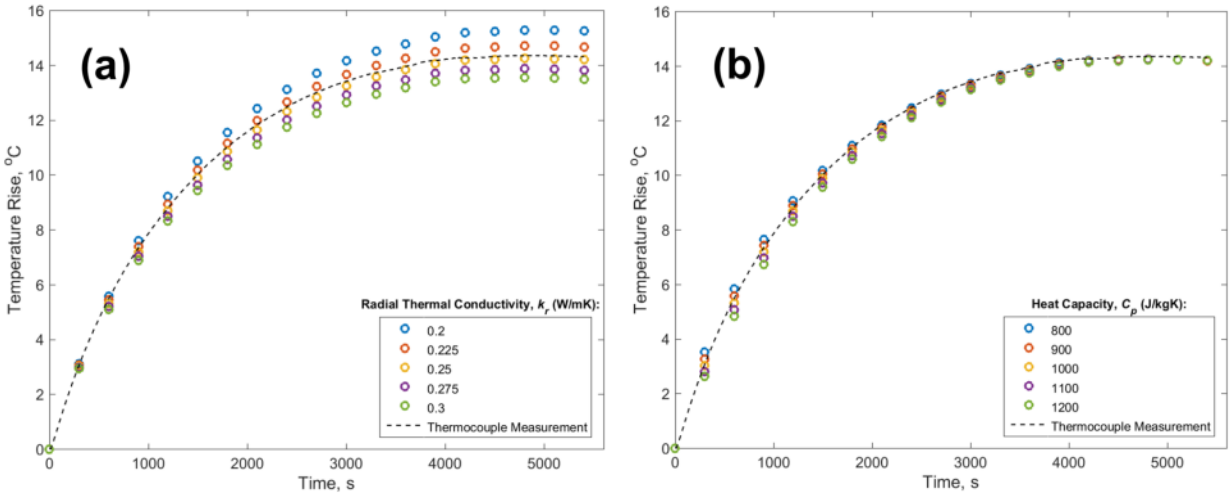

21. Figure 7: Sensitivity of the measured transient core temperature profile to (a) radial thermal conductivity, and (b) heat capacity for 0.86 W heated cylinder in free convective cooling conditions. Core temperature as a function of time from the embedded thermocouple is also plotted as a broken line.

The key limitation of the non-invasive core measurement method discussed here is that information about the thermal conductivity, heat capacity and heat generation rate of the body must be known in advance. While the thermal properties may be known if the body is made of a standard material, or through separate thermal property measurements, it may present challenges if the body is a composite. In such a case, the use of effective thermal conductivity and heat capacity may be appropriate. Information about the heat generation rate will typically come from the mechanism of heat generation. For example, for Joule heating, the heat generation rate may be obtained from current and potential difference measurements. For heating due to chemical reactions, heat generation rate may be obtained from the enthalpies and rates of reactions.

3. Methods

3.1. Theoretical Modeling

A derivation for the relationship between the core temperature as a function of time, $T_{core}(t)$ and the surface temperature distribution on the outside surface, $T_0(\theta,t)$ for an infinite cylinder is carried out using the method of undetermined parameters for solving the governing energy equation with boundary conditions that capture the measured outside surface temperature distribution. In addition, the method of Laplace transforms is used for the case of time-varying heat generation rate. Detailed derivations are provided as Supplementary Information.

3.2. Fabrication of Thermal Test Cell

Experiments described in this paper utilize a thermal test cell of 13 mm radius and 65 mm height that is capable of uniform volumetric heat generation through Joule heating in metal foil rolled and embedded within the test cell, as shown in Figures 2(a) and 2(b). Joule heating provides the advantage of close control of heat generation rate through the input electric current, and of varying heat generation as a function of time. Fabrication of the test cell has been described in detail previously [15]. In brief, a thin metal foil, insulated with Kapton tape is rolled around a thin rod and inserted inside a metal casing. A T-type thermocouple is inserted at the core of the roll at mid-height. Electric current can be passed through the metal foil through two thin metal wires. Remaining space within the casing is filled with a temperature-curable polymer, poly-dimethylsiloxane (PDMS), following which, the test cell is sealed. Air bubbles in the uncured PDMS monomer are removed in a vacuum desiccator. The curing process is allowed to occur at room temperature over 24 hours to further facilitate removal of bubbles.

The thermal test cell is designed to have similar geometry and thermal properties as a 26650 Li-ion cell, which is commonly used for high density electrochemical energy storage and conversion [27]. Heat capacity of the test cell is determined through a weighted average of the well-known heat capacities of all individual components including metal foil, Kapton tape, PDMS, metal casing, etc. Radial thermal conductivity of the cell is measured through an adiabatic heating method developed recently [19]. In brief, a thermocouple is placed at the outer surface of the test cell at mid-height using a thermal epoxy. A flexible heater is then wrapped around the outer curved surface of the test cell. The test cell is then wrapped in insulation tape, and placed inside a vacuum chamber. Transient temperature rise of the cell measured by the thermocouple, in response to a DC heat flux, is compared with an analytical thermal model to determine the radial thermal conductivity of the cell. Specifically, the intercept of the temperature vs. time plot is used to determine the radial thermal conductivity of the cell. Details of this method have been presented recently [19]. Note that the other two components of the orthotropic thermal conductivity - k_z and k_θ – are not measured, since the theoretical derivation shows that the core temperature is independent of these properties.

3.3. Calibration and Validation of IR Camera Measurements

A FLIR A6703 InSb infrared camera is used for transient surface temperature measurements needed for determination of the core temperature as a function of time. Experiments are first carried out to establish the accuracy of infrared temperature measurement, particularly in a transient setting. The accuracy of infrared based temperature measurement is strongly dependent on the quality of calibration. In this case, the same calibration settings established in past experiments are used [15], and experiments are carried out to track the known temperature of a surface as a function of time with the infrared camera. An Instec HCS662V

thermal stage is used for this purpose. The temperature of the stage can be controlled in a wide temperature range. A desired ramp rate can also be specified between two temperatures. A thermocouple embedded within the stage provides the stage temperature as a function of time, to which the infrared temperature measurement can be compared for validation.

The infrared camera is mounted above an optical breadboard, and the stage is placed directly below, as shown in the inset of Supplementary Figure S7. A thin graphite film is sprayed using a DGF aerosol spray on a small region of the thermal stage to increase surface emissivity. Starting at room temperature, the stage is set to reach a temperature of 60°C with a ramp rate of 5°C per minute. Temperature of the graphite-coated stage surface is monitored through the embedded thermocouple at 1 Hz frequency. The stage temperature is also measured using the infrared camera during this time at the same rate. Infrared measurements are carried out both without and with the specification of emissivity of the graphite surface, which are then compared with the thermocouple measurement to establish the accuracy of infrared temperature measurement.

3.4. Experimental Setup for Core Temperature Measurement

A picture of the experimental setup for measuring the transient core temperature of the test cell using transient surface temperature measurements is shown in Figure 1(a). The thermal test cell is mounted on two thin, foam risers to minimize conduction heat loss, and placed on an optical breadboard directly under the infrared camera. The outer surface of the thermal test cell is coated with the same graphite film used for calibration experiments. The measurement and data acquisition flow is shown schematically in Figure 1(b). Internal heat is generated inside the test cell through resistive heating in the metal foil due to a DC heating current sourced from a GW

INSTEK GPD-4303S power supply. The heating current can be switched on and off in order to produce time-varying heat generation rate. Potential difference across the resistive heater is also monitored using a Keithley 2100 digital multimeter controlled by LabView software in order to get measurements of heat generation rate as a function of time. A Fugetek HT-07530D12 computer fan is used in forced convection experiments to provide cooling. The fan is placed at the same height as the axis of the cell to ensure direct and symmetrical impingement of air from the fan on to the test cell. A variable resistor controller is used for fan speed control. Data acquisition from the thermocouple embedded in the core of the test cell is carried out using a NI-9213 DAQ thermocouple module and controlled by LabView software. Infrared temperature measurements as well as thermocouple measurements are taken once every 3 seconds. These measurement rates are appropriate since this system has a much larger time constant than the data acquisition interval.

3.5. Experiments

A number of experiments are carried out in a variety of heating and cooling conditions in order to measure the core temperature of the test cell as a function of time using the method described in the previous sub-section, and to compare with actual core temperature from the embedded thermocouple. In each case, the test cell starts at ambient temperature, and is supplied with a constant or time-varying heating current. The temperature field on the surface of the cell is measured as a function of time using the infrared camera until thermal steady state is reached. In order to determine the heat generation rate, the electrical resistance of the test cell is measured in advance using a small test current that minimizes self-heating. It is also confirmed that the resistance of the test cell does not increase appreciably due to temperature rise during the experiment.

Temperature distribution around the circumference of the test cell at mid-height is extracted from the temperature field data from the infrared camera at a number of time points during each experiment. Since the infrared camera views a projection of the curved surface of the cylinder, a transformation is applied on the data in order to determine the surface temperature distribution as a function of θ. The axial dependence of temperature is examined as a function of time in order to rule out significant axial thermal conduction effects. It is found that there is minimal temperature variation in the axial direction [15], which justifies the assumption of an infinite cylinder in the thermal model.

Three sets of experiments are carried out. First, the core temperature of the cell is measured as a function of time using transient surface temperature measurements at a number of heating powers while the test cell is cooled via natural convection conditions. Subsequently, a set of experiments is carried out at constant heating power with forced convection cooling from a fan operating at various speeds. Finally, experiments are carried out for each of these two cooling conditions, with time-varying Joule heating. In these experiments, heat generation in the cell is switched on and off for periods of 15 minutes each, over a total of three cycles. This mimics periodic heat generation in a Li-ion cell undergoing cyclic charge and discharge [9].

A stabilization time of five minutes is provided in each experiment with air flow from the fan before the experiment commences. An extended cool-down period is provided between experiments to ensure that each experiment begins at room temperature.

In each experiment, the transient core temperature of the cell is determined using the experimentally measured surface temperature distribution in conjunction with the theoretical model. These core temperature measurements are compared against measurements from the

embedded thermocouple in the test cell to validate the transient core temperature measurement method.

4. Conclusions

In this paper, a novel, non-intrusive method for determining the temperature inside solid bodies has been introduced and validated using experiments on a cylindrical thermal test cell. By utilizing the measured surface temperature distribution as a function of time, this method accurately predicts the core temperature as a function of time. This method, illustrated here for a cylindrical body can be easily extended to bodies of other shapes through analysis similar to one shown in this paper. A non-destructive approach for internal temperature measurement is attractive for a variety of engineering systems where insertion of a temperature sensor inside the body is simply not possible. This capability could be used for smart, thermally-aware performance optimization, as well as for ensuring thermal safety.

Acknowledgments

This material is partly based upon work supported by CAREER Award No. CBET-1554183 from the National Science Foundation. Financial support from Office of Naval Research through DURIP Award # N00014-14-1-0752 for acquisition of infrared camera is gratefully acknowledged.

Author Contributions

D.A. carried out the experimental measurements and data analysis. D.A., D.S. and A.J. carried out the theoretical derivation for the transient core temperature measurement technique. A.J. designed and supervised the project. All authors wrote and edited the paper.

SUPPLEMENTARY INFORMATION

1. Theoretical Derivation of Equation (1)

This section derives a relationship between the transient core temperature, $T_{core}(t)$ at $r=0$ and the transient surface temperature distribution, $T_0(\theta,t)$ of a heat-generating infinite cylinder. While similar solutions have been derived in the past using the method of Green's functions (for example, Özişik, M.N., Heat conduction, 2nd Ed., John Wiley & Sons, 1993), this derivation takes into account circumferential variation in T_0, as well as anisotropic thermal conduction within the cylinder.

This derivation leads to an expression for $T_{core}(t)$ that forms the basis for the technique to non-intrusively determine the core temperature.

1.1. Constant Heat Generation Rate

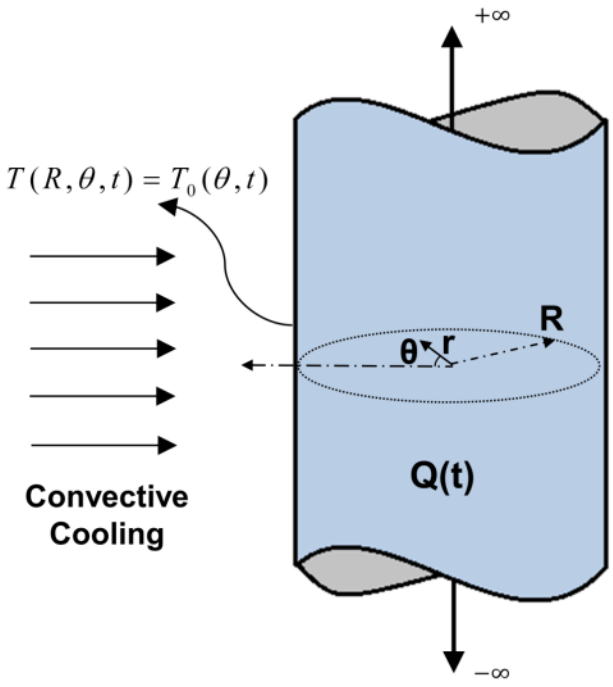

22. Supplementary Figure S1: Schematic of the geometry of a heat-generating infinite cylinder. The goal of the measurement is to determine the core temperature T(r=0,t) as a function of time from measured surface temperature $T_0(\theta,t)$ as a function of time.

This sub-section considers an infinite cylinder of radius R generating heat at a uniform and constant rate Q, shown schematically in Supplementary Figure S1. The cylinder is assumed to have orthotropic thermal conductivities, with values of k_r and k_θ in the radial and circumferential directions respectively. The circumferentially-varying, transient temperature distribution along the outer surface at $r=R$, given by $T_0(\theta,t)$ is assumed to be known, for example, through an infrared measurement. The cylinder is assumed to be at uniform temperature initially.

The transient temperature distribution in the cylinder can be determined by solving the governing energy conservation equation subject to appropriate boundary conditions. Using the separation of variables approach (Özişik, M.N., Heat Conduction, 2nd Ed., John Wiley & Sons, 1980), the temperature field may be split into two parts and assumed to be of the following form:

$$T(r,\theta,t) = T_1(r,t) + T_2(r,\theta,t) = \left[\frac{Q\left(R^2 - r^2\right)}{4k_r} + \sum_{m=0}^{\infty} A_n J_0\left(\lambda_{0n} r\right) e^{-\alpha_r \lambda_{n0}^2 \cdot t} \right] + \sum_{m=0}^{\infty} \sum_{n=1}^{\infty} B_{mn}(t) J_{m\sqrt{\frac{k_\theta}{k_r}}}\left(\lambda_{mn} r\right) \cos(m\theta) \quad \text{(S.1)}$$

Where T_1, comprising the first two terms, accounts for internal heat generation, and T_2, comprising the third term accounts for time- and θ-dependent temperature at $r=R$.

Here, J refers to the Bessel function of the first kind, and the radial norm $N_{r,n}$ is given by

$$N_{r,n} = \frac{R^2 J_1(\lambda_{0n} R)^2}{2} \quad \text{(S.2)}$$

And the eigenvalues λ_{mn} are obtained from the roots of $J_{m\sqrt{\frac{k_\theta}{k_r}}}$. Specifically, λ_{0n} are obtained from the roots of J_0. Using the orthogonality principle (Özişik, M.N., Heat Conduction, 2nd Ed., John Wiley & Sons, 1980), A_n are given by

$$A_n = \frac{-\frac{Q}{4k_r}\int_0^R \left(R^2 - r^2\right)\cdot rJ_0\left(\lambda_{0n} r\right)dr}{N_{r,n}} \tag{S.3}$$

The coefficient functions $B_{mn}(t)$ must be determined such that the solution satisfies the governing equation and boundary conditions.

Note that the core temperature $T_{core}(t)$ may be expressed in terms of the unknown coefficient functions $B_{nm}(t)$ by putting $r=0$ in equation (S.1)

$$T_{core}(t) = T_{1,core}(t) + T_{2,core}(t) = \frac{QR^2}{4k_r} + \sum_{n=1}^{\infty} A_n e^{-\alpha_r \lambda_{n0}^2 \cdot t} + \sum_{n=1}^{\infty} B_{0n}(t) \tag{S.4}$$

Equation (S.4) shows that even though all coefficient functions $B_{mn}(t)$ are needed to determine the general temperature distribution $T(r,\theta,t)$, only the coefficient functions $B_{0n}(t)$ are needed for measuring the core temperature. To do so, the expression for $T_2(r,\theta,t)$ from equation (S.1) is integrated with respect to θ to eliminate all $B_{mn}(t)$ for m>0, followed by use of the method of undetermined parameters (Myers, G.E., Analytical Methods in Conduction Heat Transfer, 2nd Ed., AMCHT Publications, 1998) to derive the following ordinary differential equation for $B_{0n}(t)$

$$\frac{dB_{0n}}{dt} = -\alpha_r \lambda_{0n}^2 B_{0n} + \frac{\alpha_r \lambda_{0n} R J_1\left(\lambda_{0n} R\right)}{2\pi N_{r,n}} \int_0^{2\pi} T_0\left(\theta, t\right) d\theta \tag{S.5}$$

Further, based on the initial condition for the temperature field, the following initial condition applies for $B_{0n}(t)$

$$B_{0n}(0) = 0 \tag{S.6}$$

A solution for equation (S.5) subject to (S.6) is given by

$$B_{0n}(t) = \frac{\alpha_r \lambda_{0n} R J_1(\lambda_{0n} R)}{N_{r,n}} \int_0^t w_{0I}(\tau) \exp\left[-\alpha_r \lambda_{0n}{}^2 (t-\tau)\right] d\tau \qquad \text{(S.7)}$$

Where $w_{0I}(\tau)$ is the circumferentially averaged value of the measured temperature at the outside surface, given by

$$w_{0I}(\tau) = \frac{1}{2\pi} \int_0^{2\pi} T_0(\theta, \tau) d\theta \qquad \text{(S.8)}$$

This completes the determination of the core temperature $T_{core}(t)$, which is given by equation (S.4), where the coefficient functions are given by equations (S.2) and (S.7).

1.2. Effect of Time Varying Heat Generation Rate

The previous sub-section assumed a time-invariant internal heat generation rate in the cylinder. In this sub-section, a more general case is considered where the heat generation varies with time, given by $Q(t)$. Time-varying heat generation is encountered in several engineering applications, where the measurement of core temperature in response to $Q(t)$ is of interest.

To develop a technique for internal temperature measurement for this case, the governing energy equation needs to be revisited. As shown in equation (S.1), the components T_1 and T_2 of the overall temperature distribution account for temperature rise due to internal heat generation and due to the time-dependent surface temperature respectively. As a result, variation in Q with time affects only the T_1 component of the temperature field. A Laplace transform approach is used to derive a solution for $T_1(r,t)$ for when Q varies with time. Taking Laplace transform of the governing equation and boundary condition for T_1 results in the following:

$$\left(\frac{d^2\overline{T}_1}{dr^2}+\frac{1}{r}\frac{d\overline{T}_1}{dr}\right)-\frac{s}{\alpha_r}\overline{T}_1+\frac{\overline{Q}(s)}{k_r}=0 \qquad \text{(S.9)}$$

Where $\overline{Q}(s)$ is the Laplace transform of the heat generation rate *Q(t)*. $\overline{T}_1$ also satisfies

$$\frac{d\overline{T}_1}{dr}=0 \qquad \text{at } r\text{=}0 \qquad \text{(S.10)}$$

And

$$\overline{T}_1=0 \qquad \text{at } r\text{=R} \qquad \text{(S.11)}$$

The solution to this ordinary differential equation can be shown to be given by

$$\overline{T}_1=\frac{\alpha_r\overline{Q}}{sk_r}\left(1-\frac{I_0\left(\sqrt{\frac{s}{\alpha_r}}r\right)}{I_0\left(\sqrt{\frac{s}{\alpha_r}}R\right)}\right) \qquad \text{(S.12)}$$

Where I_0 is the modified Bessel function of the first kind.

As a result, the core temperature $T_{core}(t)$ for an infinite cylinder can be written as

$$T_{core}(t)=T_{1,core}(t)+T_{2,core}(t)=L^{-1}\left[\frac{\alpha_r\overline{Q}}{sk_r}\left(1-\frac{1}{I_0\left(\sqrt{\frac{s}{\alpha_r}}R\right)}\right)\right]+\sum_{n=1}^{\infty}B_{0n}(t) \qquad \text{(S.13)}$$

Where L-1 refers to the inverse Laplace transform. Note that $B_{0n}(t)$ is given by equation (S.7).

For a given Q(t), the inverse Laplace transform may be determined analytically when possible, or numerically using inverse Laplace transform numerical algorithms. This provides a technique to predict the core temperature of the cylinder in presence of a time-varying heat generation within the body.

2. Supplementary Figures

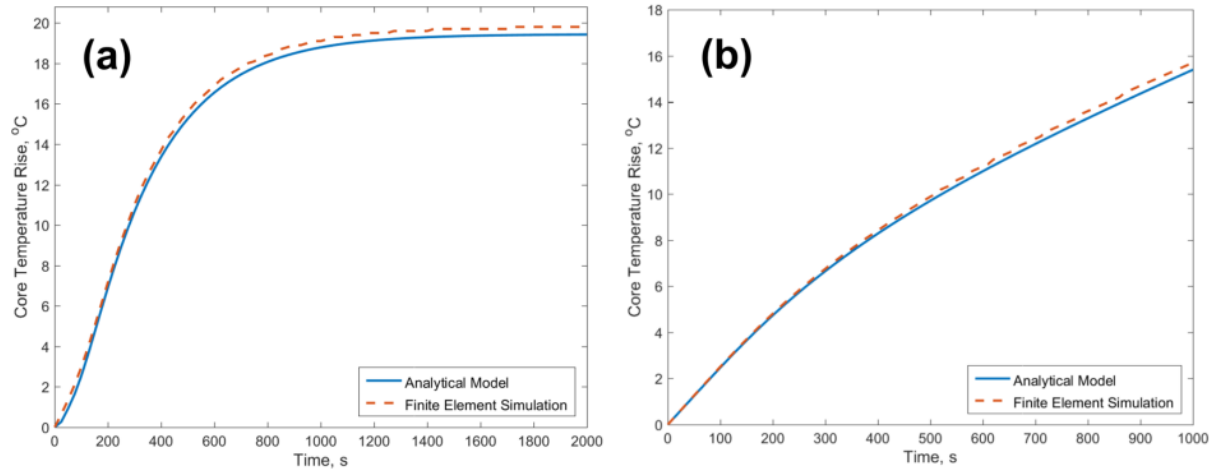

23. Supplementary Figure S2: Comparison of transient core temperature predicted by the theoretical model with finite-element simulation results for two surface temperature conditions, (a) constant T_0=10°C, (b) linearly increasing $T_0(t)$= $10\frac{t}{1000\ (s)}$ °C. Both model and finite-element simulations assume a 13 mm radius cylinder with 57,954 W/m^3 heating and the same thermal properties as the experimental thermal test cell.

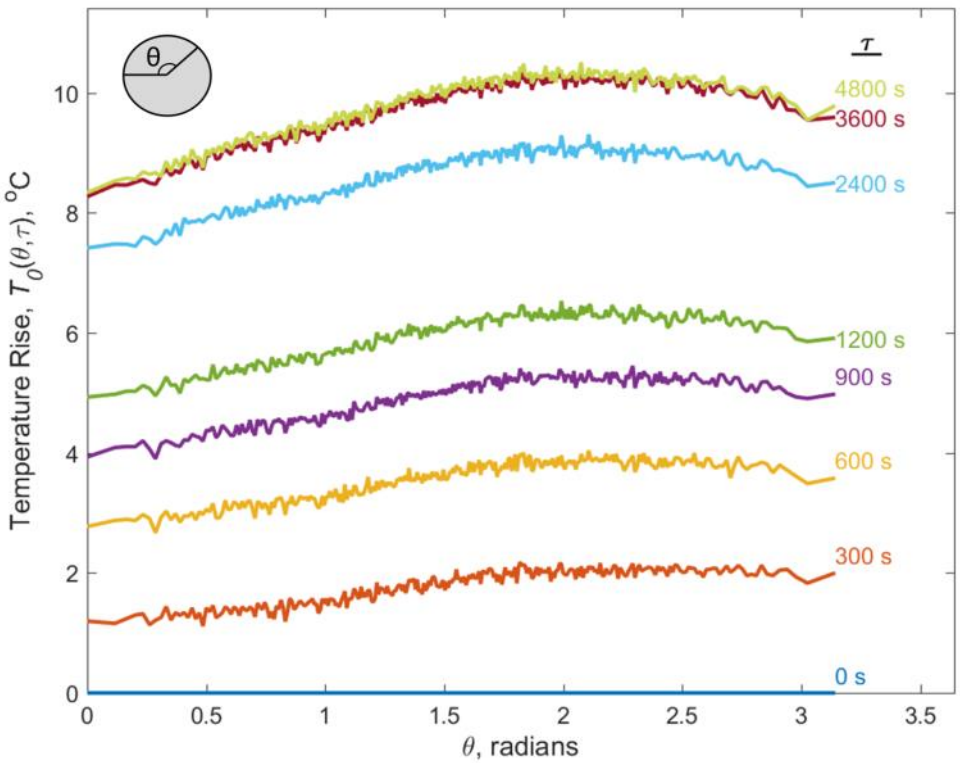

24. Supplementary Figure S3: Measured surface temperature distribution around the cylinder T0(θ,τ) at a number of times following the start of heating for 0.86 W heating power in the thermal test cell in free convection cooling conditions.

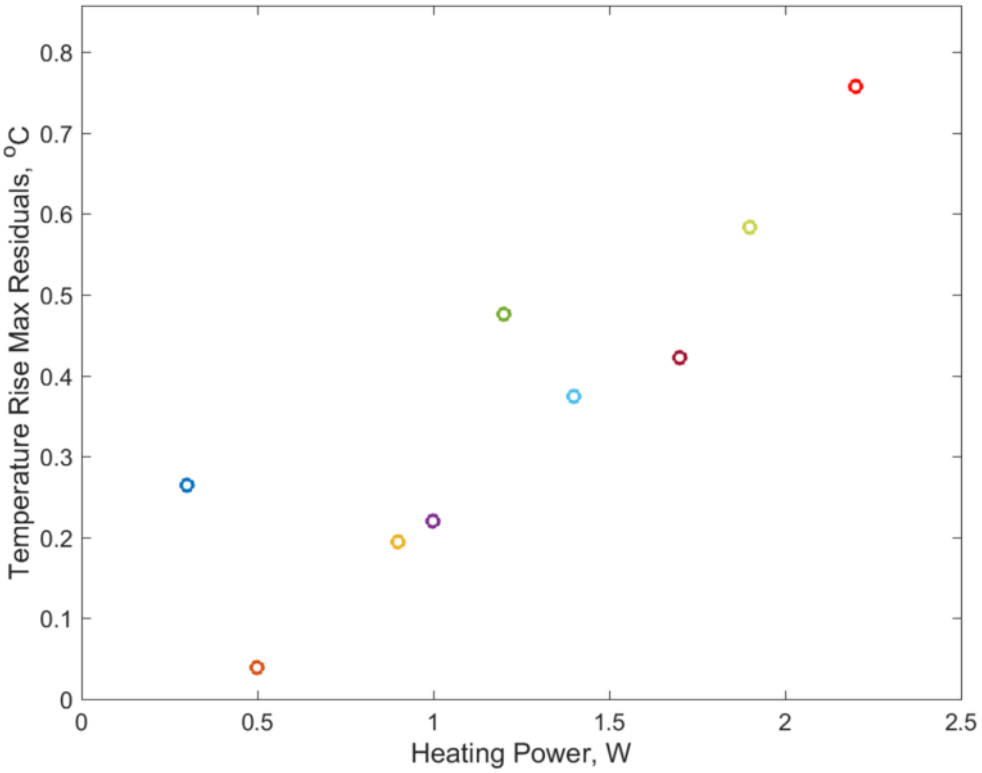

25. Supplementary Figure S4: Plot of the maximum residual over the entire experiment duration as a function of heating power for Figure 3.

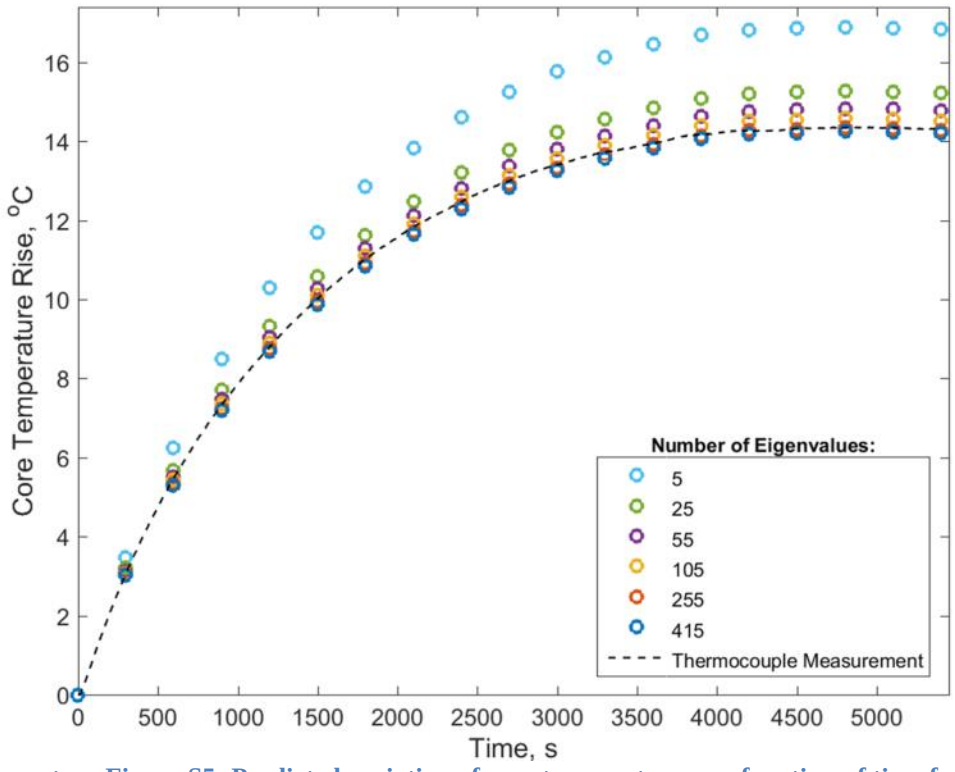

26. Supplementary Figure S5: Predicted variation of core temperature as a function of time for different number of eigenvalues considered for the B0n(t) term in equation (1). For comparison, the embedded thermocouple measurement is also shown as a broken line.

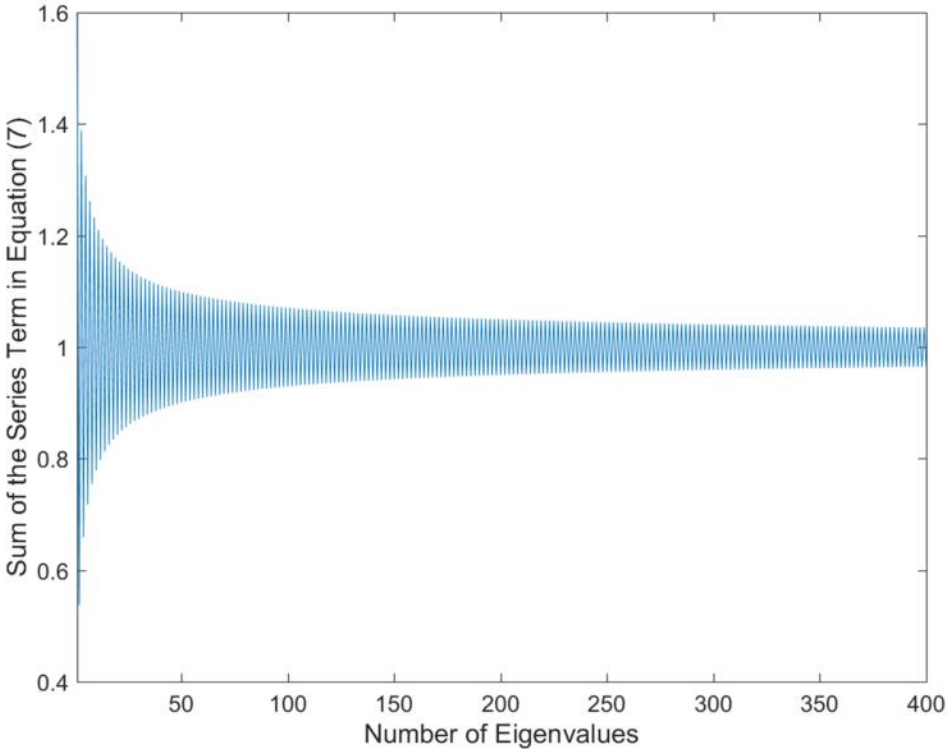

27. Supplementary Figure S6: Convergence of the infinite series in equation (7) with respect to the number of eigenvalues considered, showing slow series convergence.

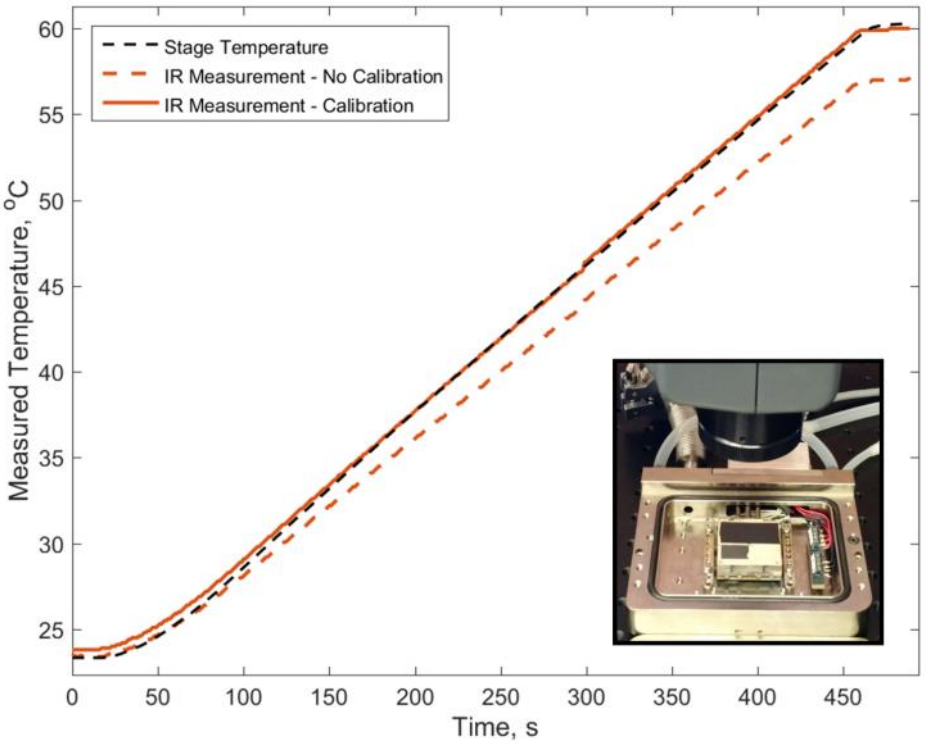

28. Supplementary Figure S7: Comparison of IR camera measured temperature of a surface with a known surface temperature as a function of time, during a temperature ramp from room temperature to 60 °C at a rate of 5 °C/min. IR data are shown both with and without calibration in red lines. The known surface temperature is also plotted in black for comparison.

References

[1] Michalski, L., Eckersdorf, K., Kucharski, J., & McGhee, J. *Temperature Measurement*, *2nd Edition* (Wiley, 2001).

[2] McGee, D.T. *Principles and Methods of Temperature Measurement* (John Wiley & Sons, 1988).

[3] Childs, P.R.N., Greenwood, J.R., & Long, C.A. Review of temperature measurement. *Rev. Scientific Instruments* **71**, 2959-2978 (2000).

[4] Raad, P.E., Komarov, P.L., & Bettiati, M.A. Thermoreflectance temperature measurements for optically emitting devices. *Microelectronics J.* **45**, 515-520 (2014).

[5] Franco J.J.L., Boemo E., Castillo, E., & Parrilla L. Ring oscillators as thermal sensors in FPGAs: Experiments in low voltage. *Proc. VI Southern Programmable Logic Conf.* 133-137 (2010).

[6] Cooper, T.E., Field, R.J., & Meyer, J.F. Liquid crystal thermography and its application to study of convective heat transfer. *ASME J. Heat Transfer* **97**, 442-450 (1975).

[7] DeWiit, D.P. and Nutter, G.D. *Theory and Practice of Radiation Thermometry*, *1st Edition* (John Wiley & Sons, 1988).

[8] Forgez, C., Do, D.V., Friedrich, G., Morcotte, M., & Delacourt, C. Thermal modeling of a cylindrical $LiFePO_4$/graphite lithium-ion battery. *J. Power Sources* **195**, 2961-2968 (2010).

[9] Drake, S.J., et al. Heat generation rate measurement in a Li-ion cell at large C-rates through temperature and heat flux measurements. *J. Power Sources* **285**, 266-273 (2015).

[10] Wang, P., et al. Real-time monitoring of internal temperature evolution of the lithium-ion coin cell battery during the charge and discharge process. *Extreme Mechanics Lett.* in press, (2016).

[11] Chyu, M.-C. and Bergles, A.E. Locating method for temperature-sensing elements inserted in solid bodies. *Exp. Therm. Fluid Sci.* **2**, 247-249 (1989).

[12] Spotnitz, R. and Franklin, J. Abuse behavior of high-power Lithium-ion cells. *J. Power Sources* **113**, 81 (2003).

[13] Ihara, I. and Tomomatsu, T. In-situ measurement of internal temperature distribution of sintered materials using ultrasonic technique. *Materials Science and Engineering* **18**, (2011).

[14] Wadley, H.N.G., Norton, S.J., Mauer, F., & Droney, B. Ultrasonic measurement of internal temperature distribution. *Phil. Trans. R. Soc. Lond. A* **320**, 341-361 (1986).

[15] Anthony, D., Sarkar, D., & Jain, A. Contactless, non-intrusive core temperature measurement of a solid body in steady-state. *Int. J. Heat Mass Transfer* **101**, 779-788 (2016).

[16] Shah, K., et al. An experimentally validated transient thermal model for cylindrical Li-ion cells. *J. Power Sources* **271**, 262-268 (2014).

[17] Lasance, C.J.M. Thermally driven reliability issues in microelectronic systems: status-quo and challenges. *Microelectrtonics Reliability* **43**, 1969-1974 (2003).

[18] Özişik, M.N., Heat conduction, 2nd Ed., John Wiley & Sons, 1993

[19] Drake, S.J., et al. Measurement of anisotropic thermophysical properties of cylindrical Li-ion cells. *J. Power Sources* **252**, 298-304 (2014).

[20] Ye, Y., Saw, L.H., Shi, Y., Somasundaram, K., & Tay, A.A. Effect of thermal contact resistances on fast charging of large format lithium ion batteries. *Electrochimica Acta* **134**, 327-337 (2014).

[21] Northrop, P., Ramadesigan, V., De., S, Subramanian, V. Coordinate transformation, orthogonal collocation, model reformulation and simulation of electrochemical-thermal behavior of Lithium-ion battery stacks. *J. Electrochem. Soc.*, **158**, A1461-A1477 (2014).

[22] de Hoog, F.R., Knight, J.H., & Stokes, A.N. An improved method for numerical inversion of Laplace transforms. *S.I.A.M. J. Sci. and Stat. Comput.* **3**, 357-366 (1982).

[23] Hollenbeck, K. J. *INVLAP.M: A matlab function for numerical inversion of Laplace transforms by the de Hoog algorithm.* (1998) Available at:

http://www.mathworks.com/matlabcentral/answers/uploaded_files/1034/invlap.m. (Accessed: 1st January 2016)

[24] Shah, K., et al. Modeling of steady-state convective cooling of cylindrical Li-ion cells. *J. Power Sources* **258**, 374-381 (2014).

[25] Choobineh, L. and Jain, A. Analytical solution for steady-state and transient temperature field in vertically integrated three-dimensional integrated circuits (3D ICs). *IEEE Trans. Components & Packaging Technologies* **2**, 2031-2039 (2012).

[26] Moffat, R.J. Describing the uncertainties in experimental results. *Experimental Thermal and Fluid Science*, **1**, 3–17 (1988).

[27] Goodenough, J. and Park, K.-S. The Li-ion rechargeable battery: a perspective. *J. Am. Chem. Soc.* **135**, 1167-1176 (2013).

CHAPTER 4:

NON-INVASIVE MEASUREMENT OF INTERNAL TEMPERATURE OF A LI-ION CELL DURING HIGH-RATE DISCHARGE

Dean Anthony[1], Derek Wong[2], David Wetz[2], Ankur Jain[1],*

[1] - Mechanical and Aerospace Engineering Department
[2] – Electrical Engineering Department
University of Texas at Arlington, Arlington, TX, USA

[*] – Corresponding Author: email: jaina@uta.edu;
500 W First St, Rm 211, Arlington, TX, USA 76019
Ph: +1 (817) 272-9338; Fax: +1 (817) 272 2952

D. Anthony, D. Wong, D. Wetz, A. Jain, Non-Invasive Measurement of Internal Temperature of a Li-ion Cell During High-Rate Discharge, *Energy*, in review, 2016.

Abstract

Although a number of methods have been used for temperature measurement in Li-ion cells, there is a lack of non-invasive techniques to determine the peak temperature at the core of the cell, which plays a key role in determining performance and safety. Measuring only the outside surface temperature is not desirable since the core temperature is in most cases much higher. This paper presents non-invasive measurement of the core temperature of a Li-ion cell using a recently developed technique that utilizes space and time integrals of the measured temperature field at the outside surface. A 26650 Li-ion cell is instrumented with an embedded thermocouple at the core. The surface temperature field is measured using infrared thermography at multiple discharge rates up to 10C, using which, the core temperature is predicted as a function of time. In each case, there is excellent agreement throughout the discharge period between the predicted core temperature and measurements from the embedded thermocouple. These measurements quantify the temperature gradient within the cell, which is particularly high at large discharge rates. These measurements demonstrate an effective, non-invasive measurement method for real-time, core temperature monitoring for performance optimization and improved safety.

Keywords: Lithium Ion Battery, Temperature Measurement, Battery Safety, Thermal Management.

1. Introduction

Accurate measurement of temperature in a Li-ion cell is a critical research challenge for ensuring performance, safety and reliability of systems that utilize Li-ion cells for energy conversion and storage [1-3]. Temperature rise occurs in a Li-ion cell due to heat generation

during energy conversion, particularly at high discharge rates [4-6]. The amount of heat generated in a typical cylindrical 26650 Li-ion cell is not extremely large. For example, about 10W heat generation has been reported for an aggressive 10C discharge [7,8]. However, due to poor thermal conductance of the cell [9] resulting from material and interfacial thermal resistances in the cell [10], this causes significant temperature rise [11,12], particularly in the core of the cell, where heat accumulation tends to occur due to the lack of a direct access for heat removal [13]. High core temperature of the cell is undesirable for performance as well as safety [14,15]. This necessitates the design and implementation of an effective thermal management strategy in order to keep the cell temperature below a threshold value and prevent undesirable conditions such as thermal runaway [16-18]. A number of thermal management strategies have been reported in the past, which have been well covered by recent review articles [14,15,19]. Most thermal management techniques focus on heat removal from the outside surface of the cell. This is accomplished either by the flow of an appropriate coolant such as air or water over the cell surface, or by cold plates [20], heat pipes [21] or phase change materials [22] in the battery pack. Other more intrusive thermal management techniques include the use of electrolyte as a coolant [23], heat absorption from current collector foils [24], as well as the integration of a heat pipe protruding out of the cell [13].

Accurate measurement of temperature of the cell, particularly the peak temperature that occurs at the core of the cell is critical for effective thermal management and thermal control. Measurement of surface temperature alone does not provide much information about the core temperature since the surface temperature may not rise much even when the core is much hotter and is in urgent need for cooling. In past experiments, for example, a temperature difference of as much as 15°C has been reported between surface and core temperatures of a Li-ion cell

undergoing high rate discharge [7,25]. Therefore, thermal management based on surface temperature measurement may lead to insufficient cooling, and a direct measurement of the core temperature is critical. This may improve not only the effectiveness of thermal management but also electrochemical performance optimization of Li-ion batteries. For example, core temperature measurement of multiple cells in a battery pack may be used for load balancing within the pack by decreasing the load on an overheated cell.

Due to its importance in thermal control, a significant effort has been expended in several other engineering systems to measure the core temperature. For example, in computer microprocessors, temperature sensors are embedded deep within the microprocessor chip where the highest temperature is expected to be encountered [26]. Similar core temperature measurement is also desirable for Li-ion cells. While the temperature on the surface of a Li-ion cell can be easily measured using thermocouples or other thermal sensors [7], measurement of the core temperature is not straight-forward. The electrochemically active environment inside a Li-ion cell presents challenges for the survival of any temperature sensor embedded within. Due to the hermetically sealed nature of the cell, connecting to an embedded sensor is also difficult. Thermocouples have been inserted in Li-ion cells [7,8,25,27], but this approach is unreliable and often causes cell failure. Some research has been carried out to utilize certain electrochemical characteristics of the cell as an indicator of its temperature [28], but this approach only yields the volume-averaged temperature, and does not give information about the peak temperature at the core of the cell. The insertion of fiber Bragg sensors has also been investigated [29], however, this approach is expensive and cumbersome, and unlikely to be a candidate for implementation at a large scale. Non-invasive temperature measurement techniques such as ultrasonic temperature measurement – in which the speed of propagation of an ultrasonic wave through a device is used

to determine the average temperature along the path [30] – is unlikely to work for a Li-ion cell due to the heterogeneous nature of Li-ion cell materials. Given the shortcomings of the current state-of-the-art, development of new, non-intrusive core temperature measurement techniques is very desirable for Li-ion cells. This is likely to have a direct impact not only on thermal management of the cell, but also on real-time performance optimization.

In the recent past, a transduction-free method for measurement of core temperature in a heat-generating cylinder based on measurement of surface temperature fields has been developed [31,32]. In this method, the steady-state [31] or transient [32] core temperature of the cylinder has been shown to be related to surface temperatures through appropriate space and time integrals. Accurate measurement of the core temperature based on non-invasive, infra-red (IR) measurement of the surface temperature field has been demonstrated. This method has the advantage of being non-intrusive and based entirely on the surface temperature, which is relatively easy to measure. Past papers [31,32] have demonstrated this method for non-electrochemical test cells in which heat is generated through Joule heating, a much simpler mechanism compared to active electrochemistry inside a Li-ion cell.

This paper presents non-invasive measurement of the core temperature of a 26650 Li-ion cell during high-rate discharge. The core temperature is determined using a theoretical model that utilizes measurements of the transient temperature field on the outside surface of the cell. Core temperature is measured in this manner for multiple discharge rates, and for a discharge process involving sudden change in discharge rate. In each case, good agreement is found with independent measurements of the core temperature using an embedded thermocouple. These experiments demonstrate an effective, non-invasive method for direct measurement of the core

temperature of an operating Li-ion cell, which may be helpful for thermal control, performance optimization as well as monitoring of thermal runaway.

2. Theoretical Model

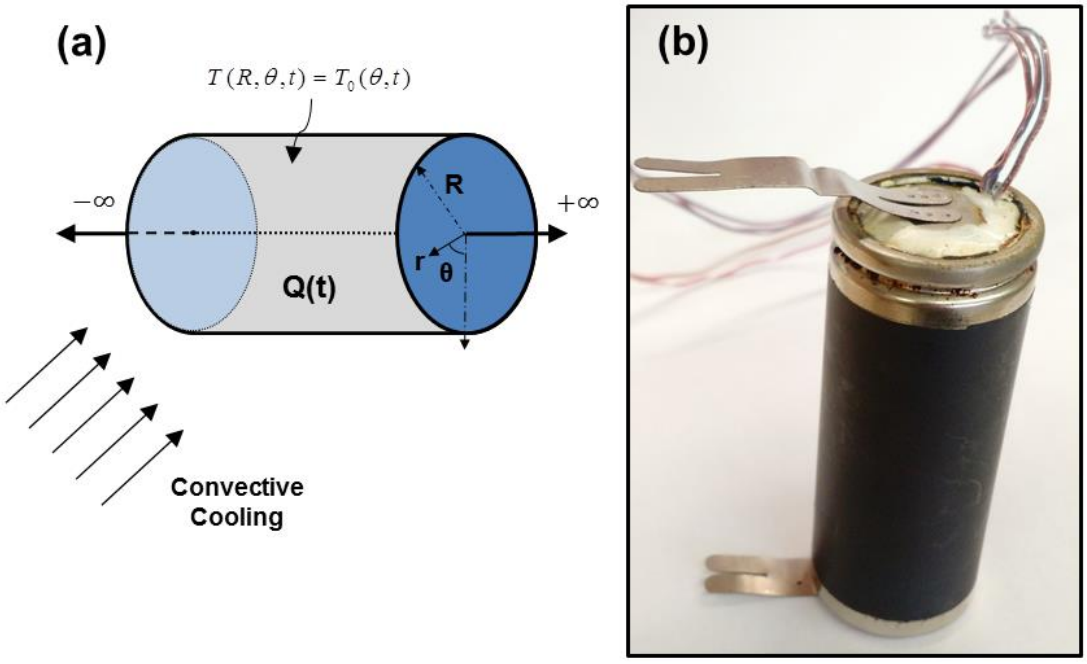

29. Figure 1: (a) Schematic of the geometry considered in this work, (b) Picture of a 26650 Li-ion cell with embedded thermocouple. Note that black graphite film on one side of the outer surface for infrared surface temperature measurements.

A theoretical model to predict the core temperature of a heat-generating cylinder as a function of time based on measurements of the temperature field on the outside surface of the cylinder has been presented in a recent paper [32]. Figure 1(a) shows a schematic of an infinite cylinder of radius R with volumetric heat generation $Q(t)$ occurring within. This model can be applied to a heat-generating, cylindrical Li-ion cell shown in Figure 1(b), for which the core temperature $T_0(t)$ is of interest. The outside surface temperature of the cylinder, $T_{out}(\theta,t)$ is measured circumferentially and as a function of time. When the heat generation rate $Q(t)$ is a constant, it has been shown [32] that utilizing the measured outside temperature as a transient boundary condition, the governing energy conservation equations can be solved using the

method of undetermined parameters. This has been shown [32] to result in the following expression for the core temperature $T_0(t)$

$$T_0(t) = T_{0,A}(t) + T_{0,B}(t) = \left[\frac{QR^2}{4k_r} + \sum_{n=1}^{\infty} u_n e^{-\alpha_r \mu_n^2 \cdot t} \right] + \sum_{n=1}^{\infty} v_{0n}(t) \tag{1}$$

Where k_r and α_r are the thermal conductivity and thermal diffusivity respectively of the cylinder material. The coefficients u_n and $v_{0,n}(t)$ are given by

$$u_n = \frac{-\frac{Q}{4k_r} \int_0^R \left(R^2 - r^2\right) \cdot r J_0(\mu_n r) dr}{N_{r,n}} \tag{2}$$

And,

$$v_{0n}(t) = \frac{\alpha_r \mu_n R J_1(\mu_n R)}{N_{r,n}} \int_0^t w_{0I}(\tau) \exp\left[-\alpha_r \mu_n^2 (t-\tau)\right] d\tau \tag{3}$$

In equations (2)-(3), $\mu_n R$ are roots of J_0, the Bessel function of the first kind and order zero. The eigenfunction normalization integral N_n is given by

$$N_n = \frac{R^2 J_1(\mu_n R)^2}{2} \tag{4}$$

Finally, $w_{0I}(\tau)$ is the circumferential integral of the outside temperature $T_{out}(\theta,\tau)$ at any time, given by

$$w_{0I}(\tau) = \frac{1}{2\pi} \int_0^{2\pi} T_{out}(\theta, \tau) d\theta \tag{5}$$

Note that when the heat generation rate Q is a function of time, the first term $T_{0,A}(t)$ in equation (1) must be replaced by

$$T_{0,A}(t) = L^{-1}\left[\frac{\alpha_r \overline{Q}}{sk_r}\left(1 - \frac{1}{I_0\left(\sqrt{\frac{s}{\alpha_r}}R\right)}\right)\right] \tag{6}$$

Where L^{-1} is the inverse Laplace transform, $\overline{Q}$ is the Laplace transform of $Q(t)$, and I_0 refers to modified Bessel function of the first kind and of order zero.

Equation (1) provides the basis for determining the core temperature of a Li-ion cell undergoing a discharge process that generates a certain amount of heat based on measurements of the outside surface temperature. Note that the core temperature at any given time depends on the measured surface temperature field at all prior times, which must be integrated in space as shown in equation (5) and then in time as shown in equation (3). Details of this key theoretical result may be obtained from a recent paper [32].

3. Experimental Methods

3.1. Assembly of Li-Ion Cell with Embedded Core Thermocouple

In order to fabricate an operating cell with a core-embedded thermocouple, Lithium iron phosphate (LFP) cells of a 26650 form factor are received from the manufacturer, as shown in Figure 2(a). The cells have no electrolyte and are unsealed, which allows for thermocouple insertion before the cell becomes electrochemically active. To precisely mimic the performance of production cells, electrolyte of the same formulation used in the production cells (1:1:1 of EC:DEC:DMC with $LiPF_6$ salt) is obtained. The production version of these cells has nominal capacity of 2.85 A-hr, and is capable of operating between a maximum range of 2.0 V to 4.1 V at a maximum rate of 42 A continuous discharge and 5 A continuous recharge. The nominal voltage

for these cells is 3.2 V during discharge at the nominal 1C rate of 2.8 A. In order to ensure the best seal possible for the cell after fabrication, a hole is first drilled in the underside pressure cap below the top nip connection on the positive terminal, as shown in Figure 2(b). During drilling, the cell is mounted on its side and the opening exposing the jelly roll is covered to prevent any metal shavings from falling in. After this is accomplished, a 2.3 mm steel rod is used to widen the space in the center of the jelly roll in order to create enough space for the thermocouple assembly to be inserted into the core.

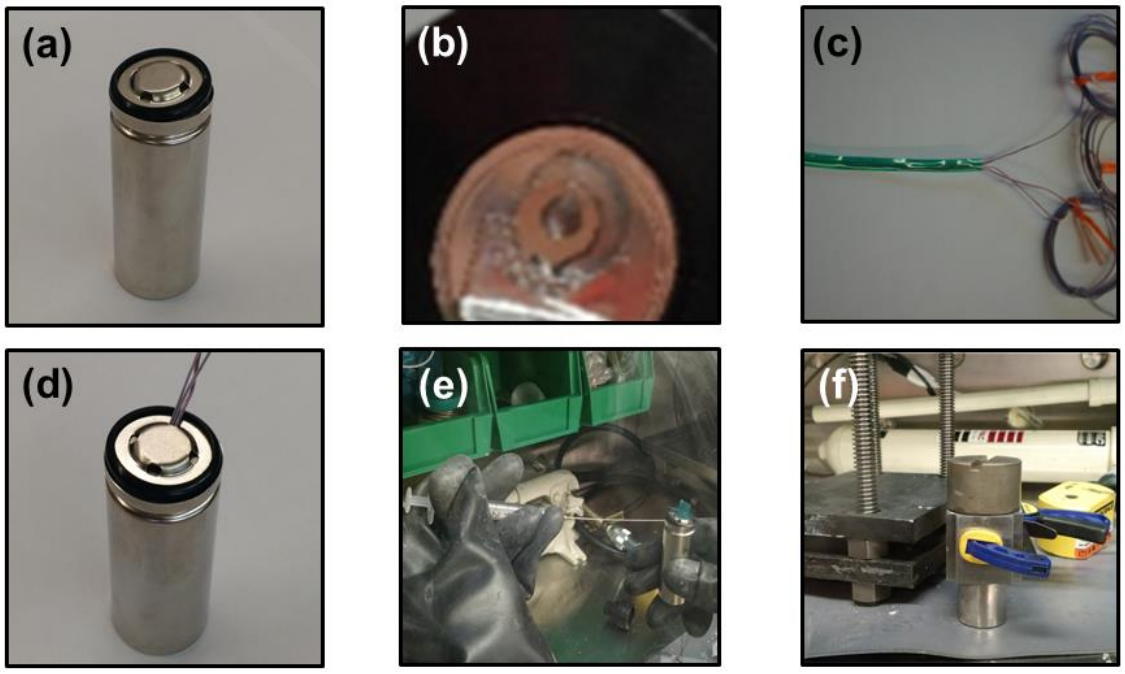

30. Figure 2: Pictures of various steps in the fabrication of a 26650 Li-ion cell with embedded thermocouple in the core of the cell.

The thermocouple assembly consists of three thermocouples, which are epoxied to the inside of a heat shrink tube at different lengths from the base of the cell, as shown in Figure 2(c). When the epoxy is dried out, a heat gun is used to collapse the heat shrink around the thermocouples. This assembly is then carefully inserted into the core of the test cell and the other end of the thermocouple wires are fed through the drilled hole and out of the small ports between the top nip and the pressure cap, as shown in Figure 2(d). The hole in the pressure cap is then

filled with marine epoxy, and the cell is mounted upside down to allow the resin to fill the entire cavity between the nip and the pressure cap. This ensures a robust seal to avoid leakage of electrolyte and reactivity with the ambient environment. The cell is then left for twenty-four hours to allow time for the epoxy to cure completely before electrolyte filling begins.

After the marine epoxy completely cures, the cell is transferred into a glove box and filled with 10 mL electrolyte solution using a 3 mL long needle syringe, as shown in Figure 2(e). The electrolyte is introduced in stages to ensure complete filling. Three to five filling stages are required to completely introduce all 10 mL into the cell. In each of these stages, electrolyte is introduced until the level is near the brim of the casing. Fifteen minutes are allowed between stages or until the level of electrolyte solution had gone down far enough for another session to begin. This ensures that the electrode films are saturated with electrolyte solution. After this is complete, the cell is ready to be crimped.

In order to press the crimping dies for these cells within the glove box, a makeshift hydraulic press is constructed by using two steel plates and a hydraulic lifting cell as shown in Figure 2(f). The first die bends the top lip into a cone shape, while the next two dies are flat, which press the bent lip firmly against the rubber seal. The dies have a through hole in the center to allow the thermocouple wires to be fed through and prevent damage from compression. After the three stages of dies have been pressed onto the cell, it is allowed to sit in the glove box for twenty-four hours to achieve chemical neutrality.

3.2. Experimental Setup for Core Temperature Measurement

A picture of the experimental setup and a schematic of the experimental data flow for non-invasively measuring the core temperature of the fabricated Li-ion cell using surface

temperature measurements, are shown in Figure 3. The Li-ion cell is placed on two thin, tapered foam risers to minimize stray heat loss, and placed on an optical breadboard directly under a FLIR A6703 InSb infrared camera. The external surface of the Li-ion cell is covered with a DGF graphite aerosol spray to ensure a high and uniform surface emissivity.

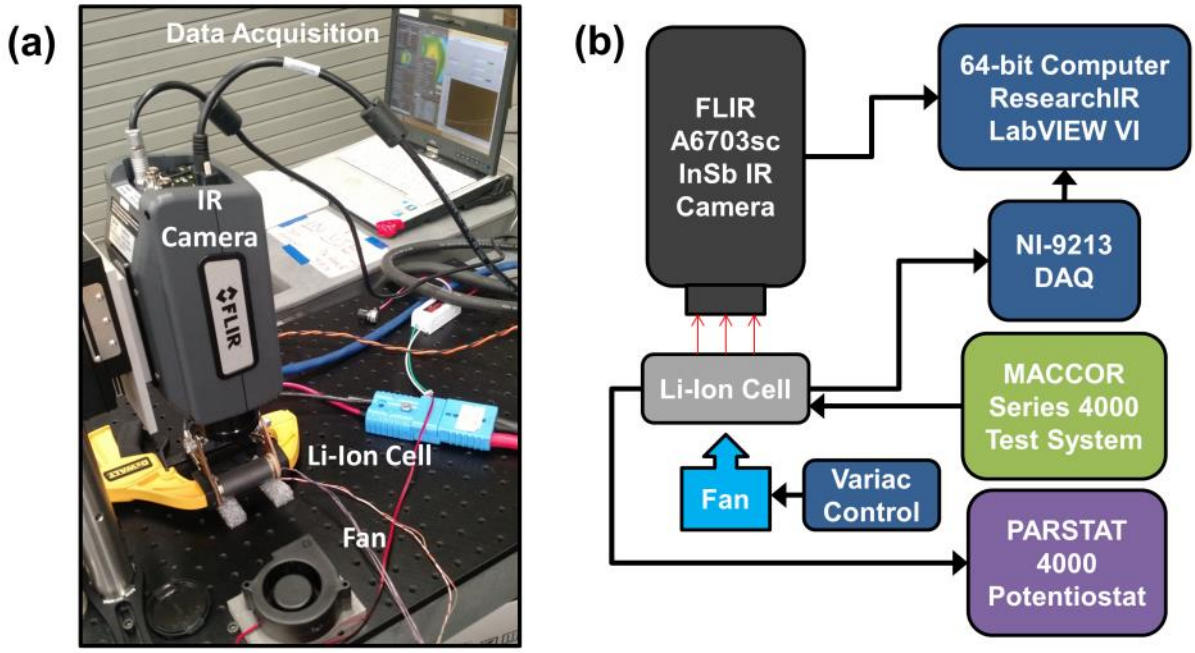

31. Figure 3: (a) Picture and (b) Schematic of the experimental setup for determining core temperature during high-rate discharge using surface temperature data acquisition and analysis.

As shown in Figure 3(a), lead wires from a MACCOR Series 4000 Automated Test System are attached to the power leads of the cell for charging and discharging the cell. A separate set of wires also connect the cell to a PARSTAT 4000 Potentiostat for EIS testing between experiments. The cell is subjected to a variety of programmable charging and discharging profiles. A small Fugetek HT-07530D12 computer fan is used for forced convection experiments to provide cooling to the Li-ion cell. The fan is placed on a metal riser in order to align the fan with the longitudinal axis of the Li-ion cell. This ensures direct and symmetrical impingement of air from the fan to the cell. A variable resistor controller is then used to control the speed of the fan for variable fan speed experiments. Air speed from the fan is measured using

an Extech mini thermo-anemometer. Thermocouples embedded in the cell are connected to a NI-9213 DAQ thermocouple module. Data acquisition is carried out through LabView software with a frequency of 1 Hz. Infrared temperature measurements are carried out using ResearchIR software, also at a frequency of 1 Hz. Both measurements are carried out once every second. This measurement rate is appropriate for this system which has a relatively larger time constant compared to the data acquisition time interval.

3.3. Electrochemical Measurements

The initial cycling procedure conducted on the test cell is intended to grow the initial layers of surface film on the electrodes. The cell is charged at 0.56 A to 4.1 V using a constant current-constant voltage profile (CC-CV) and a current cutoff of 0.30 A. While the maximum voltage for this chemistry is normally 3.65 V, the range is extended in order to promote the formation of the solid electrolyte interphase layer. This surface film is critical to the cycle life of the cell. After this step, the cell is cycled five times at the same rate using the same CC-CV procedure and a CC discharge procedure also at 0.56 A. To ensure that the cell is safe to operate, an initial discharge is conducted at approximately ten times the nominal rate (25 A).

After the high rate discharge test, the cell is recharged to 100% state of charge (SOC). An initial galvanic EIS spectrum is collected from 1 kHz to 5 mHz with a 1.00 A amplitude. For comparison, EIS of a baseline cell filled and sealed without any thermocouples inserted in its core is also carried out. The EIS spectra presented in Figure 4 show very similar electrochemical behavior when comparing the control cell (dashed line) with the thermocouple cell (solid line). There is only a slight increase in the real impedance of the cell due to insertion of the thermocouple assembly. The magnitude of the imaginary impedance in the mid-frequency semi-

circle for the thermocouple cell is only 1 mΩ less than that of the control cell. This indicates that while the Ohmic resistance of the cell is increased by the presence of the thermocouple assembly, there is no reaction with battery chemicals and active material.

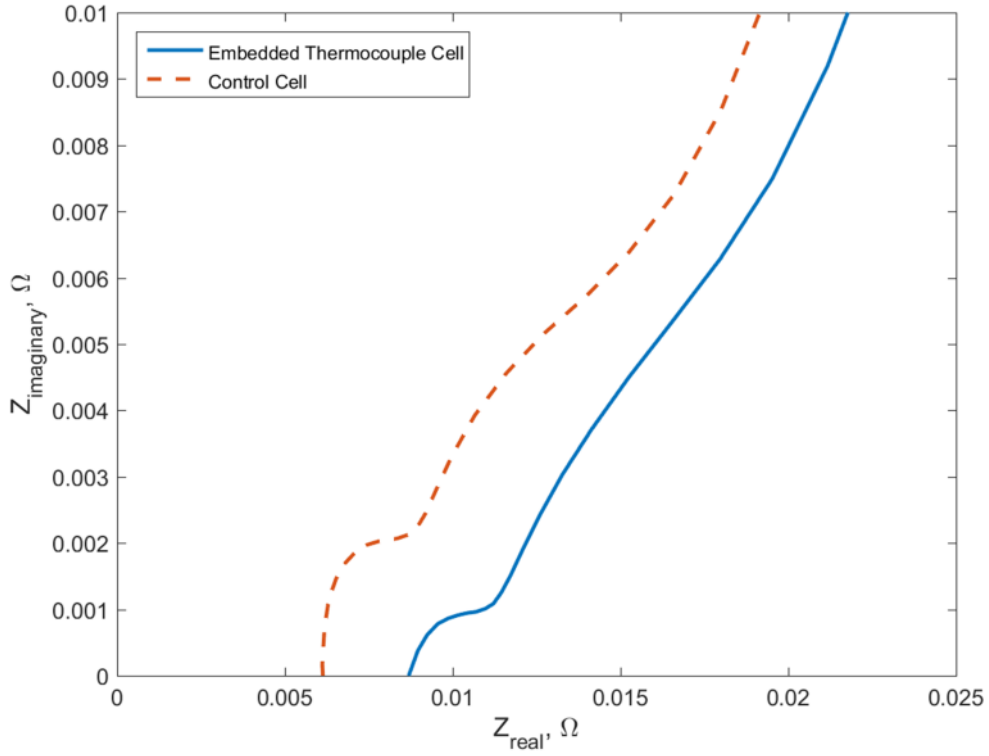

32. Figure 4: Comparison of the Nyquist plot between the 26650 cell containing an embedded thermocouple and a control cell without embedded thermocouple.

The Ohmic resistance, which is found from the x-axis intercept of the Nyquist plot, is only a few mΩ greater than that of the baseline cell. Similarity between the test and control cells is further supported by the observation that the Warburg tail in the low frequency region after the initial semi-circle remains virtually unchanged. The slope of the Warburg tail is nearly the same for the control cell and the test cell, which shows that impedance to diffusional processes such as the tunneling of Lithium-ions in electrode materials remains unaffected by the presence of the thermocouple assembly. Thus, in comparison to the control cell, the test cell does not exhibit any abrupt change in its electrochemical behavior due to the presence of the embedded thermocouple.

3.4. Core Temperature Measurements

Infrared temperature measurement usually requires exhaustive calibration. In this case, the surface of interest is coated with a graphite film, which is calibrated in advance by measuring the temperature of an Instec HCS662V thermal stage coated with the same graphite spray. Measurements of the surface temperature during a defined temperature ramp are compared with the true temperature of the stage measured by an embedded thermocouple, showing very close agreement between the two for the entire ramp duration, with a peak deviation of only 0.31°C. This establishes a baseline calibration for the camera and shows the capability of accurately measuring the temperature of a surface coated with graphite spray.

Once calibration is completed, a number of experiments are carried out at different discharge rates in order to measure the core temperature of the Li-ion cell using the method outlined in section 2. In each case, the Li-ion cell starts fully charged at ambient temperature, and a constant or time-varying discharge is conducted using the MACCOR cycler. The temperature distribution on the surface of the cell is measured in time using the infrared camera while the cell potential reaches 2.0 V. This is controlled by a shut off flag in the cycling procedure. The temperature field around the circumference of the cell at mid-height is extracted from the measured two-dimensional temperature field from the infrared camera. These data are subjected to a mathematical transformation to account for the projected view of the curved surface of the Li-ion cell as viewed by the infrared camera [32].

Three sets of experiments are carried out on the Li-ion cell. First, the core temperature of the cell is measured using surface temperature measurements at a number of discharge rates while the Li-ion cell is cooled via natural convection conditions. Then a set of experiments is

carried out for the same discharge rates, with forced convective cooling from a fan operating at various speeds. Finally, experiments are carried out to simulate an anomalous increase in heat generation, as in the case of thermal runaway [18], for each of the previously discussed cooling conditions. In these experiments, the MACCOR provides a constant 4C discharge load for a period of 7.5 minutes, followed by a much larger 10C load for the remainder of the cell capacity, for another 3 minutes.

A stabilization time of a few minutes is provided in each experiment with air flow from the fan before the experiment commences. At the conclusion of each experiment, the cell is charged at a rate of 1C and allowed to cool for a few hours. An EIS test is carried out to ensure that the EIS profile and cell internal resistance have not changed appreciably before proceeding to the next experiment. An extended cool-down period is provided between experiments to ensure that each experiment begins with the entire cell at ambient temperature. In each experiment, the core temperature of the cell is determined using the experimentally measured surface temperature distribution in conjunction with the theoretical model presented in section 2. These core temperature measurements are compared against measurements from the embedded thermocouple in the Li-ion cell to validate the temperature measurement method.

4. Results and Discussion

Figure 5 shows results from an experiment in which the 26650 cell with embedded thermocouple is subjected to 10C discharge while its surface temperature distribution is measured using infrared thermography. Using the surface temperature data and equations (1)-(5), the two components of the core temperature, $T_{0,A}$ and $T_{0,B}$ are calculated as functions of time. 415

eigenvalues are used for $T_{0,A}$ and $T_{0,B.}$ Past work suggests slow convergence of the infinite series for $T_{0,B}$ [32], which necessitates computation of a large number of terms.

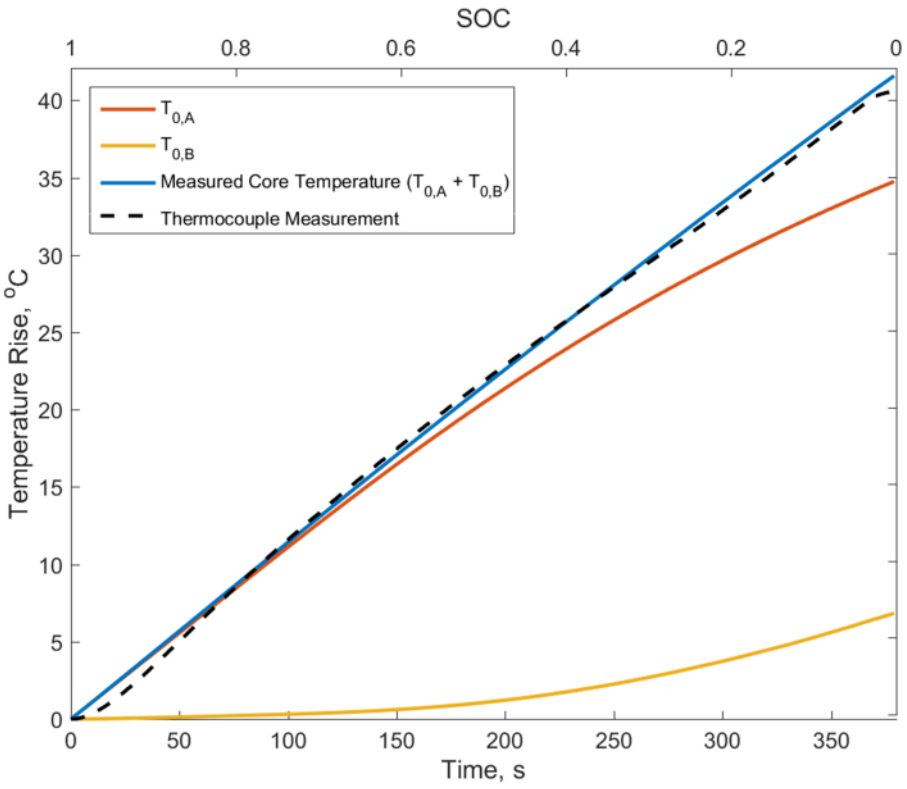

33. Figure 5: Plot of the predicted core temperature and its components $T_{0,A}$, $T_{0,B}$ as functions of time for a 10C discharge. For reference, the core temperature measured by the embedded thermocouple is also plotted.

Figure 5 plots these components as well as their sum, which, according to the theoretical model determines the core temperature of the cell as a function of time. For reference, the true core temperature of the cell, measured through the embedded thermocouple is also plotted in Figure 5. Figure 5 shows that both $T_{0,A}$ and $T_{0,B}$ increase as the discharge process progresses. $T_{0,A}$ is convex in nature, rising fast initially and then plateauing out. On the other hand, $T_{0,B}$ remains flat to begin with, and then starts rising in a concave fashion. The sum of $T_{0,A}$ and $T_{0,B}$ is found to closely match the actual core temperature of the cell, measured by the embedded thermocouple. The worst-case disagreement between the two over the entire experimental duration is less than

1°C. This demonstrates the capability of this experimental method to accurately determine the core temperature based on measurements of the surface temperature distribution.

Note that determining the core temperature in this fashion requires information about the heat generation rate in the cell, as well as various thermal properties of the cell, including thermal conductivity and specific heat. In this case, the heat generation rate is obtained from prior measurements on a 26650 cell [7] that showed that heat generation rate in a 26650 cell increases quadratically with C-rate. Further, since heat generation also depends linearly on the internal resistance of the cell, the heat generation from past measurements is scaled based on the ratio of the internal resistances from EIS measurements. The heat generation rate is assumed to be a constant, although in reality, there may be minor variations with time, particularly towards the start and finish of the discharge process [33], which may be the reason behind the increased disagreement between these measurements and thermocouple measurement of the core temperature at the start and finish of the discharge process.

Further, note that the thermal conductivity and heat capacity of the 26650 cell are obtained from past papers that have reported measurements of these thermophysical properties [9,34] for a 26650 Li-ion cell.

These experiments are repeated at a number of discharge rates. In each case, the computed core temperature based on the theoretical model is compared against core temperature measurement using the embedded thermocouple during the entire discharge period. This comparison is shown in Figure 6. As expected, the temperature rise is greater for higher C-rates due to increased heat generation rate. There is good agreement between the core temperature prediction and the thermocouple measurement over the entire discharge duration for each C-rate.

The agreement between the two is particularly good at higher discharge rates, which is also where accurate measurement of the core temperature is particularly critical due to large temperature rise and the need for effective thermal management. There is somewhat greater disagreement at lower C-rates, possibly because at lower C-rates, the temperature rise itself is so small that measurement uncertainties are relatively larger. Further, variation in heat generation rate as a function of time appears to be more significant at lower C-rates. Regardless, the disagreement between the core temperature determined through surface temperature measurements and direct thermocouple measurements is less than 1.4°C for the worst-case 1C discharge and less than 1.0°C for the 10C discharge.

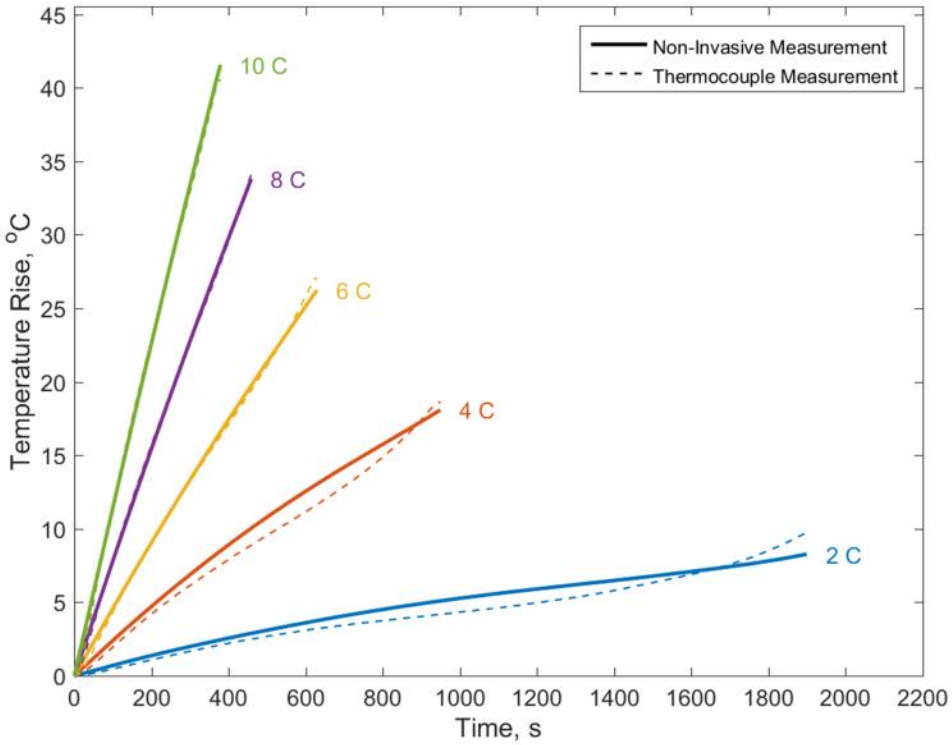

34. Figure 6: Comparison of core temperature determined from the technique described in this paper with direct measurements from the embedded thermocouple for a number of discharge rates.

In addition to constant-rate discharge, processes involving multiple rates of discharge are also common and technologically relevant. A change in the rate of discharge may occur when the power load changes, for example, in an electric vehicle due to acceleration and deceleration. In

an extreme case involving abuse of the cell, the discharge rate can also go up dramatically due to short circuit. In each case, as the discharge rate increases, so does the rate of heat generation, and hence it becomes critical to be able to monitor the core temperature of the cell during such processes. In order to demonstrate the capability of this core temperature measurement method in such a scenario, the 26650 Li-ion cell is discharged, starting at 4C, and then increasing abruptly to 10C. The core temperature of this cell, measured using the embedded thermocouple is compared with the prediction from the theoretical model using surface temperature distribution measurements.

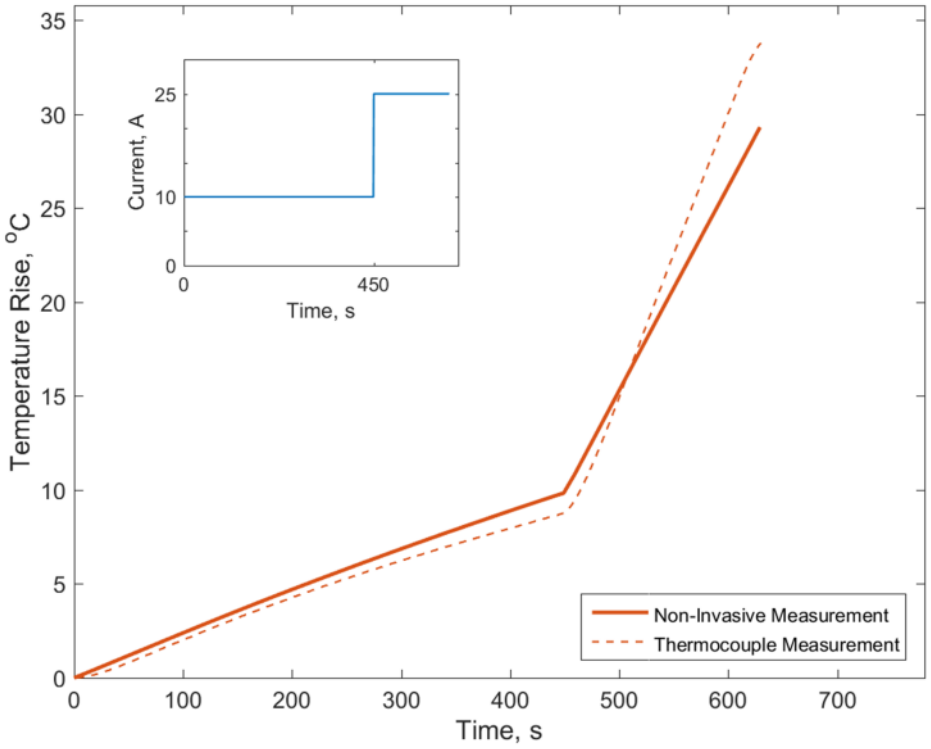

35. Figure 7: Comparison of core temperature determined from the technique described in this paper with direct measurements from the embedded thermocouple for a discharge process where the C-rate changes abruptly from 4C to 10C.

There is excellent agreement between the two, as shown in Figure 7, which shows that the temperature increases slowly during the 4C discharge, and the rate of temperature rise increases once the discharge rate goes up. During both phases of discharge, the predicted core

temperature is in good agreement with measurements from the embedded thermocouple. The predicted core temperature is somewhat lower than the thermocouple measurement towards the end of the higher-rate discharge, which could possibly be due to larger-than-expected heat generation rate towards the end of the discharge period.

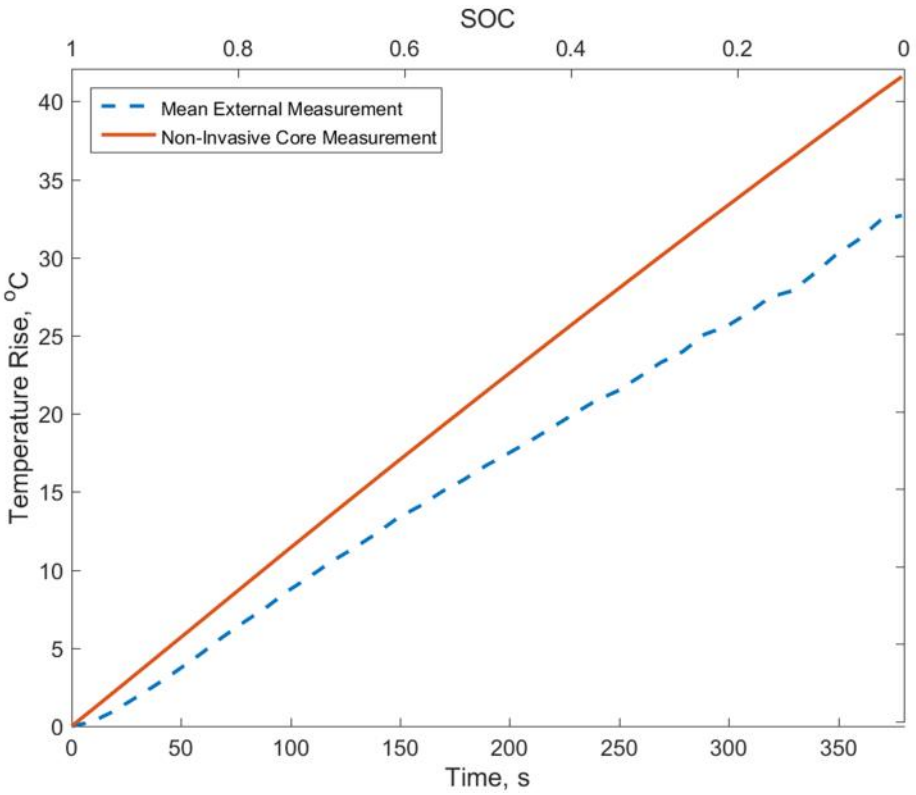

36. Figure 8: Comparison of predicted core temperature with the measured mean surface temperature for 10C discharge, showing significantly higher core temperature compared to surface temperature.

A key goal for this method of determining the core temperature of the cell is to provide a better estimate of the thermal health of the cell. In the absence of a method to determine the core temperature of the cell, thermal management and performance optimization may need to be based on surface temperature measurement alone, which is clearly not representative of the peak temperature that must be known for optimal control and thermal management, and which occurs at the core of the cell. Figure 8 plots the non-invasively measured core temperature and the circumferentially averaged surface temperature of the cell as a function of time during a 10C

discharge. These data clearly show that while the surface and core temperatures are close to each other at the start of the discharge process, the difference between the two grows as the cell discharges. By the completion of discharge, there is an almost 10°C difference between the core and surface temperatures. This demonstrates the importance of using the measured core temperature instead of surface temperature for thermal management and performance optimization. Cooling of the cell based on surface temperature will simply not be effective because the surface temperature of the cell is significantly lower than the core temperature, which may lead to under-provisioning of cooling when the core of the cell is actually much hotter and in urgent need of cooling.

4. Conclusions

Internal temperature measurement in Li-ion cells is a critical metrology need that directly affects performance and safety. The non-invasive measurement method described in this paper directly addresses this need. While measurements have been demonstrated in this paper on cylindrical cells, a similar approach could be adopted for prismatic cells as well. Information about the core temperature of the cell during operation using this method can be used for a performance management as well as for taking proactive decisions for ensuring thermal safety of the cell. This work contributes towards improved thermal and electrochemical design of energy conversion and storage systems where overheating is a concern due to high discharge rates or unforeseen events such as thermal runaway.

Acknowledgments

This material is based upon work supported by CAREER Award No. CBET-1554183 from the National Science Foundation. Support from Office of Naval Research through grant N00014-16-1-2223 is also gratefully acknowledged.

References

[1] B. Scrosati, J. Hassoun, Y.-K. Sun, Energy Environ. Sci. 4 (2011) 3287-3295. DOI: 10.1039/C1EE01388B

[2] R.A. Marsh, S. Vukson, S. Surampudi, B.V. Ratnakumar, M.C. Smart, M. Manzo, P.J. Dalton, J. Power Sources 97 (2001) 25-27. DOI: 10.1016/S0378-7753(01)00584-5

[3] A. Khaligh, Z. Li, IEEE Trans. Vehic. Technol. 59 (2010) 2806-2814. DOI: 10.1109/TVT.2010.2047877

[4] V. Srinivasan, C.Y. Wang, J. Electrochem. Soc. 150 (2003) A98-A106. DOI: 10.1149/1.1526512

[5] K.E. Thomas, J. Newman, J. Power Sources 119 (2003) 844-849. DOI: 10.1016/S0378-7753(03)00283-0

[6] D. Bernardi, E. Pawlikowski, J. Newman, J. Electrochem. Soc. 132 (1985) 5-12. DOI: 10.1149/1.2113792

[7] S.J. Drake, M. Martin, D.A. Wetz, J.K. Ostanek, S.P. Miller, J.M. Heinzel, A. Jain, J. Power Sources 285 (2015) 266-273. DOI: 10.1016/j.jpowsour.2015.03.008

[8] G. Zhang, L. Cao, S. Ge, C.Y. Wang, C.E. Shaffer, C.D. Rahn, J. Electrochem. Soc. 161 (2014) A1499-A1507. DOI: 10.1149/2.0051410jes

[9] S.J Drake, D.A. Wetz, J.K. Ostanek, S.P. Miller, J.M. Heinzel, A. Jain, J. Power Sources 252 (2014) 298-304. DOI: 10.1016/j.jpowsour.2013.11.107

[10] V. Vishwakarma, C. Waghela, Z. Wei, R. Prasher, S.C. Nagpure, J. Li, F. Liu, C. Daniel, A. Jain, J. Power Sources 300 (2015) 123-131. DOI: 10.1016/j.jpowsour.2015.09.028

[11] K. Shah, S.J. Drake, D.A. Wetz, J.K. Ostanek, S.P. Miller, J.M. Heinzel, A. Jain, J. Power Sources 271 (2014) 262-268. DOI: 10.1016/j.jpowsour.2014.07.118

[12] K. Shah, S.J. Drake, D.A. Wetz, J.K. Ostanek, S.P. Miller, J.M. Heinzel, A. Jain, J. Power Sources 258 (2014) 374-381. DOI: 10.1016/j.jpowsour.2014.01.115

[13] D. Anthony, D. Wong, D. Wetz, A. Jain, Improved Thermal Performance of a Li-ion Cell Through Heat Pipe Insertion, J. Electrochem. Soc., in review (2016).

[14] T.M. Bandhauer, S. Garimella, T. Fuller, J. Electrochem. Soc. 158 (2011) R1-R25. DOI: 10.1149/1.3515880

[15] K. Shah, V. Vishwakarma, A. Jain, ASME J. Electrochem. Energy Convers. & Storage 13 (2016) 030801:1-13. DOI: 10.1115/1.4034413

[16] Q. Wang, P. Ping, X. Zhao, G. Chu, J. Sun, C. Chen, J. Power Sources 208 (2012) 210–224. DOI: 10.1016/j.jpowsour.2012.02.038

[17] R. Spotnitz, J. Franklin, J. Power Sources 113 (2003) 81-100. DOI: 10.1016/S0378-7753(02)00488-3

[18] K. Shah, D. Chalise, A. Jain, J. Power Sources 330 (2016) 167-174. DOI: 10.1016/j.jpowsour.2016.08.133

[19] R. Zhao, S. Zhang, J. Liu, J. Gu, J. Power Sources 299 (2015) 557-577. DOI: 10.1016/j.jpowsour.2015.09.001

[20] N. Nieto, L. Diaz, J. Gastelurrutia, F. Blanco, J.C. Ramos, A. Rivas, J. Power Sources 272 (2014) 291-302. DOI: 10.1016/j.jpowsour.2014.07.169

[21] Z. Rao, S. Wang, M. Wu, Z. Lin, F. Li, Energy Convers. Manag. 65 (2013) 92-97. DOI: 10.1016/j.enconman.2012.08.014

[22] C.V. Hémery, F. Pra, J.F. Robin, P. Marty, J. Power Sources 270 (2014) 349-358. DOI: 10.1016/j.jpowsour.2014.07.147

[23] S.K. Mohammadian, Y.L. He, Y. Zhang, J. Power Sources 293 (2015) 458-466. DOI: 10.1016/j.jpowsour.2015.05.055

[24] S. Pannala, H. Wang, K. Kepler, S. Allu, Electrochem. Soc. MA2014-02 (2014) 445.

[25] C. Forgez, D.V. Do, G. Friedrich, M. Morcrette, C. Delacourt, J. Power Sources 195 (2010) 2961-2968. DOI: 10.1016/j.jpowsour.2009.10.105

[26] Thermal Sensors: Principles and Applications for Semiconductor Industries, C.M. Jha (Ed.), Springer-Verlag, NewYork, 2015. ISBN: 978-1-4939-2580-3; DOI: 10.1007/978-1-4939-2581-0

[27] M.S.K. Mutyala, J. Zhao, J. Li, H. Pan, C. Yuan, X. Li, J. Power Sources 260 (2014) 43-49. DOI: 10.1016/j.jpowsour.2014.03.004

[28] R. Srinivasan, B.G. Carkhuff, M.H. Butler, A.C. Baisden, O.M. Uy, Proc. SPIE 8035, Energy Harvest. and Storage: Mater., Devices, and Appl. II (2011) 80350D. DOI: 10.1117/12.884691

[29] S. Novais, M. Nascimento, L. Grande, M.F. Domingues, P. Antunes, N. Alberto, C. Leitão, R. Oliveira, S. Koch, G.T. Kim, S. Passerini, Sensors 16 (2016) 1394. DOI: 10.3390/s16091394

[30] S.J. Norton, L.R. Testardi, H.N.G. Wadley, Proc. Ultrasonics Symp. (1983) 852-855. DOI: 10.1109/ULTSYM.1983.198180

[31] D. Anthony, D. Sarkar, A. Jain, Int. J. Heat Mass Transfer 101 (2016) 779-788. DOI: 10.1016/j.ijheatmasstransfer.2016.05.073

[32] D. Anthony, D. Sarkar, A. Jain, Scientific Reports 6 (2016) 35886:1-10. DOI: 10.1038/srep35886

[33] Y. Ye, L.H. Saw, Y. Shi, K. Somasundaram, A.A.O. Tay, Electrochimica Acta 134 (2014) 327-337. DOI: 10.1016/j.electacta.2014.04.134.

[34] J. Zhang, B. Wu, Z. Li, J. Huang, J. Power Sources 259 (2014) 106-116. DOI: 10.1016/j.jpowsour.2014.02.079

CHAPTER 5:

IMPROVED THERMAL PERFORMANCE OF A LI-ION CELL THROUGH HEAT PIPE INSERTION

Dean Anthony[1], Derek Wong[2], David Wetz[2], Ankur Jain[1],*

[1] - Mechanical and Aerospace Engineering Department
[2] – Electrical Engineering Department
University of Texas at Arlington, Arlington, TX, USA

[*] – Corresponding Author: email: jaina@uta.edu;
500 W First St, Rm 211, Arlington, TX, USA 76019
Ph: +1 (817) 272-9338; Fax: +1 (817) 272 2952

D. Anthony, D. Wong, D. Wetz, A. Jain, Improved Thermal Performance of a Li-ion Cell Through Heat Pipe Insertion, *J. Electrochem. Soc.*, in review, 2016.

Abstract

Li-ion cells offer excellent energy storage and conversion characteristics, but also suffer from performance and safety problems related to overheating due to insufficient heat removal during operation. Traditional thermal management approaches cool the cell at its outer surface, whereas it is more critical to cool the core of the cell where heat accumulation occurs. This paper investigates thermal performance of a 26650 Li-ion cell with a heat pipe inserted into the core. Heat pipe integrated cells are assembled starting from unfilled, unsealed cells. Thermal benefit of heat pipe insertion is characterized at a number of discharge rates. Advantages of heat pipe cooling compared to traditional surface-based cooling approach are quantified. It is shown that active cooling of the protruding tip of the heat pipe results in maximum thermal benefit, which is shown to reduce the core temperature to as low as, or even lower than the surface temperature. The heat pipe is shown to reduce temperature rise in case of anomalous increase in heat generation. While heat pipe insertion involves significant manufacturing challenges to ensure long-term reliability, the thermal benefits in doing so may potentially outweigh these challenges, and offer an effective thermal management approach for future Li-ion cell designs.

*Keywords***:** Lithium Ion Battery, Thermal Management, Heat Removal, Battery Safety, Heat Pipes.

1. Introduction

Heat removal from a Li-ion cell is an important technological challenge that directly affects performance, reliability and safety of energy conversion and storage systems, including batteries for consumer electronics, electric vehicles, stationary power systems, etc. [1,2]. Heat generated during the operation of a Li-ion cell due to Ohmic losses, electrochemical reactions,

etc. [3-5] causes temperature rise. High temperature in a Li-ion cell results in reduced performance and lifetime due to capacity/power fade [6,7], self-discharge [8,9] and other reasons. Safety of Li-ion cells at high temperatures is also a critical concern due to the well-known phenomenon of thermal runaway [10,11], in which accelerated heat generation rate at higher temperatures due to a variety of physical and chemical processes may result in an ever-increasing cell temperature [12], eventually leading to catastrophic failure [10-13]. As a result, it is important to maximize heat removal from a Li-ion cell during operation.

Heat is generated inside a Li-ion cell due to a variety of electrochemical processes occurring within [3-5,14]. Heat generation is usually assumed to be spatially uniform, although there may be somewhat larger heat generation at the metal tabs due to Joule heating. Li-ion cells are traditionally cooled on the outside surface through flow of a cooling fluid such as water or air [1,2] or using a cold plate [15]. In these approaches, heat generated throughout the volume of the cell must be conducted through the cell materials to the surface. The thermal conduction process within the cell is known to be severely impeded by large thermal contact resistances between cell materials inside [16], resulting in very poor radial thermal conductivity [17-18] and as a result, a large temperature difference between the core of the cell and the outside surface [19-20]. Temperature difference of up to 15 °C has been reported for a 26650 cylindrical Li-ion cell discharging at 10C [21-22]. This large temperature gradient highlights the challenge in cooling the entire cell volume by surface-based cooling mechanisms. The influence of surface cooling is restricted only to a region close to the surface, whereas cooling is most needed at the core of the cell, which is difficult to thermally access. Some work exists on removing heat internally through current collectors [23], or by pumping electrolyte through the cell to remove heat, effectively using the electrolyte as the cooling fluid [24]. Some work also exists on fabricating

microchannels within the volume of the cell and using a cooling fluid for heat removal, although these experiments were not carried out in an actual Li-ion cell [25]. These approaches work better than external cooling in reducing the peak temperature of the cell. However, these approaches are complicated, intrusive and require significant amount of energy, for example, to pump coolant through microchannels in the cell. It is clearly desirable to develop thermal management techniques that directly access the core of the cell, while requiring minimum possible energy for operation.

Insertion of a heat pipe into a Li-ion cell may be an effective strategy for cooling the cell core. A heat pipe is a passive heat transfer device that provides highly directional heat transfer between two bodies [26-28]. The operation of a heat pipe involves the evaporation of a liquid contained inside due to heat absorption at one end, which then travels along the heat pipe due to buoyancy to the condenser end. Heat removal results in condensation back to liquid, which travels back to the evaporator end due to gravity, thereby completing the loop [26]. A porous wick structure is usually utilized to enable capillary action on the liquid inside the heat pipe. A typical heat pipe is a hollow and slender cylinder with the working fluid sealed within. While the modeling of processes that occur inside a heat pipe is quite involved [26], the operation of a heat pipe is relatively simple, and does not require active energy input such as pumping. Other advantages include the highly directed nature of cooling, ability to work in space-constrained and other challenging environments and the lack of moving parts. As a result, heat pipes have been used for a variety of thermal management requirements such as cooling of computer microprocessors [29], photovoltaic cell cooling [30], high power LEDs [31] and thermal management of electronics in space [32] where convective cooling is not possible.

Recent advances in heat pipe technology, such as oscillating heat pipes [33] and size miniaturization [34] make heat pipes appropriate for thermal management of Li-ion cells. It is still critical, however, to address manufacturing challenges related to the insertion of the heat pipe in an electrochemically active environment inside the cell. The cell needs to remain hermetically sealed despite the presence of the heat pipe, which should not deteriorate the electrochemical performance of the cell. Nevertheless, because the heat pipe directly accesses the core of the cell where cooling is most needed, there may be significant thermal benefits in the use of heat pipes that may justify these additional challenges. A trade-off between thermal benefits and manufacturing challenges may help determine the extent to which heat pipe technology can be integrated with Li-ion cells to prevent thermal runaway and enhance performance.

A limited amount of past research has investigated the use of heat pipes for the cooling of Li-ion battery packs. However, most of this research has focused on inserting heat pipes between cells in a pack, rather than into a cell itself. Thermal benefit of heat pipes placed between cells is somewhat limited. Thermal management of a Li-ion battery pack with heat pipes touching the outside surfaces of cells has been reported [35]. Thermal performance of a flat heat pipe in a battery pack has been experimentally and numerically characterized [36]. L-shaped heat pipes have been inserted in battery packs for enhanced cooling [37]. The use of flat heat pipes for cooling of a battery-like heating element on its outside surface has been reported [38]. Numerical optimization of a heat pipe based pack-level thermal management system has been reported [39]. In each of these papers, the heat pipe is located outside the Li-ion cell, and thermal performance is reported in terms of the outside surface temperature. This does not provide much information on the extent of temperature reduction at the core of the cell, where it is most needed. A recent

paper reported significant reduction in core temperature upon insertion of a heat pipe into a surrogate thermal test cell similar to a Li-ion cell [40]. However, the insertion of a heat pipe into an actual Li-ion cell has not been reported so far.

This paper carries out experimental investigation into thermal performance enhancement due to a heat pipe inserted in a cylindrical 26650 Li-ion cell. Reduction in core temperature of the Li-ion cell due to the presence of the heat pipe in a variety of operating conditions is reported. Experimental data show that by directing the heat pipe at the core of the cell where temperature is usually the highest and where cooling is most needed, the core temperature can be brought down to as low as the surface temperature, resulting in excellent cooling and thermal uniformity within the cell. The efficacy of heat pipe cooling during discharge at several C-rates is demonstrated. It is also shown that the presence of the heat pipe results in significantly lower core temperature rise in the event of a sudden increase in heat generation rate, such as in a thermal runaway situation. These experimental insights provide a fundamental characterization of thermal performance of heat pipes inserted into Li-ion cells, based on which heat pipe cooling could be evaluated for enhanced safety and performance in future Li-ion cell designs.

2. Experiments

2.1. Assembly of Li-ion Cell with Integrated Heat Pipe

The various steps involved in the assembly of a 26650 Li-ion cell with integrated heat pipe are summarized in Figure 1(a). Non-filled, non-sealed, 26650-sized, 2.8 Ahr lithium iron phosphate (LFP) cells received from the manufacturer (Figure 1(a)-i) are used to assemble working 26650 cells with integrated heat pipe. 1:1:1 of EC:DEC:DMC with 1 M of LiPF6 salt is used as electrolyte, which is the same formulation used for production cells. The cell has a rated

nominal capacity of 2.85 Ahr at a charge at half the nominal rate (C/2). The maximum voltage range in which the cell can be cycled is 2.0 V-4.1 V. The maximum continuous charge rate for the cell is 5.7 A while the maximum discharge rate is 50 A. The maximum thermal operating range of these cells is between -40°C and 85°C. In order to accommodate a protruding heat pipe, a hole is drilled from the underside of the top cap through the pressure plate and the top nip (Figure 1(a)-ii). The cell is leaned on its side during drilling to avoid metal shavings falling into the jelly roll. A T-type thermocouple is attached at mid-cell height on the outside surface of a 100mm long, 2mm diameter heat pipe from Novark Technologies, which is then insulated with polyimide tape (Figure 1(a)-iii). The drilled cell and heat pipe are transferred into an Argon glove box. The heat pipe is carefully inserted in the core of the jelly roll (Figure 1(a)-iv). The cell is then mounted upside down and cavities in the top cap are sealed with marine epoxy. The wet epoxy is pushed down in order to fill the cavity between the top nip and the base of the cap. This ensures a proper seal to prevent electrolyte leakage. The cell is left for two hours to allow time for the epoxy to dry completely.

The cell is then filled with 10 mL of electrolyte solution using a 3 mL long needle syringe. The filling is carried out in stages to allow sufficient time for electrolyte to absorb into the films. Once fully filled, the cells are sealed using a set of custom dies fabricated specifically for this cell. Three stages of dies are used to gradually compress the metallic lip around the rubber seal of the top cap. The dies have a through hole in the center to allow the protruding heat pipe to be unharmed during the sealing process. A shunt is inserted between the die and the hydraulic cylinder to protect the protruding heat pipe from bending during this process. The cells are allowed to sit in the glove box for 24 hours to observe for any leaks in the top cap, following which the initial charging of the cells is carried out.

A picture of the final, assembled Li-ion cell with integrated heat pipe is shown in Figure 1(b). This picture shows a heat pipe that protrudes about 35 mm out of the top of the cell, as well as thermocouple and power leads.

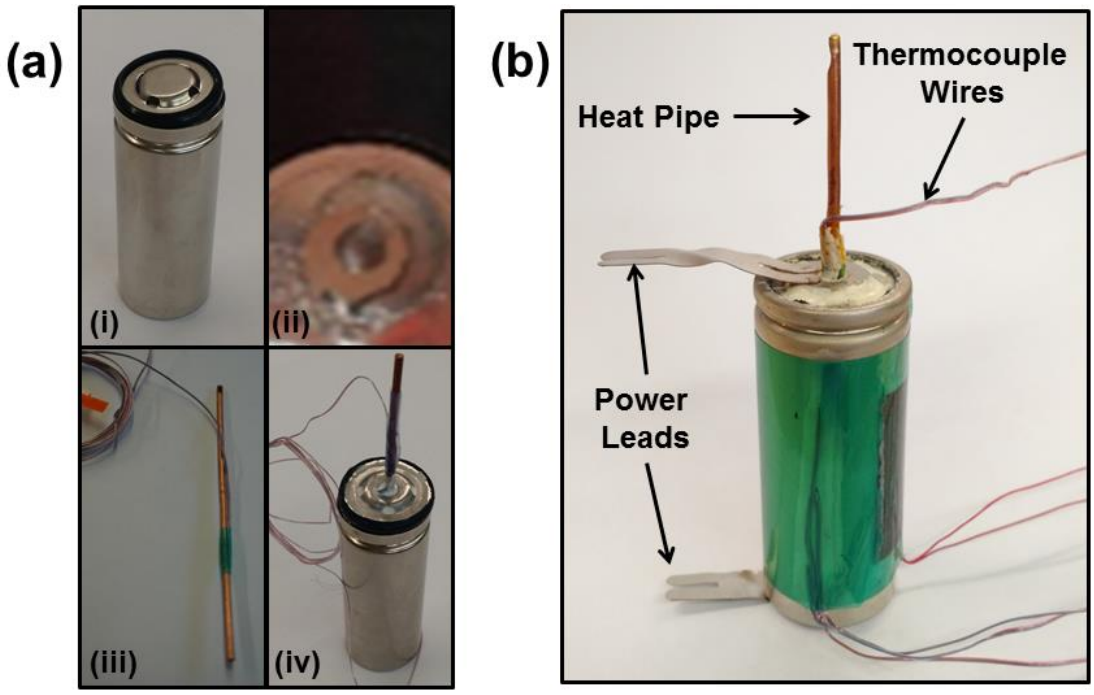

37. Figure 1: (a) Pictures of various steps in the assembly of a 26650 Li-ion cell with integrated heat pipe; (b) Picture of the final assembled Li-ion cell with heat pipe.

2.2. Electrochemical Characterization

A cell startup procedure is carried out by charging the cell at 0.56 A to 4.1 V using a constant current-constant voltage (CCCV) profile, and a current cutoff of 0.30 A using a Maccor Series 4000 Test System. While the recommended voltage cutoff for this chemistry is normally 3.65 V, the range is extended in order to promote the formation of the solid electrolyte interphase layer, which is critical to the cycle life of the cell. The cell is then cycled five times using the same charging profile, and a constant current discharge at 0.56 A while monitoring cell capacity and checking for signs of electrolyte leakage.

The cell is recharged to 100% state of charge (SOC) and an initial galvanic EIS spectrum is collected from 1 kHz to 5 mHz with a 1.00 A amplitude using a Princeton Applied Research PARSTAT 4000 series potentiostat. A similar characterization is also carried out for a control cell, which is filled and sealed without a heat pipe inserted into the core. The two EIS spectrums shown in the Nyquist plot in Figure 2 indicate very similar electrochemical behavior of the heat pipe cell and a control cell. Figure 2 shows that the heat pipe cell and control cell are similar to each other in the capacitive response (y-axis) across the entire range of scanned frequencies. This indicates that the heat pipe does not adversely affect the capability of the cell to store charge.

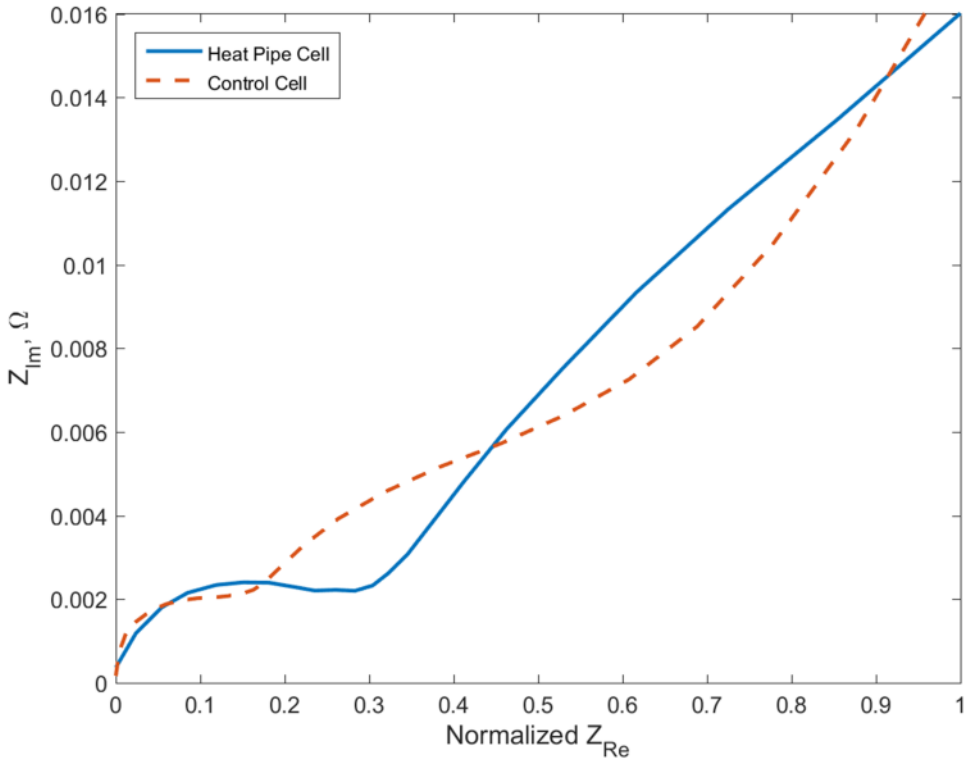

38. Figure 2: Comparison of Nyquist plots for heat pipe integrated Li-ion cell with a control cell that does not contain a heat pipe.

Further, the low frequency Warburg tail of the heat pipe cell has roughly the same slope as the control cell, indicating that diffusional impedance in the cell is unaffected by the insertion of the heat pipe. The waviness in the tail of the control cell may be explained by the incomplete

passivation of the SEI layer on the graphite anode of the control cell. Note that the 1.0 kHz equivalent series resistance (ESR) of the cell with heat pipe is greater than that of the control cell by 21.5 milliohms. Because of this real resistance shift, data in the heat pipe spectrum are normalized along the real impedance axis. This results in the expansion of the mid-frequency semi-circle in the heat pipe cell. This may be explained by slow diffusion of oxygen into the battery through the epoxy resin, causing the breakdown of solvents and conducting salts, thereby increasing the electrolyte resistance. In short, while the procedure to insert the heat pipe does reduce the shelf life of the cell, it is likely to be only due to the imperfect epoxy seal. The heat pipe itself does not appear to interfere with battery charging and discharging processes. However, large-scale implementation of heat pipes in Li-ion cells will require addressing the manufacturing challenge of integrating heat pipe without affecting long-term reliability.

2.3. Experimental Setup for Thermal Performance Measurements

The heat pipe-integrated 26650 Li-ion cell is mounted vertically, as shown in Figure 1(b), on a thin polystyrene riser to minimize conduction heat loss during experiments. Thermocouples are placed on the outer surface of the cell, at locations L/4, L/2, and 3L/4 as shown in Figure 1(b). An additional large block of polystyrene, with a 2mm diameter channel capable of completely accommodating the protruding portion of the heat pipe is used as a thermal insulation barrier for insulated heat pipe experiments. Lead wires from a MACCOR Series 4000 Automated Test System are attached to the power leads of the cell, shown in Figure 1(b). The cell is subjected to a variety of programmable charging and discharging profiles. A Fugetek HT-07530D12 computer fan is used in forced convection experiments to provide active convective cooling. The fan is placed at the same height as the tip of the heat pipe for heat pipe cooling experiments, and at cell mid-height for the cell body cooling experiments. This ensures direct

and symmetrical impingement of air from the fan on the surface to be cooled. A variable resistor controller is used for fan speed control. Air speed from the fan is measured using an Extech mini thermo-anemometer. Data acquisition from thermocouples embedded in the core and on the outside of the cell, is carried out using a NI-9213 DAQ thermocouple module, controlled by LabView software. Thermocouple measurements are taken once every second. The measurement rate is appropriate since this system has a much larger time constant than the data acquisition interval.

2.4. Thermal Performance Measurements

A number of experiments are carried out in a variety of heating and cooling conditions in order to measure the core and outer surface temperatures of the Li-ion cell with embedded heat pipe as functions of time during discharge at various currents. In each case, the Li-ion cell starts fully charged at ambient temperature, and a constant or time-varying discharge load is applied via the MACCOR Test System program.

The core and surface temperatures of the cell are measured as functions of time during discharge at a number of discharge currents. In each case, the cell is discharged until the potential difference reaches 2.0V. In one set of experiments, the protruding tip of the heat pipe is thermally insulated using a polystyrene block. In another set of experiments, the heat pipe tip is cooled through natural convection, without any forced air flow. Finally, these experiments are repeated in the presence of air flow from a fan impinging upon the tip of the heat pipe at various flowrates. In order to compare heat pipe cooling with the traditional approach of outer surface cooling, experiments are also carried out where the air flow impinges upon the outer surface of the cell instead of the heat pipe. Finally, in order to investigate the thermal effect of the heat pipe

in a situation of anomalous increase in heat generation, experiments are carried out where a 5A load is applied for a period of 5 minutes, following by a much larger, 20A load is applied for the remainder of the cell capacity, which is about 3.5 minutes.

A stabilization time of a few minutes is provided in each experiment involving air flow from the fan before the experiment commences. At the conclusion of each experiment, the cell is charged with a 2.6A current and allowed to cool for a few hours. The cell is run through an EIS test to ensure that the EIS profile and cell internal resistance have not changed appreciably before proceeding to the next experiment. An extended cool-down period is provided between experiments to ensure that each experiment begins at room temperature.

3. Results and Discussion

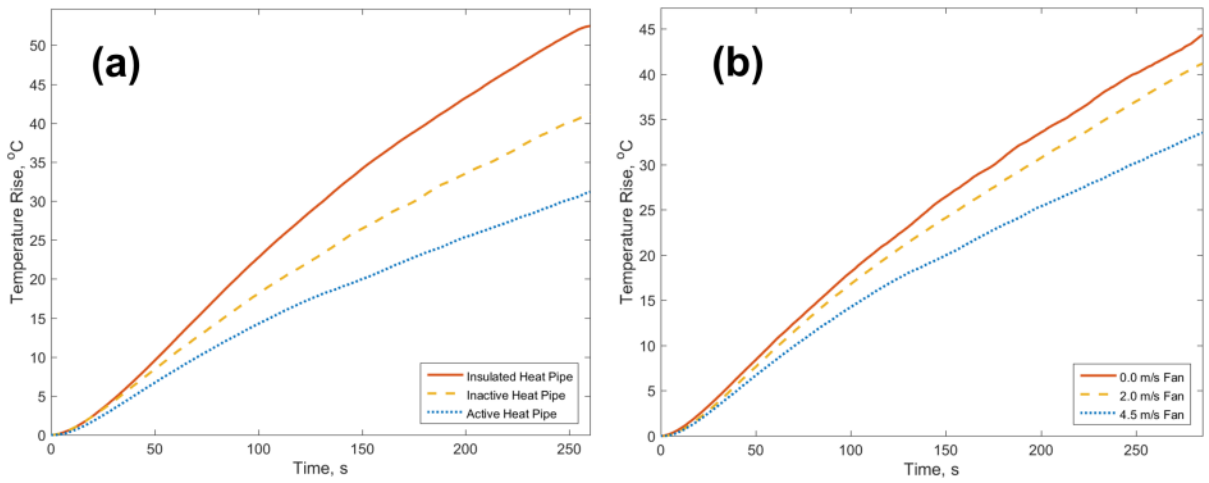

39. Figure 3: (a) Experimental measurement of core temperature as a function of time during 20A discharge in three thermal conditions related to tip of the heat pipe –insulated, cooled through natural convection, and actively cooled through forced convection using air flow at 4.5 m/s speed. (b) Experimental measurement of core temperature as a function of time during 20A discharge during active cooling of the heat pipe tip at three different air flow speeds.

While the embedded heat pipe is capable of transferring heat from the core of the cell to the condenser end located at the tip of the heat pipe, effective use of the heat pipe also requires heat removal from the condenser end. Otherwise, heat accumulation occurs at the condenser end,

thereby limiting overall heat pipe effectiveness. To investigate this, thermal performance of the heat pipe is measured in three separate cases. In the first case, the protruding portion of the heat pipe is covered with polystyrene insulation. In the second case, the protruding portion of the heat pipe is exposed to ambient air, so that heat removal occurs through natural convection – this case is referred to as an inactive heat pipe. A fan is used in the third case to provide active convective cooling of the heat pipe tip. Figure 3(a) plots the measured temperature rise at the core of the cell at mid-height for these cases as functions of time during 20A discharge, equivalent to about 12C. These data show a significant reduction in temperature rise of up to 20 °C between Case 1, where the heat pipe plays no role in cooling due to being insulated, and Case 3, where the heat pipe has the highest thermal effect. Even when the heat pipe is merely inserted without any active cooling of the condenser tip (Case 2), there is substantial improvement in thermal performance compared to the baseline Case 1. Ensuring effective heat removal from the heat pipe tip through forced convection (Case 3) results in the optimal utilization of the heat removal capability of the heat pipe. This is further investigated in experiments where the speed of air flow from the cooling fan is varied. Results plotted in Figure 3(b) for three different speeds show, as expected, that the temperature of the core reduces as the fan speed increases, due to improved heat removal from the condenser tip of the heat pipe.

A comparison of the core temperature with the surface temperature of the Li-ion cell is also of interest. It is desirable to bring the two as close to each other as possible in order to minimize spatial temperature gradients within the cell. Figure 4(a) plots both core and surface temperatures measured as functions of time during 20A discharge, and compares the temperature response for the cases of insulated and actively cooled heat pipe tip. Compared to the insulated heat pipe tip case, where the heat pipe plays minimal role in heat transfer, the actively cooled

heat pipe tip case results in lower values for both core and surface temperatures. Equally importantly, there is a significant temperature difference between the core and surface temperatures in the insulated heat pipe case. This happens because while the outside surface of the cell loses heat to the ambient air, there is no cooling mechanism available at the cell core, which gets much hotter than the surface. On the other hand, when the heat pipe tip is being actively cooled, thereby providing a mechanism for direct heat removal from the core, the core and surface temperatures are very close to each other throughout the discharge period, as shown in Figure 4(a). Figure 4(b) plots the temperature gradient measured within the cell during the discharge process, indicating a gradient of around 13 °C by the end of discharge for the insulated heat pipe case, whereas when the heat pipe is actively cooled, the temperature gradient is very small, even negative towards the last half of the discharge process. This interesting result shows that the heat pipe is capable of cooling the core of the cell down to a temperature similar to, or even lower than the surface temperature. This is simply not possible with the current paradigm of cooling cells on the outside surface, which is effective at removing heat close to the cell surface, but not from the core of the cell.

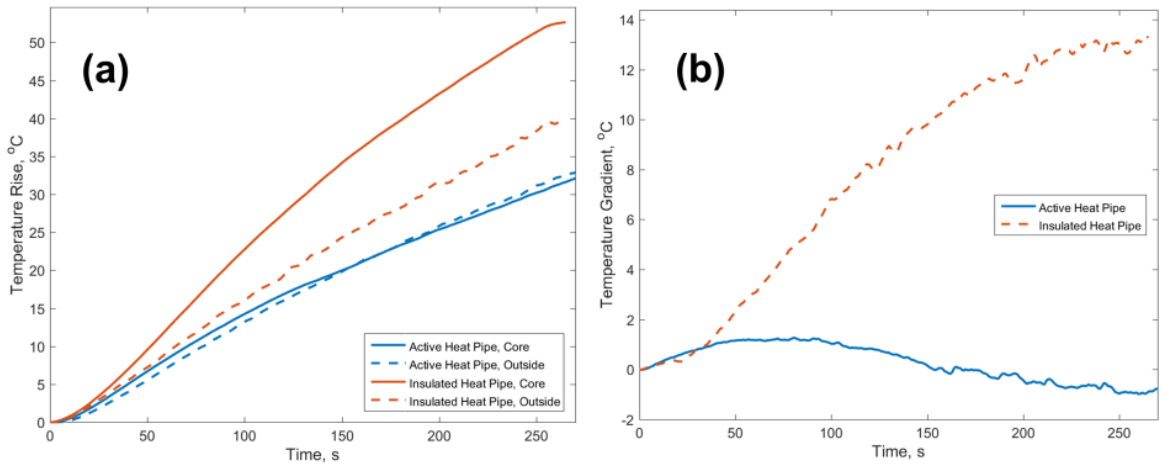

40. Figure 4: (a) Core and outside surface temperatures as functions of time without and with heat pipe (forced convective cooling) during 20A discharge, (b) Temperature difference between core and outside surface temperatures.

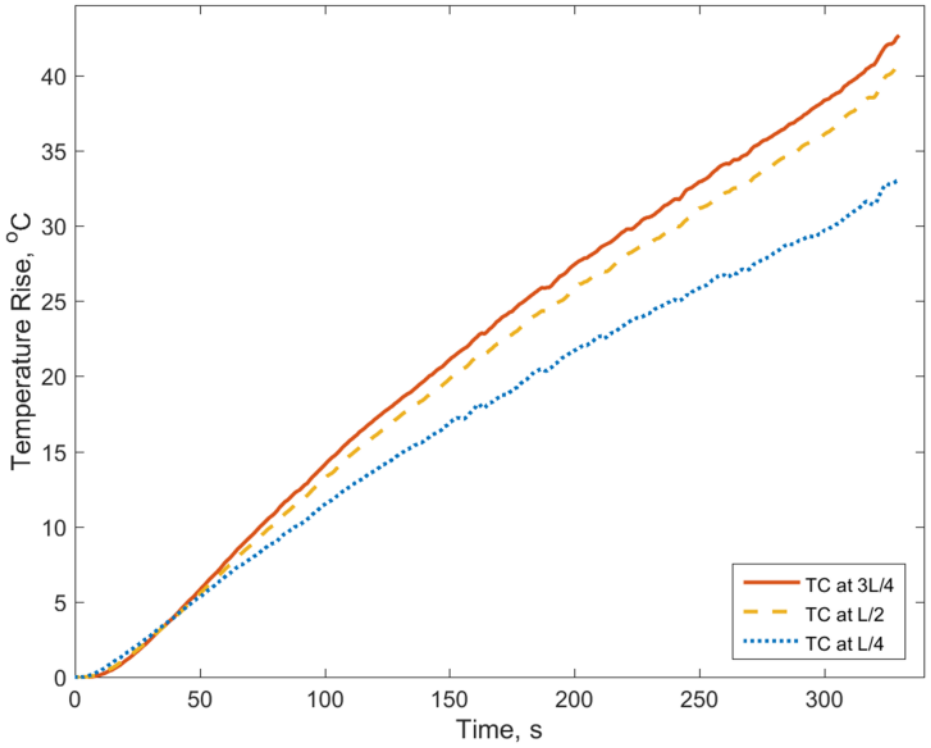

41. Figure 5: Axial variation in the core temperature during 20A discharge in the presence of the heat pipe, with forced convective cooling of the heat pipe tip.

Axial variation in temperature along the core of the cell is also of interest. Figure 5 plots temperature measurement from thermocouples located at three axial locations along the heat pipe inserted in the cell. These data are presented for a 20A discharge while the tip of the heat pipe is being actively cooled with 4.5 m/s air flow. The thermocouple at three-fourth height – closest to the heat pipe tip – is the hottest, whereas the thermocouple farthest from the heat pipe tip is the coolest. This trend is consistent with the operating principles behind a heat pipe, which indicate that the evaporator section of the heat pipe, farthest away from the condenser tip protruding out from the cell, is expected to have the lowest temperature [26].

Further experiments are conducted to investigate the importance of effective cooling of the heat pipe tip. In the first set of experiments, the cell is discharged at a number of discharge currents in both inactive and active heat pipe modes. Results summarized in Figure 6 indicate

that in each case, the temperature rise in the active heat pipe mode is lower than when the heat pipe is not active. As expected, temperature rise is higher at higher discharge currents due to greater heat generation.

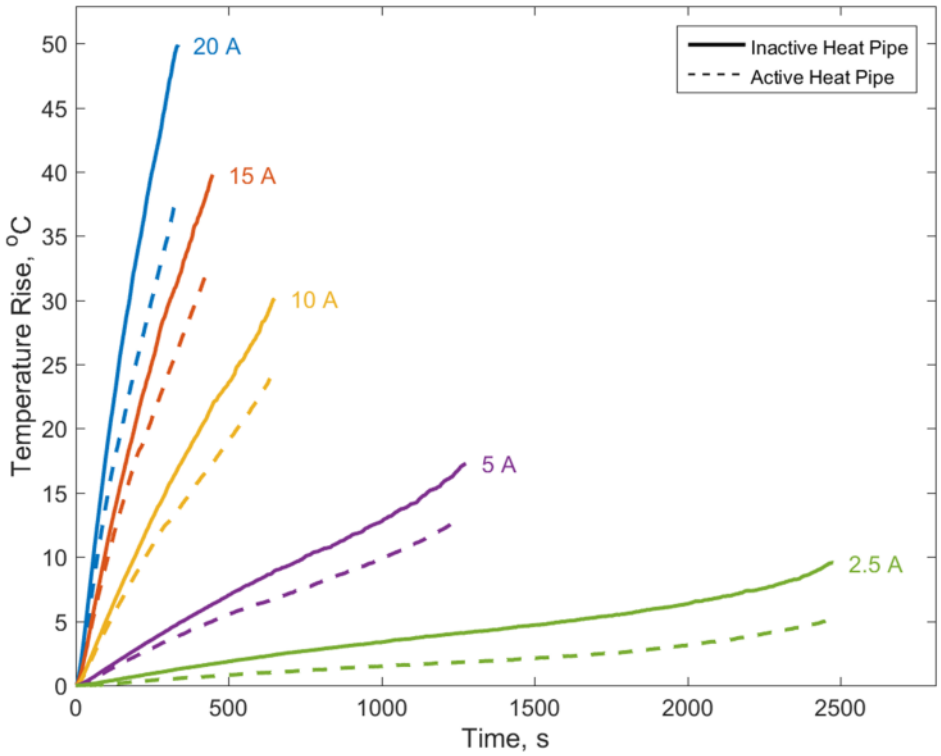

42. Figure 6: Comparison of core temperatures for multiple discharge rates with inactive and active heat pipe.

The role of the heat pipe in case of an anomalous increase in heat generation rate from the cell is of interest. Such a scenario may occur, for example, if the cell is thermally or mechanically abused, or if there is a failure of the battery management system. Specifically, an experiment is carried out where the discharge current of the cell suddenly jumps from 5A to 20A, representing approximately 16-fold increase in the heat generation rate. Such a large increase in heat generation subjects the cell to a thermal shock, and makes it critical to remove the heat generated in order to prevent large temperature rise leading to thermal runaway. Figure 7 plots the measured core temperature of the cell as a function of time in this scenario for inactive

and active heat pipe cases. During the initial phase of the experiment, the two cases are quite similar, with a slightly larger temperature rise in the inactive heat pipe case. However, when the anomalous heat generation occurs, core temperature in the cell with inactive heat pipe rises very rapidly, whereas when the heat pipe is active, the temperature rise is a lot less steep. Figure 7 shows that within the short period of the anomalous heat generation, temperature rise in the inactive heat pipe case is about 10 °C greater than in the active heat pipe case.

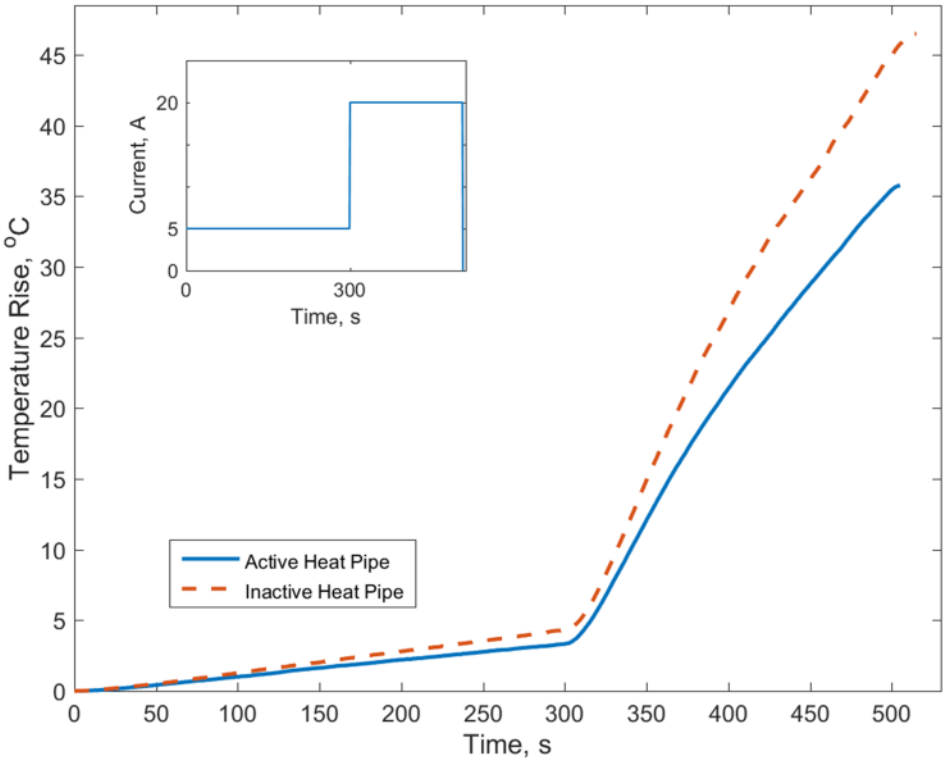

43. Figure 7: Thermal response of the core temperature to a sudden increase in discharge rate, without and with heat pipe.

Finally, heat pipe based cooling is compared with the present paradigm of outer surface-based cooling where coolant flow over the outer surface of the cell results in convective heat transfer. Experiments are carried out where the same air flowrate impinges either over the protruding tip of the heat pipe, or over the cell surface itself, as shown in the inset of Figure 8. Figure 8(a) plots the measured core and surface temperatures in both cases as functions of time

during a 20A discharge. Direct cell cooling results in a very low cell surface temperature, but fails to similarly reduce the core temperature, primarily due to the large thermal resistance between the core and the surface. On the other hand, when heat pipe cooling is used, the core temperature drops significantly, and, as shown in Figure 8(b), the temperature gradient within the cell is much lower throughout the experiment for the heat pipe cooled cell compared to the cell being cooled at the outer surface. This highlights the capability of heat pipe based thermal management to effectively cool the core of the cell, where cooling is most needed, thereby reducing the temperature gradient within the cell.

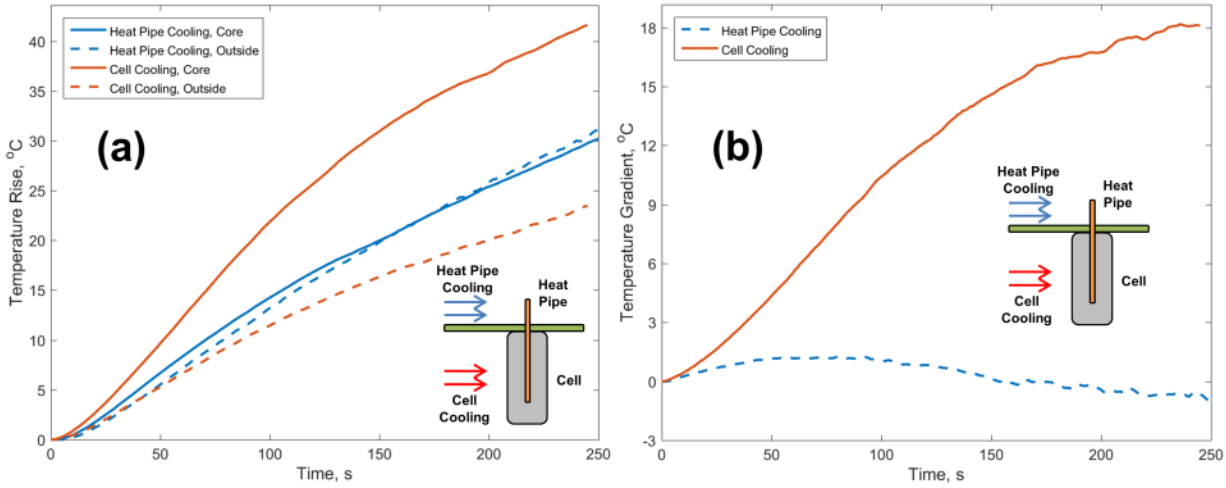

44. Figure 8: Comparison of (a) core and outside surface temperatures and (b) temperature gradient for heat pipe based cooling with traditional approach of cooling the outer surface.

4. Conclusions

Heat pipe technology is an attractive approach for reducing operating temperature and improving thermal uniformity in Li-ion cells. This work advances the application of heat pipe in Li-ion cell cooling by inserting a heat pipe into a cell and measuring its thermal benefit during high-rate discharge of the cell. This is a significant improvement over past efforts where the heat pipe was only inserted between cells in a battery pack, because insertion into a cell facilitates heat removal directly from the core of the cell which is in greatest need of cooling. Experiments

carried out here show a large temperature reduction due to the presence of the heat pipe, particularly when the protruding tip of the heat pipe is actively cooled in order to promote overall heat transfer. Results indicate that the heat pipe can cause the core temperature to become as low as, or even slightly lower than the outer surface temperature of the cell.

While the insertion of a heat pipe into a Li-ion cell poses several manufacturing challenges, the experimental data presented in this paper suggests that there may be several thermal benefits in doing so. Further investigation of these manufacturing challenges, particularly to ensure long-term cell reliability in the presence of the heat pipe, is necessary to evaluate this thermal management approach for future Li-ion cell designs. Novel cell designs need to be investigated that accommodate a heat pipe in the cell, for example by providing an axial channel in which to insert the heat pipe. Further, it is also essential to model and optimize the design of the heat pipe itself. This may further improve the thermal performance obtained from the use of heat pipes.

Acknowledgments

This material is based upon work supported by CAREER Award No. CBET-1554183 from the National Science Foundation. Support from Office of Naval Research through grant N00014-16-1-2223 is also gratefully acknowledged. Heat pipe assistance from Dr. Winston Zhang, Novark Technology Inc. is gratefully acknowledged.

References

[1] K. Shah, V. Vishwakarma, A. Jain, ASME J. Electrochem. Energy Convers. Storage (in press), 2016. DOI: 10.1016/j.jpowsour.2016.08.133

[2] T.M. Bandhauer, S. Garimella, T. Fuller, J. Electrochem. Soc. 158 (2011) R1-R25. DOI: 10.1149/1.3515880

[3] V. Srinivasan, C.Y. Wang, J. Electrochem. Soc. 150 (2003) A98-A106. DOI: 10.1149/1.1526512

[4] K.E. Thomas, J. Newman, J. Power Sources, 119-121 (2003) 844-849. DOI: 10.1016/S0378-7753(03)00283-0

[5] D. Bernardi, E. Pawlikowski, J. Newman, J. Electrochem. Soc. 132 (1985) 5-12. DOI: 10.1149/1.2113792

[6] M. Broussely, Aging Mechanisms and Calendar-Life Predictions, in: W.A.V. Schalkwijk and B. Scrosati (Eds.), Advances in Lithium-Ion Batteries, Kluwer Academic/Plenum Publishers, New York, 2002, pp. 393-432. ISBN: ISBN 978-0-306-47508-5

[7] P. Arora, R.E. White, M. Doyle, J. Electrochem. Soc. 145 (1998) 3647-3667. DOI: 10.1149/1.1838857

[8] D. Aurbach, J. Power Sources 146 (2005) 71-78. DOI: dx.doi.org/10.1016/j.jpowsour.2005.03.151.

[9] B.A. Johnson, R.E. White, J. Power Sources 70 (1998) 48-54. DOI: 10.1016/S0378-7753(97)02659-1

[10] Q. Wang, P. Ping, X. Zhao, G. Chu, J. Sun, C. Chen, J. Power Sources 208 (2012) 210-224. DOI: 10.1016/j.jpowsour.2012.02.038

[11] R. Spotnitz, J. Franklin, J. Power Sources 113 (2003) 81-100. DOI: 10.1016/S0378-7753(02)00488-3

[12] K. Shah, D. Chalise, A. Jain, J. Power Sources 330 (2016) 167-174. DOI: 10.1016/j.jpowsour.2016.08.133

[13] H. Maleki, G. Deng, A. Anani, J. Howard, J. Electrochem. Soc. 146 (1999) 3224-3229. DOI: 10.1149/1.1392458

[14] Y. Ye, Y. Shi, N. Cai, J. Lee, X. He, J. Power Sources 199 (2012) 227-238. DOI: 10.1016/j.jpowsour.2011.10.027

[15] N. Nieto, L. Diaz, J. Gastelurrutia, F. Blanco, J.C. Ramos, A. Rivas, J. Power Sources 272 (2014) 291-302. DOI: 10.1016/j.jpowsour.2014.07.169

[16] V. Vishwakarma, C. Waghela, Z. Wei, R. Prasher, S.C. Nagpure, J. Li, F. Liu, C. Daniel, A. Jain, J. Power Sources 300 (2015) 123-131. DOI: 10.1016/j.jpowsour.2015.09.028

[17] S.J. Drake, D.A. Wetz, J.K. Ostanek, S.P. Miller, J.M. Heinzel, A. Jain, J. Power Sources 252 (2014) 298-304. DOI: 10.1016/j.jpowsour.2013.11.107

[18] J. Zhang, B. Wu, Z. Li, J. Huang, J. Power Sources 259 (2014) 106-116. DOI: 10.1016/j.jpowsour.2014.02.079

[19] K. Shah, S.J. Drake, D.A. Wetz, J.K. Ostanek, S.P. Miller, J.M. Heinzel, A. Jain, J. Power Sources 271 (2014) 262-268. DOI: 10.1016/j.jpowsour.2014.07.118

[20] K. Shah, S.J. Drake, D.A. Wetz, J.K. Ostanek, S.P. Miller, J.M. Heinzel, A. Jain, J. Power Sources 258 (2014) 374-381. DOI: 10.1016/j.jpowsour.2014.01.115

[21] S. Drake, M. Martin, D.A. Wetz, J.K. Ostanek, S.P. Miller, J.M. Heinzel, A. Jain, J. Power Sources 285 (2015) 266-273. DOI: 10.1016/j.jpowsour.2015.03.008

[22] C. Forgez, D.V. Do, G. Friedrich, M. Morcrette, C. Delacourt, J. Power Sources 195 (2010) 2961-2968. DOI: 10.1016/j.jpowsour.2009.10.105

[23] S. Pannala, H. Wang, K. Kepler, S. Allu, Electrochem. Soc. MA2014-02 (2014) 445.

[24] S.K. Mohammadian, Y.L. He, Y. Zhang, J. Power Sources 293 (2015) 458-466. DOI: 10.1016/j.jpowsour.2015.05.055

[25] T.M. Bandhauer, S. Garimella, Appl. Therm. Eng. 61 (2013) 756-769. DOI: 10.1016/j.applthermaleng.2013.08.004

[26] A. Faghri, Review and Advances in Heat Pipe Science and Technology, J. Heat Transfer 134 (2012) 123001. DOI: 10.1115/1.4007407

[227] S.W. Chi, Heat pipe theory and practice: a sourcebook, Hemisphere Publishing Corporation, Washington, D.C., 1976. ISBN: 0070107181

[28] P.D. Dunn, D.A. Reay, Heat Pipes, third ed., Pergamon Press Inc., New York, 1982. ISBN: 0080293565.

[29] R. Mahajan, C.P. Chiu, G. Chrysler, Proc. IEEE 94 (2006) 1476-1485. DOI: 10.1109/JPROC.2006.879800

[30] A. Akbarzadeh, T. Wadowski, Appl. Therm. Eng. 16 (1996) 81-87. DOI: 10.1016/1359-4311(95)00012-3

[31] X.Y. Lu, T.C. Hua, M.J. Liu, Y.X. Cheng, Thermochim. Acta 493 (2009) 25-29. DOI: 10.1016/j.tca.2009.03.016

[32] R.R. Riehl, T. Dutra, Appl. Therm. Eng. 25 (2005) 101-112. DOI: 10.1016/j.applthermaleng.2004.05.010

[33] H.B. Ma, B. Borgmeyer, P. Cheng, Y. Zhang, J. Heat Transf. 130 (2008) 081501. DOI: 10.1115/1.2909081

[34] V.Y. Kravets, Y.E. Nikolaenko, Y.V. Nekrashevich, Heat Transf. Res. 38 (2007) 553-563. DOI: 10.1615/HeatTransRes.v38.i6.70

[35] Z. Rao, S. Wang, M. Wu, Z. Lin, F. Li, Energy Convers. Manag. 65 (2013) 92-97. DOI: 10.1016/j.enconman.2012.08.014

[36] T.H. Tran, S. Harmand, B. Desmet, S. Filangi, Appl. Therm. Eng. 63 (2014) 551-558. DOI: 10.1016/j.applthermaleng.2013.11.048

[37] Q. Wang, B. Jiang, Q.F. Xue, H.L. Sun, B. Li, H.M. Zou, Y.Y. Yan, Appl. Therm. Eng. 88 (2014) 54-60. DOI: 10.1016/j.applthermaleng.2014.09.083

[38] N. Putra, B. Ariantara, R.A. Pamungkas, Appl. Therm. Eng. 99 (2016) 784-789. DOI: 10.1016/j.applthermaleng.2016.01.123

[39] Y. Ye, L.H. Saw, Y. Shi, A.A.O. Tay, Appl. Therm. Eng. 86 (2015) 281-291. DOI: 10.1016/j.applthermaleng.2015.04.066

[40] K. Shah, C. McKee, D. Chalise, A. Jain, Energy 113 (2016) 852-860. DOI: 10.1016/j.energy.2016.07.076

CHAPTER 6

CONCLUSION

Non-invasive measurement of temperature inside solid bodies is of great importance for a wide variety of engineering applications where the temperature of the body governs safety, performance, and reliability. In this thesis, a novel, non-invasive method for determining the core temperature of solid, heat generating bodies has been introduced and validated using experiments on a cylindrical thermal test cell and on a cylindrical Li-ion cell during discharge periods. By utilizing the measured surface temperature distribution, this method accurately predicts the core temperature as a function of time. The method presented here can be easily extended to bodies of other shapes, so long as the thermal conduction problem can be solved for the particular geometry, to derive a relationship between the core and outside temperatures, as previously described in this work. These results validate a novel metrology method for non-invasive, internal temperature measurement of solid bodies, which contributes towards thermal design and optimization of a wide variety of engineering systems. This capability could be used for smart, thermally-aware performance optimization, as well as for ensuring thermal safety. This work contributes towards fundamental thermal metrology, improved thermal and electrochemical design of energy conversion, and storage systems where overheating is a concern and requires careful monitoring.

Heat pipe technology is an attractive approach for reducing operating temperature and improving thermal uniformity in Li-ion cells. This work justifies the use of heat pipes in Li-ion cell cooling by utilizing an embedded a heat pipe in a uniquely manufactured cell and measuring its thermal benefit during high-rate discharge periods. The experiments performed show a large

temperature reduction due to the presence of the heat pipe, specifically when the exposed tip of the heat pipe is actively cooled, facilitating greater heat transfer. Experimental data show that the heat pipe can allow the core temperature of the cell to become as low as, or even lower than the external surface temperature of the cell. The insertion of a heat pipe into a Li-ion cell may pose several manufacturing challenges, but the results presented in this work suggest that there is a serious thermal benefit in utilizing this method. This work contributes toward improved thermal design and electrochemical performance of Li-ion batteries from a manufacturing standpoint.

BIOGRAPHY

Dean Raymond Anthony was born in 1988 in St. Louis, Missouri. He spent much of his childhood growing up in Tempe, Arizona. He attended the University of Arizona for his undergrad where he studied Teaching Physics and Italian. He now resides in Fort Worth, Texas where he is completing a Masters in Mechanical Engineering from the University of Texas at Arlington in 2016.

Contact: dean.anthony@mavs.uta.edu